DEVELOPING A SYSTEM OF SCALABLE COMPLEXITY FOR IN VITRO MODELS OF CELL MIGRATION

By

William J. Ashby

Dissertation

Submitted to the Faculty of the

Graduate School of Vanderbilt University

in partial fulfillment of the requirements

for the degree of

DOCTOR OF PHILOSOPHY

in

Chemical and Physical Biology

December, 2012

Nashville, Tennessee

Approved:

Professor David W. Piston

Professor Franz J. Baudenbacher

Professor Christopher J. Janetopoulos

Professor Alissa M. Weaver

Professor John P. Wikswo

To my wife
for accompanying me on this journey
always and in all ways

ACKNOWLEDGEMENTS

Just as cell migration results from the integration of numerous inputs from various sources (see Fig. 2), this dissertation results from the integrated inputs of various people in my life.

First of all, I thank my mentor Dr. Zijlstra whose enthusiasm and eagerness to create better approaches for biological studies provided the impetus and freedom essential to our joint successes such as the patent pending magnetically attachable stencils and magnetically sealed live-cell imaging chamber presented herein.

Secondly, my thanks goes to Dr. John Wikswo my co-mentor who has provided time and expertise necessary to move my research and the development of these tools forward.

Third, I thank Dr. Dave Piston for imparting an unwavering sense of confidence in my ability and for the opportunity to rotate in his lab thus crossing paths with my soon-to-be postdoctoral mentor Dr. Chris Easley.

Fourth, my thanks goes to Al Beth and Hassane Mchauorab who spearheaded the creation and implementation of this Ph.D. program which has been a perfect fit for me.

Fifth, I thank Lindsay Meyers for assistance with numerous menial tasks and questions and for many invitations to lunch with Chemical and Physical Biology recruits.

Sixth, my thanks goes to Dr. Michal Kliman for being a true Christian and a true friend to me and my family.

Last, I thank with all my heart my wife Lisa for her sacrifice through these six years which has indeed been greater than my own.

TABLE OF CONTENTS

LIST OF TABLES

LIST OF FIGURES

LIST OF VIDEOS

Videos

LIST OF ABBREVIATIONS

2D	two-dimensional
3D	three-dimensional
A555	Alexa Fluor® 555
BSA	bovine serum albumin
CAM	chorioallantoic membrane
CCM	cultureware, camera, microscope
CN	collagen
CNC	computer numerical control
DIC	differential interference contrast
DME/M	Dulbecco's modified Eagle's/medium
ECIS	electric cell impedance sensing
ECM	extracellular matrix
EMT	epithelial-mesenchymal transition
FBS	fetal bovine serum
FN	fibronectin
FITC	fluorescein isothiocyanate
GFP	green fluorescent protein
H&E	haematoxylin & eosin
hr	hour
MAt(s)	magnetically attachable stencil(s)
MAT(s)	magnetically attachable template(s)
MMC	murine mammary carcinoma
min	minute

MSLIC(s)	magnetically sealed live-cell imaging chamber(s)
NdFeB	neodymium iron boron
OD	outer diameter
PAA	polyacrylamide
PBS	phosphate buffered saline
PDL	poly-D-lysine
PDMS	polydimethylsiloxane
PDMS-M	polydimethylsiloxane-magnetite
PVA	polyvinyl alcohol
RPMI	Roswell Park Memorial Institute
SANPAH	succinimidyl-6-(4'-azido-2'-nitrophenylamino) hexanoate
SD	standard deviation
SEM	standard error of the mean
SLR	single-lens reflex
TEMED	tetramethylethylenediamine
UV	ultraviolet
μTAS	micro-total analysis system
VIIBRE	Vanderbilt Institute for Integrative Biosystems Research and Education

CHAPTER I

INTRODUCTION

Current medical ability to diagnose and treat disease remains limited for many chronic diseases such as cancer, carcinoids, diabetes, and obesity. Basic research promises to advance our understanding of such conditions and ultimately improve treatment. However, basic research relies upon models and assays that recreate in vitro a portion of the enormous complexity found in vivo and that enable robust quantitative analysis. The tools of research must combine biologically-relevant complexity with analytical ability. Development of such tools requires skills and collaboration across disciplines. Furthermore successful implementation is most likely for tools that are versatile and easy-to-use. This dissertation presents research on the development and implementation of two versatile, combinable tools that allow portions of in vivo complexity to be recreated in vitro in a scalable manner: magnetically attachable stencils (MAts) and magnetically sealed live-cell imaging chambers (MSLICs). By integrating these two tools a greater range of complexity can be scaled. In combination these tools constitute a system of scalable complexity ranging from simple 2D cell assays under static conditions to fluidically controlled 3D cell assays.

Historical Perspective on Scalable Complexity

Scalable complexity is the ability to add in a controlled and analyzable manner important aspects of the in vivo environment to in vitro models. It requires both the incorporation of complexity into in vitro models and the ability to perform detailed analysis. Not all aspects of biological complexity need to be or can be scalable in a given system; however, complexity outside of experimental control needs to be reproducible and carefully consid-

ered when interpreting data. The objective of this dissertation is the creation and implementation of tools that provide such scalable complexity for cancer metastasis research. It should be noted that these tools are applicable to all fields involving cell migration and not just cancer metastasis.

Historically experimental models have been split between two extremes: in vitro and in vivo models. Both present unique challenges or constraints to biological research. In vitro models oversimplify the biology in order to provide greater analytical ability (Fig. 1). This oversimplification may diminish relevance and can lead to false expectations and subsequent failure as research is translated into in vivo models and clinical use. On the other hand in vivo models provide complexity similar to a living human being but limit analytical capacity, often allowing only mere snapshots of dynamic biological processes. The differences be-

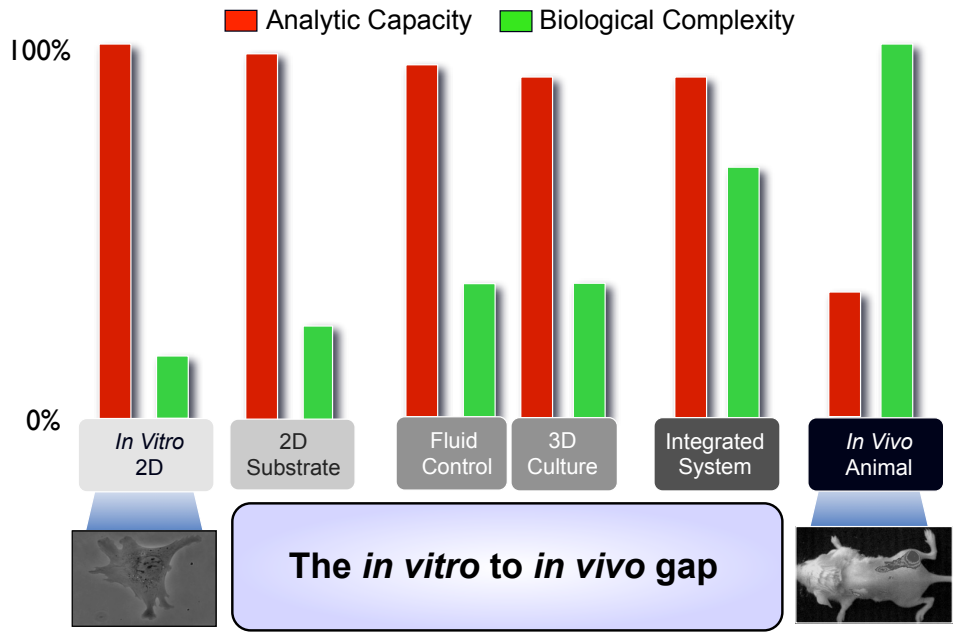

Figure 1. The gap between standard in vitro and in vivo models. In vitro models provide superior analytical capacity but lack complexity and therefore may also lack relevance . Scaling the complexity of in vitro and in vivo biology is possible without significant loss of analytical capacity. This dissertation specifically presents a system of integrated in vitro tools capable of 2D substrate, fluid, and 3D culture complexity thus filling the gap between in vitro and in vivo models.

tween these two approaches represent a critical gap in society's research capabilities.

The purposes for creating scalable complexity are to fill the gap between simple in vitro models and complex in vivo models, improve translational research efficiency, reveal the aspects of in vivo complexity that are critical for a given area of research, and ultimately increase society's ability to prevent, diagnose, and treat disease. Many individual tools have already been created to fill this gap and are delivering results. For example, in 2009 the first long-term culture model of intestinal epithelium was developed [1]. This model was capable of sustaining intestinal stem cell niches for >350 days because it incorporated the necessary complexity into in vitro organoid culture. Specifically a 3D culture matrix of collagen, a liquid-air interface, cellular myofibroblast architecture, and appropriate stimulation of Wnt and Notch signaling were required [1]. Other technological advancements are filling this gap between in vitro and in vivo models and have illustrated the importance of various parameters to in vitro research such as mechanical matrix properties, fluid composition and dynamics, cell-cell interactions, and intrinsic cellular properties [2-9]. Chapter II provides a review of these advancements relevant to two-dimensional (2D) in vitro cell migration. However, none of these advances alone constitutes a system capable of scaling through multiple aspects of biological complexity. The absence of scalable complexity in existing models and the need for our laboratory to use such a tool for scientific inquiry motivated my pursuit to develop a system of scalable complexity.

Developing a System of Scalable Complexity

The objectives of this dissertation research are development and implementation of tools that both fill the gap between in vitro and in vivo models and combine to form a system of scalable complexity. The product of this thesis is a series of tools including magnetically attachable stencils (MAts), magnetically sealed live-cell imaging chambers (MSLICs),

and the angiogenesis disk. The biological focus of this dissertation has been cancer cell migration as it relates to metastasis. However, the tools presented herein are applicable to all fields of biological research utilizing cell migration and other live-cell assays. The development phase of the research involved numerous iterations and prototypes in order to achieve the capability and versatility essential to scalable complexity for cell migration. Implementation of the developed tools resulted in more prototyping in order to achieve ease-of-use for endpoint users. Consequently, the tools presented herein are versatile delivering to cell migration studies scalable complexity of 2D substrate conditions, fluid conditions, and 3D matrix conditions. Yet they remain easy-to-use. For this reason they have been implemented in laboratories throughout Vanderbilt University and beyond.

2D substrate complexity

In order to scale the complexity of substrate conditions for 2D migration of densely organized cells, a tool is required that can create a void between cells without disruption or modification of the matrix onto which the cells will migrate. Existing cell migration methods fail to accomplish this for a wide range of substrate conditions. MAts fill this gap and enable migration analysis on various protein coatings and surface materials such as glass, plastic, nanofibers, and elastic hydrogels. This is possible because MAts utilize magnetic force to attach to these substrates. The magnetic force can be tailored to the substrate in order to protect the substrate during placement and removal of the MAts. Implementation of MAts on various substrates and the resulting biological insights are reported in Chapter III. Notably, research with MAts revealed unexpected migratory inhibition as dense cell populations migrated across an interface of two matrix proteins. Such migration across matrix protein interfaces occurs regularly in the process of cancer cell migration in vivo and represents an important component of the biological complexity of metastasis.

Fluid complexity

Another component of biological complexity oversimplified in vitro is fluid dynamics. Many systems such as commercial bioreactors and microfluidics have been developed to incorporate fluid dynamics into cell growth and analysis. However most systems are designed for specific applications and lack the versatility and ease-of-use essential to broad implementation in life science research. In order to meet this need and create fluidic control in a platform compatible with MAts, we developed the magnetically sealed live-cell imaging chamber (MSLIC) which is presented in Chapter IV. Fluidically controlled systems are complex by necessity because of the required tubing and pumps. Efforts to make MSLICs as easy-to-use as possible led to the use of magnetic force to seal the chambers. Furthermore the chambers can be used statically without tubing and pumps or syringes. MSLICs enable scalable complexity of the fluid environment such as temporally controlled delivery of treatments, soluble factors, or oxygen and CO_2.

3D complexity

Incorporating 3D complexity into the tools of this dissertation was extremely important to achieving the desired range of complexity. Extensive research and development of 3D materials for cellular environments has been done. For this reason our efforts focused on simply incorporating already developed 3D culture techniques into MSLICs. The use of MSLICs for 3D culture is discussed in Chapter IV and in the Future Directions section of Chapter V.

CHAPTER II

ESTABLISHED AND NOVEL METHODS OF INTERROGATING TWO-DIMENSIONAL CELL MIGRATION*

Summary

The regulation of cell motility is central to living systems. Consequently, cell migration assays are some of the most frequently used in vitro assays. This article provide a comprehensive, detailed review of in vitro cell migration assays both currently in use and possible with existing technology. Emphasis is given to two-dimensional migration assays using densely organized cells such as the scratch assay. Assays are compared and categorized in an outline format according to their primary biological readout and physical parameters. The individual benefits of the various methods and quantification strategies are also discussed. This review provides an in-depth, structured overview of in vitro cell migration assays as a means of enabling the reader to make informed decisions among the growing number of options available for their specific cell migration application.

Introduction

Cell migration is a dynamic and complex process guided by a vast array of chemical and physical signals. Controlled cell migration allows for normal development and function; whereas, misregulated motility potentates a multitude of pathologies, including inflammation and cancer metastasis. Not surprisingly, a variety of cell migration assays have been de-

---

*This chapter is pending publication as W. J. Ashby and A. Zijlstra, "Established and Novel Methods of Interrogating Two-Dimensional Cell Migration," Integrative Biology. doi://10.1039/C2IB20154B

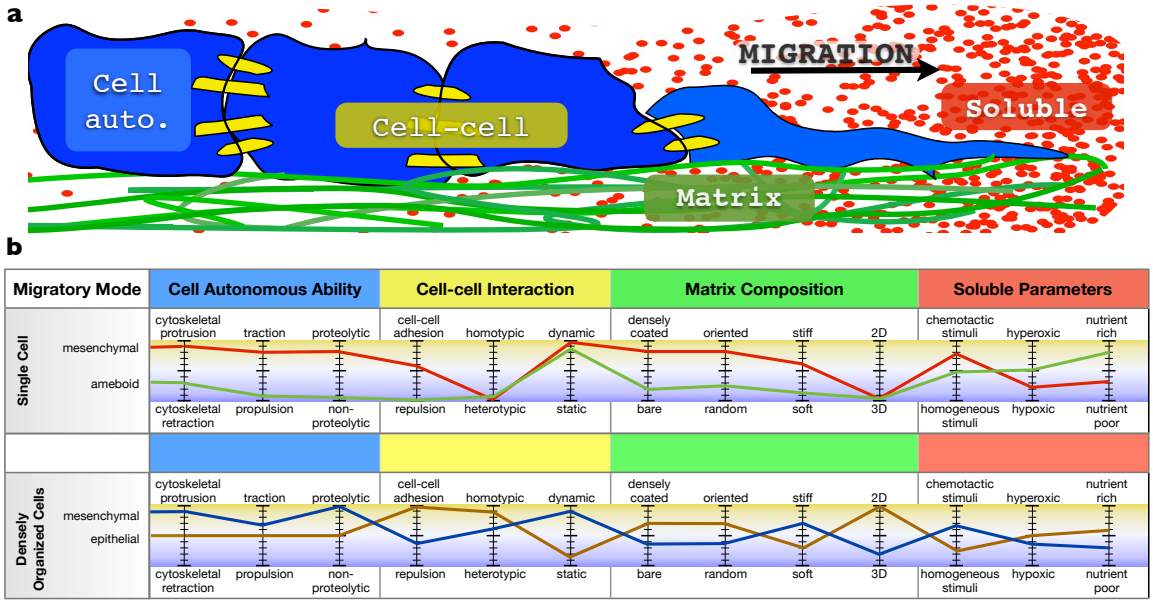

Figure 2. Parameters of cell migration. A multi-scale model of cell migration presents multiple interdependent parameters classified under four distinct categories (cell autonomous ability, cell-cell interaction, matrix composition and soluble parameters. **(a)** Cells are constantly integrating elements that contribute to their ability to migrate including those from within (cell autonomous ability), those created by interacting with neighboring cells (cell-cell interaction) or with the surrounding matrix composition and by those received as soluble stimuli (soluble parameters). The integration of these parameters determines the mode and capacity of migration. **(b)** The range of many migratory parameters can be displayed in a tuning model similar to those commonly used in audio equalizers (supplement). The magnitude of any parameter influences its impact on the mode and means of migration as well as the influence of related parameters. Each migration mode is represented by a colored line, and the position at which this line crosses each tuner represents the magnitude of that parameter for this migration mode. This enables a visual display of the general conditions for various types of cell migration including single isolated mesenchymal cells (red line) and ameboid cells (green line) as well as densely organized mesenchymal (blue line) and epithelial cells(brown line). For additional interpretation and definitions of terms see supplemental Figure C1 and Table CI.

signed in order to investigate the critical components that control cell movement. These assays have unique strengths and weaknesses that define their utility. To judiciously select one assay from among the growing number of assays, a knowledge of both the assay's capabilities and the surrounding context are needed. This review expounds on the capabilities and shortcomings of existing assays including a side-by-side comparison of current 2D cell migration assays. More importantly by including potential methods for new assays, this review provides the full context needed to readily understand both existing and future assays.

The landscape of cell migration consists of numerous variables that fit into various categories (Fig. 2). Four broad categories useful for capturing the various influences on migration are 1) cell autonomous properties, 2) soluble factors, 3) matrix properties, 4) cell-to-cell interactions [10]. To visualize these categories and further stratify the migratory landscape, we expanded Friedl's tuning model of migration to include variables within each of the four broad groups (Fig. 2B) [11]. The various conditions possible for each variable are represented as possible vertical positions which together constitute the bandwidth of the tuning model. Specific conditions of variables across these four categories result in specific modes of migration. Unique modes of migration such as dense and single cell mesenchymal migration, collective cell migration, and single cell ameboid migration are illustrated as lines cutting across the bandwidth of the tuning model. This model helps convey the multifactorial nature of the various controls over cell migration.

For a review of cell migration itself this landscape and the various migratory modes would be sufficient; however, understanding the context of cell migration assays requires incorporation of the assays' physical means of operation into this migration-focused landscape. These means of operation are given in the two left-most columns of Table 1. In two-dimensional migration assays cells are either removed from the substrate or excluded. Cell removal methods utilize mechanical, electrical, chemical, and potentially thermal and optical means to remove or destroy cells and thus enable migration into the disrupted area. Exclusion methods rely on solids, gels, liquids, air interfaces, and potentially electromagnetic forces to prevent cells from adhering to the area into which they later migrate. These physical modes of operation each have limitations. Combining the cell migration landscape with the physical modes of operation creates a full context for understanding 2D cell migration assays.

With this complete context in mind the capabilities of specific assays can be readily compared and understood even without prior knowledge of the individual assays (Table 1). Just as a mode of migration can be displayed by a line across the bandwidth of the tuning model, each migration assay can be displayed as a custom bandwidth according to the assay's

Table 1. Bandwidth of 2D migration assays.

Assay Bandwidth (Upper Range / Full Range / Lower Range; ? = unknown; NA = not applicable)		Geometry		Cell-cell Interaction		Matrix Composition				Soluble Parameters		
		rectangular	voids	homotypic	dynamic	densely coated	oriented	stiff	2D	chemotactic stimuli	hyperoxic	migration inducing factors
		circular	nests	heterotypic	static	bare	random	soft	3D	homogeneous stimuli	hypoxic	inhibiting factors
Isolated, Individual Cells												
	Single Cell Tracking	NA	NA	NA	NA							
Densely Organized Cells												
Cell Removal (Wounding)												
Mechanical	Scratch Assay											
	Scratch Variations	or	or									
Electrical	ECIS											
Chemical	Laminar Flow of Trypsin											
Undeveloped **Thermal**	Thermal Damage	?	?									
Undeveloped **Optical**	Laser Ablation	?	?									
Cell Exclusion (Void Filling)												
Solids	Stencils											
	Stoppers											
	MAtS											
Gels	Barricade Gels											
Liquids	Immiscible Solutions											
	Laminar Flow											
Air	Droplets											
	Microfluidic Surface Tension											
Electromagnetic	Magnetic Particles	?	?									
Undeveloped	Electric Cell Repulsion	?										
Undeveloped	Optical Trapping											

ability or lack of ability to provide experimental control of important variables such as geometry, cell-cell interaction, matrix composition, and soluble parameters. By comparing an assay's custom bandwidth (Table 1) to a mode-of-migration line (Fig. 2B), the ability of a

given assay to study a specific mode of migration can be crudely estimated.For example single cell migration assays are, as expected, highly compatible with the single cell ameboid and single cell mesenchymal migration modes, and magnetically attachable stencil (MAts) assays are well-suited for studies of dense mesenchymal and epithelial migration. Visually depicting the capability and limitations of each assay facilitates rapid side-by-side comparison and thus selection of suitable migration assays (see Fig. C2 for examples). This visual depiction can be readily expanded to accommodate new assays as they are developed.

In vivo, most migration occurs in three dimensions, and for this reason many three-dimensional in vitro migration assays are in development. Unfortunately, there are currently few consistent guidelines regarding the set up and analysis of 3D assays. Furthermore, 3D assays require greater data collection and more advanced image analysis than 2D assays. Considering this, we have restricted our review to the more common two-dimensional in vitro migration assays. In this publication densely organized cell migration is used to refer to both collective epithelial cell migration and migration of densely organized mesenchymal cells.

Migration of Densely Organized Cells

1 Cell-Removing Methods

Cell-removing methods are frequently referred to as "wound healing" assays because of the damage caused by removing or destroying cells within a defined area of the culture surface. Migration of the cells into this denuded void can be recorded and analyzed under various experimental conditions. Cell removing (and cell excluding techniques) can be made with rectangular or circular voids or nests (see Fig. 3) and then quantified by various methods (see Fig. 4).

Pros: The main advantages of cell-removing assays is their simplicity and ease. Few, if any, modifications are made to the routine culture conditions under which cells are maintained and the experimenter can choose among a variety of removal options ranging from simple mechanical removal to enzymatic detachment. In some instances the damage caused by cell removal is advantageous, since it may simulate a migratory response representative of in vivo processes such as wound healing [12].

Cons: Damage to the cells and the underlying matrix is a significant limitation of cell-removing assays. Generally physical cell removal damages and removes the matrix to which the migrating cells should adhere. Since the extent of damage to cells and matrix cannot be readily assessed its contribution to the migratory behavior is usually unknown. Another disadvantage is that as cells form a dense population they modify the underlying substrate. As these cells are removed from the monolayer the composition of the void into which they migrate will be influenced by 1) the culture surface material (glass or plastic), 2) the matrix protein coated onto this surface prior to cell plating, 3) the deposition, removal, and/or modification of matrix by cells during monolayer formation, and 4) the irregular disruption of the matrix during cell removal. For these reasons cell-removing methods though simple and easy to perform offer little control over underlying matrix conditions.

1.1 Mechanical Removal

Scratch Assay

Expertise: low Throughput: single to 384-well plates

Equipment: cultureware, camera, microscope (CCM)

The scratch assay is by far the most published method discussed in this review (see Table 2). It is well-established, versatile, and easy to perform. The basic scratch assay is implemented by creating a continuous monolayer of cells and then manually scratching away a

portion of the cells with a plastic pipette tip or similar mechanical pin [13]. The cells adjacent to the scratch remain attached and migrate into the void or "wound" which is generally 300 to 900 μm wide. The primary advantage of the scratch assay is compatibility with most lab cultureware and cell culture microscopes. Positioning plates or dishes for imaging is often done manually by making fiducial marks on the bottom of the culture dish. The scratch assay is not restricted to specific culture dishes and can be performed on a variety of plastic and glassware of different sizes. Therefore, the assay is easily adaptable to standard cell culture protocols.

Table 2. Comparison and publications of cell migration assays.

Migration Assay		Defining characteristic	Examples and (references)	Custom substrates		Compatible with variety of culture dishes		Google Scholar search term/s	Publications (2011)
Cell Removing									
	Scratch Assay	scraping	pipette tip, silicone wedge, (4-9)	**no**	scratch disrupts the substrate	**yes**		"scratch assay"	**488**
	Electric Impedance	electric readout of cell adhesion and migration	electric cell-substrate impedance sensing (ECIS), (11-12)	**no**	confluent cells alter the substrate	**no**	requires special plates with electrodes	migration "cell-substrate impedance sensing"	**96**
Miscellaneous									
	Microfluidics	small fluidic channels and chambers	cell trypsinization, cell patterning via capillary force, (13-14, 35-36)	**?**	varies with each device	**no**	requires microfluidic device and equipment	microfluidic "wound healing" "cell migration"	**214**
	Colony Migration	growth of small cell population into collective colony for migration analysis	oil drop assay, collective migration on elastic substrate, (16,34)	**yes**	requires either exposing substrate to atmosphere or to oil drops while cells attach	**yes**		colony expansion "collective migration"	**17**
Cell Blocking									
	Stencils	contact between stencil and substrate relies on auto-adhesion	PDMS membrane, Culture-Inserts by Ibidi, (26-32)	**no**	substrate must be completely dry prior to attaching inserts	**yes**	requires uncoated or dry surface	"collective cell migration" OR "collective migration" PDMS membrane OR stencil / Ibidi culture inserts migration	**121**
	Stoppers	wedging into specific size wells ensures contact of stopper and substrate	Cytoselect™ Wound Healing Inserts, Oris™ Cell migration assay, teflon stoppers, (22-25)	**?**	physical insertion of stoppers may disrupt the substrate	**no**	requires specific dimensions	Oris cell migration / Cytoselect cell migration	**211**
	Barricade Gels	blocking cell adhesion with a dissolvable gel	Radius™ Gel, Oris™ Pro (NA)	**no**	manufacturer determines substrate which must be dryable	**no**	sold in limited variety of plates	"Radius gel" OR "Oris Pro" cell migration	**6**
	MAts	magnetic force maintains contact between stencil and substrate	magnetically attachable stencils, MAts (33)	**yes**	magnetic force attaches MAts without disrupting the substrate	**yes**		n/a published in 2012 (reference 33)	**n/a**

Beside damaging cells and matrix which is a limitation of cell removing methods in general, scratch assays often create irregular voids with jagged edges and occasionally cause cells to pile-up densely alongside the void. Such piled-up cells rapidly expand back to normal density within a few hours. These variables decrease the accuracy of the scratch assay and

confound analysis and interpretation of the results. These complications have motivated many modifications of the assays.

Variations of the Scratch Assay

Variations of the scratch assay generally involve alternative scratch mechanisms and alternative cell patterns. The scratching mechanism can significantly alter the amount of damage to both cells and substrate. Because metal objects readily damage plastic, they are rarely used to make scratches. Plastic pipette tips are the standard tool; however, silicone tips and teflon wedges have been used to reduce damage to cells and substrate. Within these scratch variations rectangular voids are still most common. Drill presses have been used to create circular geometries by gently pressing spinning silicone tips against the cells [14,15]. By placing the silicone tip off-center in the drill press, circular nests can be created [16]. Scratch-making devices may reduce human error and improve reproducibility but are most-often employed in order to achieve high throughput [17,18]. Although each of these variations offers some improvement over the standard scratch assay, the basic strategy is the same, and maintaining a defined substrate is not possible.

Stamp Wound Assay

Expertise: low Throughput: single to 24-well plates

Equipment: CCM, PDMS stamps, and weights

Rather than scraping a silicone tip across a surface, stamp wounds are created by pressing polydimethylsiloxane (PDMS) stamps against a dense cell population using weights. After several minutes the weights and PDMS stamps are removed leaving behind an area of cell debris into which the surrounding cells migrate [19]. By stamping rather than scratching, the matrix generally remains intact as do many parts of the removed cells. Unfortunately

stamping still requires the formation of a monolayer and therefore the underlying matrix may be modified by the occupying cells. This prevents analysis of a clean homogeneous matrix, In specific studies like those involving migration through dead or damaged tissue, the cell debris left after stamping may provide a more relevant environment.

1.2 Electrical Removal of Cells

Electric cell impedance sensing (ECIS)

Expertise: low-medium Throughput: multiwell plates

Equipment: CCM, ECIS plates and control system

Electric cell impedance sensing (ECIS) is an increasingly popular alternative to both traditional scratch and transwell migration assays. ECIS systems measure impedance which results from interactions between cells and an electrode-containing substrate. Changes in impedance occur as cells proliferate, migrate, spread, scatter, and alter cell-to-cell or cell-to-matrix adhesions [20]. This makes ECIS useful in a broad range of studies including epithelial barrier function [21]. ECIS platforms are available in a variety of formats; however, only the application of ECIS to migration is directly relevant to this publication. After establishing a dense cell population over the electrode-containing substrate, which can be coated with matrix proteins, pulses of high voltage are applied to the electrode resulting in electroporation and cell death after several seconds. The result is a a circular void (though other geometries should be possible) over the electrode. As cells migrate and cover the electrode, the impedance changes. With proper calibration this impedance change can be used to indirectly measure cell migration.

ECIS provides several advantages over scratch assays and introduces a few disadvantages. ECIS measurements can be made in real-time without removing cells from a controlled environment such as a cell culture incubator. The void for migration is automatically

created with a pulsating high voltage electric field eliminating human error. Irregularities in cells and substrate may still occur from this process but are much less likely than for scratching or stamping. However, special plates designed for ECIS-readout of scratch assays are also available.

The major disadvantage of ECIS migration studies is the diversity of cell behaviors that change impedance. Changes in adhesion and cell density will alter the impedance. These changes are indistinguishable from changes due to migration. For this reason, the judicious use of controls and microscopic verification of cell migration are necessary to avoid misinterpreting impedance data.

1.3 Chemical Removal

Laminar Flow

Expertise: medium Throughput: varies with microfluidic design

Equipment: CCM, microfluidic systems

Cells are routinely removed by chemical means such as trypsin. Using laminar flow within microfluidic devices can create rectangular voids and nests of cells when chemically removing cells with trypsin or other reagents [22,23]. Laminar flow is the flow of two different solutions side by side without mixing except by diffusion because of the absence of fluid velocity in the direction perpendicular to the flow. It's occurence depends on fluid viscosity and spatial dimensions. In the micrometer dimensions of microfluidic devices, fluids such as water and cell culture medium undergo laminar flow. After flowing cells into a microfluidic channel and allowing them to attach, two or more inputs into the large channel establish the laminar flow of trypsin (or another cell-removing agent) bounded by normal medium. As trypsin degrades cellular attachment proteins the cells detach from a portion of the substrate

and are subsequently flushed away with fresh medium. The remaining cells migrate into the trypsinized area.

In general microfluidics are especially useful for experiments requiring rare or costly reagents because they can utilize small volumes. An additional benefit of chemically removing cells via laminar flow is that the matrix left in the cell-free void is more uniform and predictable than the scratch assay's void.

The major disadvantage is that successful application of microfluidic devices requires expertise. Air bubbles, clumping of cells, and maintaining proper cell culture medium conditions are challenges common to microfluidic cell-based experiments. Fortunately, these challenges have been surmounted by several groups. For example, VanderMeer et al. implemented devices for migration analysis using pumps to exchange and thus maintain proper medium conditions. Alternatively, Nie et al. implemented devices that use passive flow of medium which is driven by gravity, and evaporation and occupy little space in a cell culture incubator [22,23]. The latter devices are attractive options because they are easier to use.

1.4 New, Developing methods of Cell Removal

While organizing existing cell-removal methods, it became apparent that optical and thermal methods for initiating cell migration could be developed. A survey of the scientific literature revealed potential techniques that could be but are not yet applied to the migration of densely organized cells.

Chemical Removal: Alternatives to Laminar Flow

Although chemical removal is routinely achieved with microfluidic devices, it is also possible without them. Peterbauer et al. used a robotic clone selecting system (CellCelector, Aviso, Greiz-Gommla, Germany) to selectively remove small colonies of cells [24]. This ap-

proach should be adaptable to creating voids in densely organized cells. Alternatively, aqueous two-phase systems can pattern proteins or transfect cells with ~400 μm resolution [25]. Adaptation of this approach to selectively remove patterns of cells with trypsin or other chemical reagents should also be possible; however, a more promising approach would be to selectively pattern cells with aqueous two-phase solutions and thereby avoid cell-based substrate alterations (see "Immiscible Solutions").

Thermal wounding

Thermal cell wounding is an undeveloped method, despite the existence of two technologies that could be readily adapted for creating voids in densely organized cells. First, electrical current flowing through a thermoresistive material embedded on a culture surface could be used to wound a portion of the cells. Existing ECIS systems already provide the needed electronics to controllably heat such thermoresistive strips. Although cells may not be removed by thermal damage, the subsequent migration of cells into the lifeless void may be very informative for studies of burn healing. The expertise and requirements for such a thermal cell "removing" migration assay would be very similar to those of ECIS. The second technology capable of thermal wounding cell populations is the heating of small volumes using infrared laser light [26]. By scanning such a laser across a cell-coated dish countless patterns could be created for cell migration. Both techniques could be utilized to heat and wound small areas and possibly induce heat shock without ablating cells or causing apoptosis. The ability to modify existing ECIS systems to study migration or heat response make such thermal wounding systems an attractive candidate for future development.

Optical Removal via Laser Ablation

Ultraviolet lasers are routinely used to perform microsurgery. These lasers successfully ablate cell monolayers in vitro [27] and in vivo in the drosophila embryo [28]. This laser ablation is significantly different from thermal wounding with infrared lasers because it relies on the brief formation of a plasma and cavitation bubbles to destroy individual cells [29]. Though already employed for cell migration and cell tension studies, the cost and maintenance of sophisticated lasers and optics currently prevent wide adoption. However, improvements in on-chip lasers and optics as found in micro-total analysis systems (μTAS) may enable wide adoption in the future.

2 Cell Excluding Methods

The alternative to removing cells from an area is to exclude them from settling into an area. The past two decades have introduced a variety of novel techniques for cell exclusion ranging from elastomeric solid barriers to laminar flow in microfluidic devices. Like cell removing methods, methods for excluding cells also employ rectangular or cylindrical nests and voids (see Fig. 3). The resulting images are also quantified with the same approaches used for cell removing methods (see Fig. 4).

Pros: Cell excluding methods have significant advantages over cell removing methods and will undoubtedly prove beneficial to our understanding of the role and effect of the environment of cells. The most significant advantage of excluding cells is that the matrix in the void is not altered directly by the cells because they are not allowed to cover the void until migration is initiated. Another important advantage is that certain methods can accommodate additional matrix complexity such as pliable surfaces, protein patterns and even textured surfaces.

Cons: The primary disadvantage of cell exclusion methods is the additional components required to exclude cells as they adhere and form dense populations. A disadvantage of certain cell excluding assays is that the barrier may leave residues on the matrix or in solution which may alter cell behavior.

2.1 Solid Barriers

The earliest documented method for excluding cells is the solid barrier. Originally, solid barriers were fabricated from nickel or stainless steel and could only exclude cells during adhesion [30]. Modern solid barriers are fabricated from elastomers and are able to prevent cell protrusion and migration until the barrier is removed [31]. These barriers are forcefully held against the bottom of a culture dish in order to successfully seal against the matrix, prevent cell protrusions, and protect the condition of the matrix. The original metal stencils relied on gravity to maintain contact and remain immobile on the culture surface. Current barrier strategies are held in place with forces generated from wedging, autoadhesion, or magnetism rather than relying upon gravity.

Wedging, Stoppers

Expertise: low Throughput: low-high

Equipment: CCM, specific cultureware, and stoppers

Stoppers utilize friction and compression to wedge into a dish and press against the bottom of the dish. This wedging provides the force needed to seal against the substrate on the bottom of the dish. For this reason stoppers are large (even when the void created is small ~1.5 mm). Because they must wedge against the walls of a culture dish, they can function only in the specific dishes for which they were designed. They can be solid or hollow in the center [31,32].

The main advantage of stoppers is that they can be sealed against wet, protein-coated surfaces in order to study the effect of matrix conditions on cell migration [31,33,34]. However, excessive force while inserting the stopper can disrupt matrix proteins coated onto the culture surface. To avoid this problem, preinserted stoppers can be purchased in protein-coated plates. Alternatively, the risk of matrix disruption can be minimized to a small perimeter using stoppers with a hollow center [31,33].

Regardless of being hollow or solid in the center, the main weakness of stoppers is the need to insert them into the well which must be done manually for custom-made substrates. Excessive force during insertion can disrupt matrix proteins and insufficient force will result in an incomplete seal allowing cells to enter into the void prior to the start of the migration assay.

Adhesion, Stencils

Expertise: low Throughput: low-medium

Equipment: CCM, Stencils

Most modern stencils rely on autoadhesion rather than gravity. Autoadhesion provides a tight seal against the matrix but limits the application to hydrophobic materials and in a few cases to dry matrix proteins. Rudimentary stencils have been cut out of Parafilm [35]. High precision stencils are made using microfabrication techniques from PDMS [36,37] or parylene-c [38]. Though most stencils are thin membranes less than 200 μm in height, some are large such as Ibidi's Culture Inserts, 5 mm tall [39]. Stencils can also be made from a hybrid of rigid and conformal materials [40,41].

Regardless of height or composition, a major advantage of stencils is their similarity to the scratch assay. The expertise and hardware for stencil assays is nearly identical to the scratch assay.

The main weakness of stencils is that autoadhesion requires a dry, generally clean. hydrophobic surface. Autoadhesion to wet protein-coated substrates is not possible and in many situations stencils placed on dry hydrophilic surfaces fail to successfully prevent cells from protruding into the void.

Magnetic Attraction, Magnetically Attachable Stencils (MAts)

Expertise: low Throughput: low-high

Equipment: CCM, MAts, and magnets

Magnetically Attachable Stencils (MAts) are fabricated from PDMS and magnetite. These stencils seal against a wide variety of substrates via magnetic attraction to magnets placed underneath the culture dish. Although they can be produced in various geometries, the most commonly used MAts are star-shaped with four arms that are 7 mm in length and 5 mm tall. Because MAts are attracted to magnets placed under the substrate, they seal successfully on wet, protein-coated surfaces, elastic polyacrylamide substrates, and polycaprolactone nanofibers (Nanofiber Solutions).

The highly controlled magnetic force minimizes user damage to the matrix and also improves reproducibility between experiments. By positioning MAts manually a few millimeters above the bottom of a dish containing several millimeters of solution and then releasing the MAts, the impact of the MAts on the matrix becomes more dependent upon the magnetic force than the user. This eliminates the risk of the user damaging the substrate during MAts attachment. Another advantage of magnetic force is it can be customized to achieve similar compression on substrates of varying elasticity.

The disadvantage of MAts, which is shared by stencils and stoppers, is their manual removal. Like stencils and stoppers, careless MAt removal can damage cells or substrates, or possibly both. However, with proper care MAts successfully pattern densely organized cells

while protecting the underlying matrix. The matrix can have various conditions ranging from coated to uncoated, oriented to randomly oriented, and stiff to soft (see Table 1).

2.2 Gel Barriers

Degradable gel droplets

Expertise: low Throughput: 24- to 384-well plates

Equipment: CCM, gel-containing plates

Rather than placing and removing a solid barrier on a substrate, gels can be used to prevent cell adhesion to a defined area. Gels are printed onto the center of multiwell plates and dried or polymerized prior to adding cells. After cells have adhered the gel is dissolved allowing migration into the void. These gels are currently proprietary technologies available as the Oris™Pro and Radius™ cell migration assays. Two strategies have been taken to dissolving gel barriers. One is to create gels which automatically dissolve in solution after a certain amount of time. This enables an assay to be setup and left in an automated analyzer; however, the disadvantage is that the edges of the gel which are thinner dissolve sooner resulting in irregularities along cell boundaries. Alternatively, a dissolving reagent can be used to initiate the dissolution of the gel. If done after cells are well adhered, this dissolution technique results in crisper cell boundaries at the initial time-point [32].

The advantage gels over solid barriers is that the gel dissolves without any manual manipulation other than adding solutions. This eliminates the human error inherent in the removal of stencils, stoppers, and MAts.

The disadvantage of gels revolves around application of the gel before it polymerizes. This is currently done commercially with proprietary systems on 24, 96, and 384-well plates which are sold uncoated or collagen-coated. Other proteins and possibly custom-made

matrices may be available upon request. In any case the matrix proteins have to be dried limiting the ability to investigate various cell-matrix interactions.

2.3 Liquid Barriers

Similar to gels, liquid barriers ensure that substrate conditions remain unchanged by physical damage from solid objects while excluding cells and preventing cell alteration of the substrate. Considering the advantages of liquid barriers, their limited use is surprising and may reflect lack of awareness of the technique or concerns of affecting migration with the additional reagents required to create two-phase solutions. We anticipate increased use of liquid barriers in migration assays as two-phase aqueous systems are adapted to cell patterning and as microfluidics become more commonplace.

Immiscible Solutions

Expertise: low-med Throughput: low-high

Equipment: CCM, immiscible solutions

Liquids can function as barriers to cells. By placing cells in one part of an immiscible or two-phase solution, cells can be patterned as they adhere to a substrate. Immiscible solutions such as mineral oil and cell culture medium can create 2-3 mm diameter cell colonies [42]. However, better resolution is achievable. Tavana et al. recently used aqueous two-phase system consisting of polyethylene glycol and dextran solutions to pattern droplets ranging from 400 to 1400 μm diameter for substrate coating and cell transfection. With this system complex patterns can be created by dispensing a stream of dextran solution from a moving tip [25]. Adapting this approach to the patterning of cells should enable sub-millimeter features ranging from simple droplets to complex printed patterns on even softest of substrates and can likely be applied repeatedly to pattern multiple protein and cell containing solutions.

The major advantage of these techniques is that with proper care cells can be patterned on delicate matrices that would readily be altered by solid objects such as soft collagen gels.

The main disadvantage is the requirement of using solutions uncommon to cell culture which may affect cell behavior and migration or possibly alter matrix conditions. Further research is needed to verify or dismiss the possibility of such effects.

Laminar Flow in Microfluidics

Expertise: medium Throughput: varies with microfluidic design

Equipment: CCM, microfluidic systems

Because of the small dimensions of microfluidic devices, laminar flow can be achieved with various solutions such as cell culture medium. This has enabled chemical removal of cells as addressed earlier, patterning of protein gradients [43], and patterning of cells for migration [44]. Utilizing liquids to pattern cells removes risks of substrate damage that is inherent with solid barriers.

However, microfluidic flow provides additional advantages. Medium conditions can be controlled dynamically to deliver treatments or used to maintain very stable conditions regardless of cell metabolism. Gradients in solution can be created and maintained, a feature that is important for many studies such as chemotaxis.

A disadvantage unique to excluding cells using laminar flow is that as cells adhere there is no surface tension or physical force to prevent cells from immediately migrating into the void after they adhere.

2.4 Air Interface as a Barrier

Droplets

Expertise: low Throughput: low-med

Equipment: CCM

One of the simplest approaches to patterning cells in liquid is to add droplets of cells to a dry substrate. Essentially the air interface acts as a barrier because of the surface tension of the medium. After cells in droplets have begun to adhere (30-60 minutes), medium is added to re-immerse the dry surface surrounding the droplet preventing evaporation or exhaustion of the limited nutrients within the droplet, and subsequent cell death.

Key advantages of using droplets are that they do not require novel tools and cells can easily be patterned on delicate materials. Though cell patterning achieved in this way is highly variable, the approach has enabled analysis of cells migrating collectively on soft elastic polyacrylamide gels [45]. This represents one of the first investigations of collective cell migration on materials capable of recreating soft tissues such as breast.

The major disadvantages of this approach are that the cells used must be capable of adhering in a short period of time, the matrix outside the cell-occupied zone must be dried temporarily, and the cell patterns achieved are variable.

Microfluidics

Expertise: medium Throughput: varies with microfluidic design

Equipment: CCM, microfluidic systems

Surface tension at the liquid air interface can also be used to create precise patterns of cells inside microfluidic devices. Generally, a large, main channel bordered by several small channels is filled with cells. Liquid does not enter the small channels because of surface tension. After the cells have adhered, migration is initiated by applying sufficient vac-

uum to the small channels to overcome the surface tension and fill them with culture medium [46].

This approach has multiple advantages. The cell patterns are precise and reproducible. The substrate remains untouched until migration is initiated. Cells have ample time to adhere and form stable monolayers because culture medium can be replenished without initiating migration.

The disadvantages of the approach are that the matrix must be temporarily dried while cells adhere and unlike droplets microfluidic devices are not currently compatible with elastic surfaces such as polyacrylamide.

2.5 New, Developing Methods for Excluding Cells

Electric Fields. ECIS migration assays rely on the removal of cells by brief, pulsed, intense electric fields that electroporate and disrupt cell monolayers. However, it may be possible to exclude cells from the void with a pulsating electric field, referred to as an "electric fence", during the adhesion and growth of cells. Turning off the fence initiates migration into the void which can be measured by changes in impedance [47].

There are three advantages of the "electric fence" approach. First, it can be implemented using existing ECIS dishes and controllers. Second, the matrix does not have to be dried. Third, the matrix in the void is not modified by physical contact with solids, gels, or cells.

The main disadvantage is the unknown effect of oscillating electric fields on nearby cells, substrate, and possibly cell culture medium. However, protein coatings are expected to remain intact in the presence of the electric fence enabling densely organized cell migration onto custom, protein-coated substrates [47].

Magnetic Particles

Various magnetic beads are routinely used to manipulate cells and perform magnetic based separations. Two technologies exist that could be implemented for cell migration assays. First, cells in solution can be patterned by exposure to cationic liposomes containing magnetite followed by application of static magnetic fields [48-50]. The second technology consists of, dynamic magnetic manipulators currently used in making force measurements on individual cells [51,52]. Both technologies could potentially enable magnetic particle-based cell patterning for cell migration assays.

Optical Traps

Since the introduction of optical traps for manipulating viruses and cells in 1987 [53], traps have found diverse applications ranging from subcellular and molecular manipulation to label-free discrimination of cancerous and non-cancerous cells [54,55]. State-of-the-art holographic optical tweezers enable dynamic control of the shape and position of large traps or numerous small tweezers simultaneously. Such capabilities can exclude and sort cells in real-time [56] and should allow cell exclusion from a defined region during adhesion. This would enable analysis of both single and densely organized cell migration on a variety of substrates including extremely soft materials. Another important application of optical traps will be to dynamically manipulate and probe cells while they migrate.

3 Geometry

Densely organized cells can be arranged to migrate towards one another or away from one another by creating voids or nests of cells, respectively. Various shapes can also be created though generally only rectangles and circles are employed as shown in Fig. 3. Understanding the differences between geometries is important to choosing and properly executing

migration assays. Theoretically, the migration between void and nest geometries will be identical for rectangular geometries when experimental conditions and times are carefully selected to avoid increased or decreased migration due to contact inhibition as a void closes or cell density changes as a nest expands. For the circular geometry, voids and nests behave differently because migration causes the perimeter, and thus the cell density at the perimeter, to shrink or grow respectively.

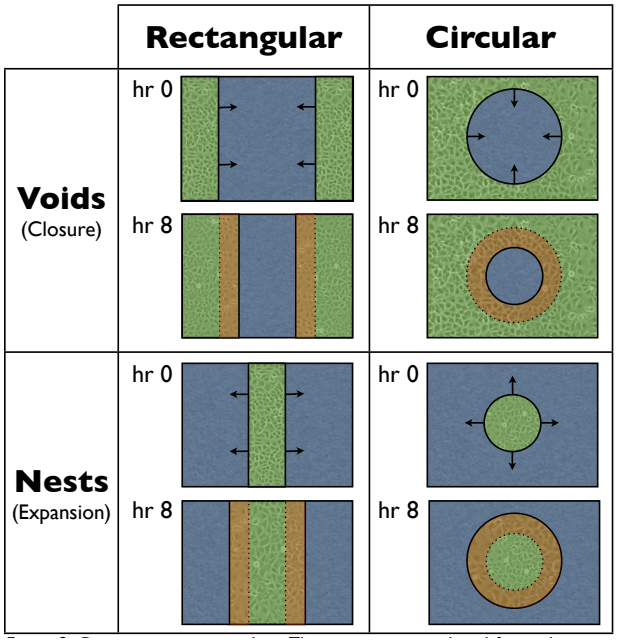

Figure 3. Common geometries of cell migration assays. The geometries employed for analyzing in vitro two-dimensional migration of densely organized cells are classified by direction of migration or by shape. Generally cell migration is measured as an inward closure of a void or outward expansion of a nest of cells. Both voids and nests can be created with rectangular and circular shapes. However, average migration rates are generally only calculated from rectangles.

3.1 Voids

Voids are often created in large dense cell populations in order to measure migration. Generally culture surfaces are completely covered with cells except for the void. In this situa-

tion a large number of cells must be nourished by a limited volume of medium. As a result migration can be affected by changes in medium condition. Furthermore, time points must be selected carefully for each cell type in order to minimize variations in migration rate that occur as voids begin to close and cells undergo contact inhibition of migration.

Rectangular Voids

Traditional scratch assays create rectangular voids. Many other assays also use this geometry. The width of the void is generally less than 900 μm, and lengths may range from a few millimeters to a few centimeters. Acquisition of rectangular voids should include both sides of the void and employ fiducial marks or another positioning scheme. Alternatively time-lapse microscopy and automated microscope stages can be used to ensure proper positioning throughout all time points. This is necessary for precise quantitation of migration rates or percent closure,. Fortunately, the rectangular geometry is forgiving of minor misalignment as long as both sides of the void remain completely visible in the image.

Circular Voids

Circular voids are popular in high-throughput formats where space is limited and often the entire culture surface is imaged. In some situations acquisition is possible for only partial images of the void and very precise alignment must be achieved using automated live-cell microscope systems or fiducial marks combined with image registration. Circular voids are quantified almost exclusively by percent closure because converting circular closure to a linear migration rate is mathematically complex and the migration rate itself is altered by the quadratic decrease in the area of the void as cells migrate inward. In some instances cells capable of rapidly closing a rectangular void may be seriously retarded when closing a circular void. Though this is most often considered a disadvantage, in some situations, this retar-

dation may be beneficial by providing extra time to compare control and experimental groups.

3.2 Nests

Nest assays overcome the spatial hindrance that retards migration cells as they fill voids. Nests are dense populations of cells that migrate away from each other into a large open space. Nests use fewer cells for a given volume which can be beneficial when working with highly metabolic cell types but may result in dilution of factors that stimulate migration. Like voids, nest migration rates may also decrease in migration after a period of normal migration. The cause of such retardation is primarily because the cell density decreases rapidly as the nest empties into the surrounding area. By judiciously selecting the time frame and conditions for migration, these differences can be minimized.

Rectangular Nests

With proper care for medium conditions and time points, the migration of rectangular nests is theoretically identical to rectangular voids. In fact, if two or more rectangular nests are created side by side, one or more rectangular voids will be created between them. For many of the stencil assays such patterns are purposefully created and migration can be viewed as a rectangular void or nest. Like voids, images generally contain both sides of a nest in order to reduce the need for precise horizontal alignment.

Circular Nests

Unlike rectangular geometries, circular voids and circular nests will behave differently despite giving careful consideration to medium conditions and time points. This difference occurs because circular nests experience a quadratic increase in available surface area as they

migrate outward whereas the area for circular voids decreases as cells migrate inward. Like circular voids, circular nests should be imaged in their entirety if possible. This eliminates the need for precise image alignment. An advantage of circular nests is their resemblance to the migration of cells away from a dense population such as a tumor.

4. Quantification

Equally important to the execution of cell migration experiments is the quantitative analysis of the resulting data. Generally, a couple pictures or time series of pictures are taken

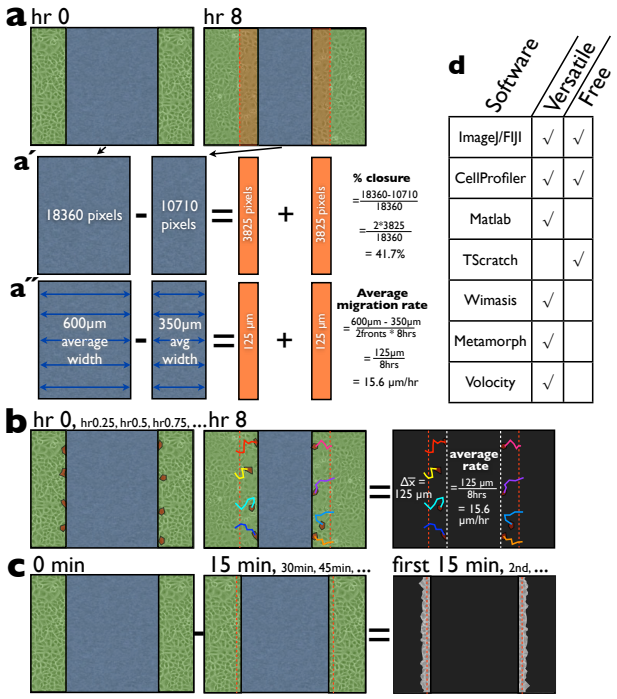

Figure 4. Methods for quantifying migration data. **(a)** Cell covered areas are determined from corresponding images of initial and final timepoints. **(a´)** The open area for each is calculated precisely or **(a´´)** the open average width is estimated by measuring lengths of 5 lines. The percent closure or average migration rate are calculated from the values. **(b)** Individual cells are tracked through all timepoints. The distance traveled is averaged and used to calculate average migration rate. **(c)** By substracting the current image and following image a movie is created showing movement of cells both migrating into the void and mobilizing behind the initial cell boundary (red line). **(d)** Commonly used commercial and free software for migration analysis.

and subsequently analyzed to determine widths between cells, migration rates, and/or percent closure. The two simplest analyses consist of determining the open area and the average width of the void. Though such analyses are suitable for answering many biological questions, much more information can be obtained by tracking cells or performing image-based calculations on a time series.

4.1 Area Analysis

The simplest and probably most common method of analyzing densely organized cell migration is to compare the void area of images from two time-points (Fig. 4a). This can be done by counting pixels uncovered by cells for both time-points and then calculating the percent closure (Fig. 4a´). For rectangular geometries this percent closure can be converted to average migration rate if the actual width of the image is known. Alternatively, average widths between cells can be obtained by measuring multiple horizontal lines (Fig. 4a˝). From these widths the average migration rate or percent wound closure can be calculated which both represent the average productive movement into the void. The authors prefer average migration rate because percent closure varies depending on the initial size of the void.

For area analysis, TScratch stands out among the software platforms known by the authors (Fig. 4d). TScratch focuses on cell migration assays such as the scratch assay and therefor lacks the versatility of other softwares. However, it can successfully distinguish between cells and background artifacts and provides a graphical user interface to facilitate user manipulation of void areas as needed [57]. Alternatively, various standalone software as well as packages/algorithms for ImageJ [58], Cell Profiler [59], and Matlab (Mathworks) are readily available.

4.2 Individual Tracking

In order to obtain more information about the migratory behavior of individual cells at the periphery and within the population, time series images can be used to track individual cells (Fig. 4b). After creating x,y coordinates of the cell tracks, a variety of parameters. such as turn angle, persistence, velocity, and displacement can be extrapolated. To facilitate the extraction of such parameters and to minimize the possibility of human error, an open-source, peer-reviewed software package called Cell_motility was created by Martens et al. [60]. Comparing behavior of cells at various distances from the periphery will provide insight into how and when cells in a dense population are mobilized.

4.3 Image Calculations

To better understand how cells at the periphery and within a dense population migrate and change, various image-based calculations have been implemented as alternatives to individual cell tracking. By calculating pixel by pixel the difference between phase contrast images separated by 15 minute increments, Matsubayashi, Razzell, and Martin visualized and quantified the mobilization of periphery cells and cells within the population with a growing "white wave" (Fig. 4c) [61]. Similarly, Poujade et al. applied particle image velocimetry to phase contrast time-lapse images of cell monolayers and created velocity fields showing complex motions among cells within the population and at the periphery [37]. Automated image calculations can provide quantification of additional parameters such as the shape of both individual cells and the migratory front, proliferation rates, and cell turning [62,63]. These calculations provide insight into the behavior of cells throughout the population not just at the periphery and enable visualization of otherwise unnoticeable phenomenon.

5. Assay Selection

Deciding on the migration assay that is most suitable for a specific experimental objective can be challenging. A decision diagram has been included (Fig. 5) to facilitate this process. The decisions are based on the primary research objective, cell density, the analytical requirements, cost and available expertise. Although the suitability of any assay must be confirmed empirically, Fig. 5 provides an overview of possible approaches suitable for specific research objectives. In all instances selection of the specific assay will involve balancing the complexity of the scientific question and the analytic requirements with the time, cost and resources available to the investigator.

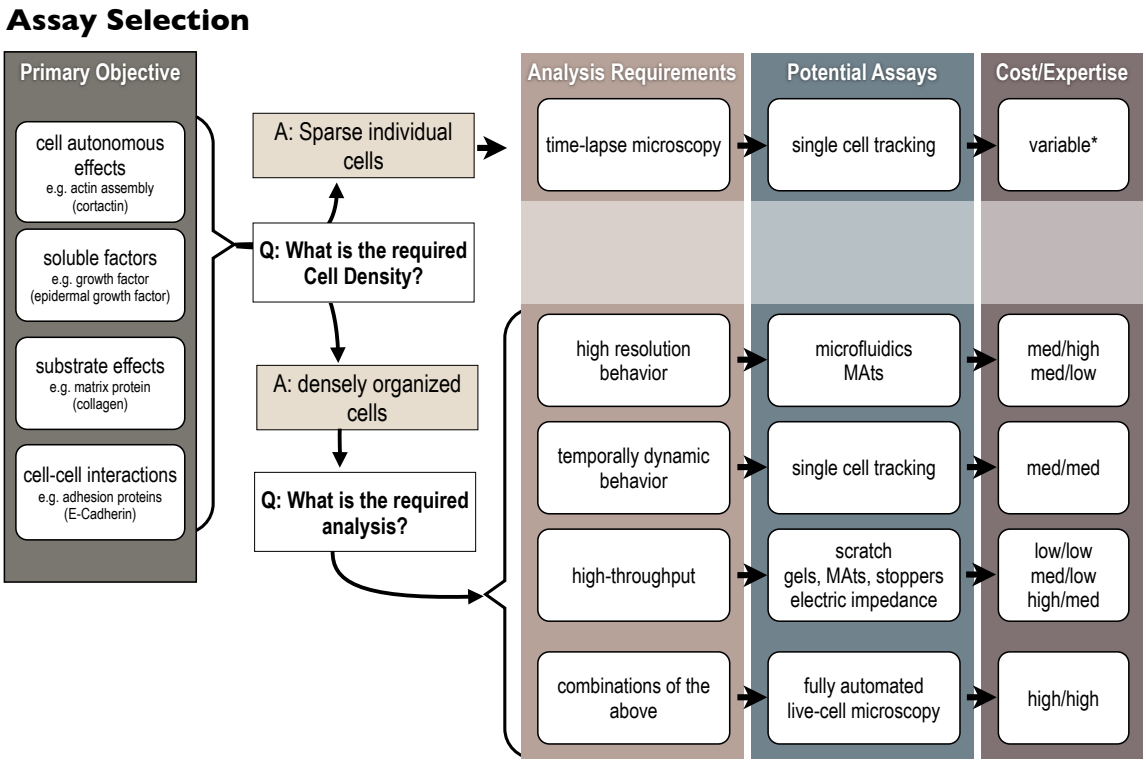

Figure 5. Assay selection. The first step in assay selection is to consider the study's research objective ("Primary Objective"). Once the research objective is defined, the cell density at which migration is analyzed must be determined. Selecting the analytical parameters ("Analysis Requirements") guide the final selection of an assay ("Potential Assays") most appropriate for the research objective. Frequently there are several options that are appropriate and the final choice is determined by the available resources and expertise ("Cost/Expertise").

Conclusions

Migration assays have been and will continue to be important tools in our investigation of the mechanisms that control both normal biology and pathology. The implementation and diversity of methods for analyzing cell migration have increased dramatically over the past two decades. In vitro 2D densely organized cell migration assays often require less equipment and are generally simpler to analyze and quantify than single cell migration assays. Recent technological advances enable unprecedented 2D migration studies of densely populated cells on a variety of substrates ranging from custom-coated tissue culture plastics to pliable hydrogels and microfabricated surfaces. Such assays are able to integrate multiple aspects of the four broad factors influencing migration: 1) cell autonomous properties, 2) soluble factors, 3) matrix properties, 4) cell-to-cell interactions (Fig. 2). This level of control and integration enables more relevant in vitro investigation of development, disease, and other biological processes that depend on cell migration.

Of the currently available densely organized cell migration assays, several demonstrate unique strengths. ECIS is unsurpassed in ability to perform nearly real-time acquisition. To achieve similar time-lapse results with other assays would require live-cell microscopy systems capable of observing multiple wells in parallel. The scratch assay remains unrivaled in cost since it can be performed with standard equipment already available in labs performing cell culture. However, as cell excluding methods, such as stencils, stoppers, MAts, and gels, become more common, their costs will decrease making them more and more competitive. Of the cell excluding methods, the simplest and most versatile is the magnetically attachable stencil, MAts. Any dish under which a magnet can be placed can be used with MAts and magnetic force can be customized to accommodate soft and stiff substrates.

Analyzing the fundamental mode of operation of existing assays reveals undeveloped methods with promise. Though thermal wounding has been performed on animals to

better understand healing of burns, the technique has not been applied in vitro to the migration of cells. Such studies could provide insights into burn healing and also to other heat-related conditions. Another promising method for studying cell migration is the application of two phase aqueous solutions to form sub-millimeter diameter droplets or patterns of cells and proteins. Because contact between a solid material and substrate is completely avoided, two-phase aqueous solutions are an attractive approach to patterning cells on very delicate substrates. In terms of control and ability to manipulate cells and even molecules during migration, the capabilities of holographic optical tweezers are unrivaled. Implementation of the above techniques for cell migration studies promise to provide significant, unique insights into the behavior of individual and densely organized cells. Furthermore, such studies are expected to reveal ways to improve the relevance of 2D migration assays to in vivo cell migration.

By analyzing existing assays and areas for future assay development, this review illuminates the unique qualities of individual assays and provides the necessary context for readily understanding the strengths and weaknesses of individual assays. Though the specific assays included in this review will evolve over time, the organization of their fundamental modes of operation provides a context that will remain important to understanding 2D cell migration assays far into the future.

Acknowledgements

We thank the many authors in the field of cell migration whose work made this review possible and apologize to those authors not referenced for our limitations and oversights. We thank Elias Horn of Ibidi GmbH for sharing his expertise in cell-based assays by reviewing the pre-submission manuscript; John Wikswo of the Vanderbilt Institute for Integrative Biological Research and Education for initial motivation to begin writing this review;

and Trenis Palmer, a member of the Zijlstra lab and graduate student of the Department of Pathology, Microbiology, & Immunology at Vanderbilt University for insightful discussions on the broad categories of factors influencing migration. Andries Zijlstra and William Ashby were supported by R01 CA143081 and P01 CA040035.

CHAPTER III

MAGNETICALLY ATTACHABLE STENCILS AND THE NON-DESTRUCTIVE ANALYSIS OF THE CONTRIBUTION MADE BY THE UNDERLYING MATRIX TO CELL MIGRATION

Summary

Cell migration is controlled by the integration of numerous distinct components. Consequently, the analysis of cell migration is advancing towards comprehensive, multifaceted in vitro models. To accurately evaluate the contribution of an underlying substrate to cell motility in complex cellular environments we developed a migration assay using magnetically attachable stencils (MAts). When attached to a culture surface, MAts create a defined void in the cell monolayer without disrupting the cells or damaging the underlying substrate. Quantitative analysis of migration into this void reveals the substrate's contribution to migration. The magnetically-guided placement of a microfabricated stencil allows for full experimental control of the substrate on which migration is analyzed. MAts enable the evaluation of intact, defined matrix, and make it possible to analyze migration on unique surfaces such as micropatterned proteins, nano-textured surfaces, and pliable hydrogels. These studies also revealed that mechanical disruption, including the damage that occurs during scratch assays, diminishes migration and confounds the analysis of individual cell behavior. Analysis of migration on increasingly complex biomaterials reveals that the contribution of the underlying matrix depends not only on its molecular composition but also its organization and the context in which it is presented.

---

*This chapter was published as W. J. Ashby, J. P. Wikswo, and A. Zijlstra, "Magnetically attachable stencils and the non-destructive analysis of the contribution made by the underlying matrix to cell migration.," Biomaterials, vol. 33, no. 33, pp. 8189–8203, Nov. 2012.

Introduction

Cell migration is a multifactorial process controlled by many different molecular components that can be parsed into four distinct categories: 1) cell autonomous characteristics, including the genetic and epigenetic regulation of cell signaling molecules; 2) cell-matrix adhesion, including its regulation by the matrix composition and elasticity; 3) cell-to-cell interactions through the formation of cell-cell adhesions; and 4) soluble communication through factors such as small molecules, cellular metabolites, and secreted proteins (Fig. 6a and Fig. 2) [10,11]. The spatial and temporal integration of these fundamentally different elements determines the successful initiation, progression, and eventual completion of cell migration.

Because migration is the product of a multifactorial integration of many different mechanisms, the specific contribution of any single factor can only be studied within the context of the other participating components. The migratory response to a soluble cytokine, for example, can be augmented by the presence of mature cell-cell adhesions or the composition of the matrix to which the cells adhere. Although migration in vitro is frequently done with isolated cells, migration in vivo occurs within the context of a physical tissue architecture and densely organized cellular populations [64]. In vivo single cells rarely have the opportunity to migrate alone across a cell-free expanse of matrix because both the neighboring cells and the surrounding matrix inhibit motility. In vitro recreation of these in vivo conditions is challenging because existing assays do not enable investigators to control matrix conditions while analyzing migration of dense cell populations [65].

Traditional scratch assays disrupt the matrix, and the accurate patterning of cells on fragile, bioactive substrates is technically challenging and does not accommodate many existing experimental strategies. Therefore, depending on the importance of cell-matrix interactions versus cell-cell contact, in vitro cell migration studies have generally been divided into

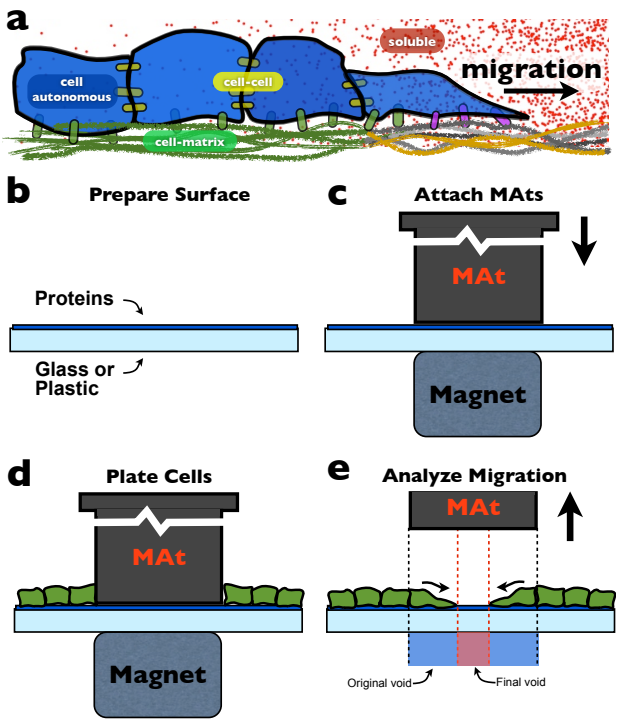

f

In Vitro Migration		Cell Autonomous	Soluble	Cell-cell Interactions		Matrix Composition		
Method	Assay			absent (single cell)	present (dense cells)	proteins	oriented	elastic
Single Cell	Migration	√	√	√	x	√	√	√
Wound Healing	Scratch	√	√	x	√	x	x	x
Space Filling	MAt	√	√	x	√	√	√	√

Figure 6. Role of matrix in cell migration and its protection using MAts. **(a)** A schematic depiction of the elements that contribute to cell migration: Cell migration in tissues is determined by the integration of cell autonomous ability, soluble communication, cell-cell adhesion and matrix interaction. The presentation of a new or modified substrate and the acquisition of new matrix adhesive properties (lower right) have a powerful influence on cell migration. (b-e) Schematic depiction of the MAt assay: **(b)** The culture surface, such as tissue culture plastic or glass, is coated with relevant protein. **(c)** A magnet is placed underneath the culture surface and a MAt is subsequently attached. The magnet not only secures the MAt to the surface, it also provides sufficient force to seal the stencil on wet, protein-coated surfaces without disrupting the underlying substrate. **(d)** Cells are plated around the MAt. **(e)** The MAt is removed, thereby creating a void adjacent to the cells, and cell migration into the void is analyzed by comparing pictures between initial and final time-points. **(f)** Comparison of the MAt assay with scratch and single cell migration assays in their ability to address the four elements that contribute to migration.

two distinct approaches: 1) the analysis of single cells on intact matrix and 2) the analysis of densely organized cells engaged in cell-cell contact on a wounded or modified monolayer

(Fig. 6f). A few exceptions to this general dichotomy are scatter assays [66], the dispersal of confluent populations from droplets [42,45], and the analysis of collective cell migration using electrically controllable substrates [67].

In order to overcome these limitations and study the permissive or non-permissive nature of the underlying substrate during migration, we created a non-destructive space-filling assay using magnetically attachable stencils (MAts). MAts are attached magnetically to a culture surface and kept in place during cell culture. The migration assay is initiated by removing the MAt to create a void into which the cells migrate (Fig. 6b-e & Video C1). The rate at which cells migrate into the void is the product of the composition of the substrate in the void, cell autonomous properties, soluble factors, and cell-cell interactions. MAts provide the ability to accurately and non-destructively pattern cells on a wide variety of substrates, including culture surfaces coated with matrix proteins, micropatterned and nanofabricated surfaces, pliable gels (Fig. 6f). In this way MAts integrate both cell-matrix and cell-cell interactions at high density and enable the investigator to determine the contribution of the underlying matrix to cell migration.

Materials and Methods

The following materials and methods were used unless specifically stated otherwise in the text.

Materials

Rare-earth (NdFeB) magnets were obtained from K&J Magnetics. The 1/4″x1/8″x1/8″ grade N42 magnets (B422) were used to attach MAts to t.c. plastic dishes. Polyacrylamide gels used identical magnets for stiff gels and 1/4″x1/8″x1/16″ grade N42 magnets (B421) for soft gels. Standard MAts were cast in brass molds using polydimethylsiloxane (PDMS,

Sylgard 184, Dow Corning) mixed with magnetite (~2μm particle size, Pirox 200HP, Pittsburgh Iron Oxides LLC) at a 2:1 ratio by weight, homogenized in an AR-100 mixer (Thinky), and cured at 60ºC in an oven. Glass and t.c. plastic substrates, specifically 6- and 12-well plates (Costar 3516 and 3513, Corning) were coated with collagen (rat tail type I, 354249, BD Biosciences), human plasma fibronectin, murine laminin (L2020, Sigma), poly-D-lysine (P7280, Sigma), and FITC gelatin (G13187, Fisher). Collagen refers to collagen type I isolated from rat tails unless stated otherwise. Alexa fluor 555-conjugated bovine serum albumin (A555-BSA, A34786, Invitrogen) and fraction V BSA (A8412, Sigma) were used for blocking substrates. DME medium (11965, Gibco), Roswell Park Memorial Institute 1640 medium (RPMI, 21870, Gibco), Optimem (31985, Gibco) were used with cells. Polyacrylamide (PAA) substrates were made using acrylamide (40%, 161-0140, BioRad), bis-acrylamide (2%, 161-0142, BioRad), ammonium persulfate (248614, Sigma), and TEMED (161-0800, BioRad) on 22 mm diameter #1.5 glass coverslips (Electron Microscopy Services). Gelatin (G1890, Sigma) and collagen (rat tail type I, 354249, BD Biosciences) were conjugated to polyacrylamide surfaces by activating N-Sulfosuccinimidyl-6-(4'-azido-2'-nitrophenylamino) hexanoate (sulfo-SANPAH, 22589, Thermo Scientific) with black light blue UV bulbs (~340 nm) 3-4 inches from the PAA surface in a UV Stratalinker 2400 (Stratagene). Solidworks (Dassault Systems) and GibbsCAM (Gibbs and Associates) software was used in the design and fabrication of MAt molds for computer-numeric-control (CNC) milling. Images were calibrated to achieve actual distances using a micro-ruler (1 mm total length, 100 x 10 μm divisions, Graticules, Ltd., Tonbridge England). Nanofiber substrates came from Nanofiber Solutions LLC.

Cell Culture

Cell cultures of human head and neck carcinoma HEp3, human lung carcinoma A549 cell lines, murine brain endothelial cells bEnd.3, and primary murine mammary carcinoma cells (MMC) were cultured in DME medium, RPMI, DME medium and according to the procedures of Ramirez et al. [68] DMEM and RPMI were supplemented with penn/strep, HEPES buffer, non-essential amino acids, and 10% fetal bovine serum. Cells were cultured at 37ºC in a humidified 5% CO_2 incubator and passaged every 2-4 days.

Mold Production

Brass molds were constructed in two layers in order to ensure a smooth contact surface free of tool marks that also transitions sharply without any curvature at the bottom edge. The bottom layer consists of a 3˝ x 3˝ x 0.25˝ piece of brass, with a 3 by 3 array of bolt holes surrounded by 2 reamed holes on each side that was later pressure-fitted with steel dowels serving as guide pins for the brass cubes. The top layer was made of an outer frame and a 3 by 3 array of 0.5˝ x 0.5˝ x 0.25˝ cubes of brass with rounded corners (3/32˝ diameter), a 5º taper all around, a central threaded hole, and two holes to each side for the guide pins. After grinding and polishing the base to a mirror finish, dowels were pressed into the base. Then the brass cubes were inserted over the dowels and individually fastened into place with screws (Fig. C4a). MAts were cast in the void between the cubes, resulting in a 2 by 2 array of connected MAts (Fig. C4b-d). Molds for larger arrays are under development and will utilize a replaceable mirror-finish plastic sheet sandwiched between the base and brass cubes.

Preparing and Sterilizing MAts

MAts were fabricated according to the following steps. Polydimethylsiloxane prepolymer was made by mixing 10 parts base to 1 part curing agent by weight, as recommended by the manufacturer. Then magnetite was measured into the prepolymer to achieve a 33% magnetite mixture by weight. The magnetite was mixed briefly by hand and then homogenized in an AR-100 mixer. PDMS-magnetite mixture (PDMS-m) was poured into the brass molds and degassed by applying sufficient vacuum to cause large (2 mm) bubbles to rise, at which point the vacuum was released. This degassing procedure was repeated once. The PDMS-m was cured in the molds at 60ºC for at least 4 hours, after which the connected 2 by 2 of MAts was removed from the molds and cut with a clean razor blade (Fig. C4, b-d). As expected, cured PDMS-m was noticeably stiffer than plain PDMS [69]. MAts were stored with the contact surface against the bottom of clean plastic petri dishes. To prepare MAts for use, the contact surface was sprayed vigorously with 70% ethanol to both remove dust and provide sterilization. Ethanol was immediately aspirated from the surfaces of the MAts in the cell culture hood. After this, MAts were placed upside down to dry. For greater sterilization MAts may be soaked in 70% ethanol for ≥ 10 minutes, following which they must be dried in an oven at 50-60ºC for ≥ 2 hours in order to evaporate and remove ethanol from within the PDMS-m.

Magnetic Attachment

MAts were attached to a culture surface by placing magnets underneath, in direct contact with the t.c. plastic. The magnetic force is determined by the strength of the magnet, amount and susceptibility of the magnetite in the stencil, and the distance between the magnet and stencil. For simplicity we chose to maintain 33% magnetite in the MAts, though this concentration could be decreased to achieve less force. Different magnetic arrangements

were tested for their ability to facilitate alignment of the MAts. The arrangement of four small magnets rotated by 90º around a central point and pressed into plus-shaped grooves was chosen because it visually and magnetically facilitates alignment of Star MAts (Fig. C4f-g). Magnet arrangements for 6- and 12-well plates were created this way. Magnet arrangments for 96-well plates were also created using a single 1/8˝ diameter 1/16˝ tall grade N52 magnets (D21B-N52) for each well. An appropriate level of force was determined empirically. The 1/4˝ x 1/8˝ x 1/8˝ grade N42 magnets (B422, K&J Magnetics, Inc.) were chosen based on their ability to prevent cell protrusions underneath MAts in 6-well plates by generating sufficient force to seal but not deform the MAts. The magnetic field across the contact surface of the MAts using these magnets and 6- or 12-well plates was 0.17 ±0.01 T. Stiff and soft PAA gels used fields calculated by the vendor of 0.14 ±0.01 T and 0.10 ±0.01 T by using arrangements of 1/4˝x1/8˝x1/8˝ and 1/4˝x1/8˝x1/16˝ grade N42 magnets (B422 and B421, K&J Magnetics, Inc.), respectively. These magnetic fields were calculated by the vendor using product testing results, and the error was determined according to the error of our measurements of the distance between MAts and magnet arrangements.

Protein Patterning

Protein patterns were created around Star MAts (Fig. 8c-d) as follows. Tissue culture plastic was coated with 100 μg/ml FITC gelatin and rinsed three times with PBS. With PBS in the culture dish, the MAts were positioned near the culture surface and released, allowing the magnets to pull the MAts against the surface. A PBS solution containing 3 μg/ml human plasma fibronectin was added and allowed to incubate around the MAts for 2 hours at 37ºC. After rinsing three times with PBS, the plate was removed from the magnets, the MAts were detached, and the culture surface was rinsed twice more with PBS. Then rabbit antibodies against human fibronectin were added at 2 μg/ml in PBS containing 0.5% BSA and incu-

bated for 1 hour at 37ºC. The surface was rinsed, and an anti-rabbit goat antibody labeled with Alexa-546 at 2 μg/ml in PBS containing 0.5% BSA was added for 1 hour at 37ºC. After rinsing three times with PBS, the surface was imaged.

Micropatterned Proteins

Microfluidic channels made of PDMS-m by casting the prepolymer over SU-8 patterns on silicon wafers provided by the Vanderbilt Institute for Integrative Biosystems Research and Education were sealed against 6-well plates with custom magnet arrangements. In Fig. 9, the microchannels created alternating lanes of collagen and A555-BSA. PBS containing 100 μg/ml collagen was pipetted into the microchannels and incubated for 2 hours at 37ºC. The collagen solution was washed away by rinsing and aspirating fluid through the microchannels 3 times. After removal of the microfluidic channels, the substrate was rinsed twice with PBS. The entire surface was subsequently blocked with 3 μg/ml Alexa555-BSA in PBS for 1 hour at 37ºC. Collagen bound to the surface in alternating lanes blocked most of the Alexa555-BSA binding and thus appears as dark red lanes in Fig. 9. The culture surface was rinsed twice, filled with cell culture medium, and MAts were attached perpendicular to the direction of the lanes of collagen for cell patterning.

Nanofiber Substrates

Parallel and randomly oriented poly(ε-capralactone) nanofiber substrates (Fig. 10) in 24-well plates were graciously provided by Nanofiber Solutions (Columbus, OH). Wells were coated with 100 μg/ml of collagen (rat tail type I, BD) in PBS for 2 hours at 37ºC. The substrates were rinsed twice, fresh cell culture medium was added, and MAts were magnetically attached. The assembly of MAts, 24-well plate, and magnets was incubated at 37ºC and 5%

CO_2 for approximately 15 minutes while HEp3 GFP cells were trypsinized and counted. Cells were plated at a quantity of 250,000 cells per well (131,000 cells per cm2) and incubated for 8 hours prior to MAt removal. Images were taken immediately after removal. Plates were then incubated for 8 hours, after which the final images were taken.

Polyacrylamide Substrates of Varying Elasticity

Polyacrylamide substrates of soft or stiff rigidity (Fig. 11) were made following the protocol of Pelham and Wang [70]. Briefly, 8% acrylamide and 0.05% bis-acrylamide (soft PAA) or 0.35% bis-acrylamide (stiff PAA) were cross-linked using 0.05% ammonium persulfate and 0.05% TEMED solution on 22 mm diameter glass coverslips. Spacers were used to create 170 μm thick polyacrylamide gels. The polyacrylamide surface was coated with 1% gelatin for 3 minutes, then the gelatin was aspirated and dried in the vertical position for 45 minutes. After this the gelatin on the polyacrylamide was cross-linked with 0.5% glutaraldehyde in PBS for 45 minutes and washed with repeated changes of PBS over a 15-minute period. Prior to plating cells, the prepared soft and stiff substrates were incubated for 1 hour with cell culture medium. The elastic modulus of soft polyacrylamide as made above has been reported as 1 kPa and the hard polyacrylamide has been reported as 10 kPa [71] which is similar to the elastic modulus of muscle tissue [72]. In order to avoid distorting the soft substrate by compressing it significantly more than the stiff substrates, magnetic arrangements for soft substrates were assembled using 1/4˝ x 1/8˝ x 1/16˝ (length, width, height). The standard 1/4˝ x 1/8˝ x 1/8˝ magnets were used on stiff PAA substrates.

Matrix Protein Interfaces

Using large (8 mm x 4 mm x 5 mm) Block MAts, interfaces between matrix proteins were created (Fig. 14a-b). A Block MAt was attached to each well of 6-well plates using the standard magnet arrangement, fiducial marks were made with the tip of stainless steel tweezers, and the wells were coated with the proteins onto which cells later migrated, specifically collagen 100 μg/ml, poly-D-lysine 0.05 mg/ml, fibronectin 10 μg/ml, and laminin 10 μg/ml in PBS for 1 hour at 37ºC. Wells were rinsed thrice with PBS, blocked with 0.5% BSA for 2 hours at 37ºC, and rinsed twice with PBS. In each well a second Block MAt were placed adjacent to the first block MAt and the first Block MAt was carefully removed, exposing an uncoated area of t.c. plastic. Collagen (100 μg/ml), poly-D-lysine (0.05 mg/ml), fibronectin (10 μg/ml), or laminin (10 μg/ml) were added to the wells thereby creating the matrix onto which the cells adhered. HEp3 cells were plated at 800,000 cells per well overnight. The medium was changed to Optimem containing 0.5% BSA 1 hour prior to removing the MAts. Cell migration was documented at hour 0, 8, and 16 through a 10x 0.25NA objective on an Axiovert 135 (Zeiss) microscope. To analyze migration across these matrix interfaces, fiducial marks were created on each end of the migration zone, individual 10x images were stitched together using the ImageJ plugin "Grid/Collection Stitching" [73], registered manually or registered automatically with the "Descriptor-based series registration" plugin [74], then cropped and quantified.

MAt Migration Assay

Extracellular matrix proteins (collagen 100 μg/ml in PBS and/or fibronectin 10 μg/ml in PBS) were coated onto glass or plastic culture surfaces for 1 hour at 37ºC and 5% CO_2. After being coated, the culture dish was rinsed 3 times with PBS and securely affixed above an array of magnets (Fig. C4f). Medium was added to the wells (1-2 ml for a 6-well plate),

MAts were lowered into position slightly above the culture surface and released, allowing the magnetic force to pull MAts against the wet protein-coated surface and thus avoiding scraping proteins off the surface. Cells were added (800,000 - 100,000 cells per cm2 depending on cell type) and allowed to adhere. After incubating for 16 hours or more, the culture dish was released from the array of magnets and MAts were subsequently removed to reveal the underlying void. Fresh cell culture medium containing 10% FBS was added. Images were taken immediately after removal of the MAts and at indicated times (generally 8, 12, 16, and/or 24 hours). For further protocol details and notes refer to Appendix A. For a direct comparison between MAts and scratches, the scratch and MAt assays were performed in the same well, thereby ensuring that identical culture conditions were applied to each. For Fig. 13 MAts were attached to half the wells of 12-well plates. Collagen was added to all wells for 1 hour at 37ºC. After rinsing thrice, the wells were blocked with 0.5% BSA and for Fig. 13b the wells were additionally coated with human plasma fibronectin 10 μg/ml in PBS for 1 hour at 37ºC. Cells were serum-starved overnight and migration was analyzed in medium containing 10% serum.

Scratch Migration Assay

The culture surfaces were coated with matrix proteins as described for the MAt assay. Cells were added (800,000-100,000 cells per cm2 depending on cell type). After achieving a confluent cell population, a void or "scratch" was created by dragging a plastic 200 μl pipette tip through dense cell population, according to the protocol of Liang et al. [13]. The culture was rinsed with PBS or medium to remove debris. Fresh cell culture medium containing 10% FBS was added. Images were taken immediately after void formation and at indicated times (generally 8, 12, 16, and/or 24 hours).

Image Acquisition

The microscope systems used to capture images are as follows unless specified otherwise in the text:

The upright microscope is a BX61 (Olympus). Images were taken using a 10x 0.4NA objective via DIC contrast or fluorescence using an ORCA-ER camera (Hamamatsu) and Volocity (PerkinElmer).

The shared spinning disk confocal consists of a CSU-10 confocal unit (Yokogawa) on an Axiovert 200 (Zeiss). Images were recorded through the 63x 1.4NA oil-immersion objective with an ORCA-ER camera (Hamamatsu) using Metamorph (Molecular Devices).

The cell culture microscope is a TMS-F (Nikon). Images were taken with a 10x 0.25NA objective and recorded using a D90 SLR camera (Nikon) attached to the trinocular.

The shared inverted microscope is an Axiovert 135 (Zeiss). Images were taken via phase contrast or fluorescence with a 10x 0.25NA objective and recorded with with a Retiga 200R camera (QImaging) using QCapture (QImaging)

The stereomicroscope is a Lumar V12 (Zeiss). Images were recorded through a NeoLumar 1.5x objective at 80x magnification using a Retiga Exi camera (QImaging) and Volocity (PerkinElmer) unless specified otherwise

Migration Quantified by Area Using TScratch

For both MAt and scratch assays, we acquired data microscopically as digital images using phase contrast, differential interference contrast (DIC), and/or fluorescence. Generally, images captured the entire void and cells along both sides of the void. The void between cell monolayers was quantified as a percentage of the total image area using TScratch [57]. The average width of the void was calculated by multiplying the percent area from TScratch

by the width (in μm) of the image. This is only possible when the height of the migration area is the same as the height of the image so that

$$\%area = \frac{width_{wound} * height_{wound}}{width_{image} * height_{image}} * 100$$

can be reduced and rearranged to

$$width_{wound} = \frac{\%area}{100} * width_{image}$$

By orienting the edge of the population of migrating cells vertically in the field of view, the height of the image and wound were always equal. The migration rate was subsequently calculated by dividing the difference of the wound widths in microns by the time (in hours) and as needed dividing this result by 2 to account for the migration of two cell boundaries towards each other.

Migration Qantified by Area Using ImageJ

For time-lapse data, ImageJ macros were written to automatically prepare images and determine the open area. Briefly, the contrast was adjusted, edges were detected, and the images were thresholded to create a binary image. These binary images were dilated in order to connect any disconnected edges before running ImageJ's Analyze Particle command. Analyze Particle parameters were selected to identify the large cell population and ignore individual cells. The open areas were converted to average widths as described, negative values resulting from improper area selection were omitted, and the results are shown in Fig. 12d. Cell boundaries (Fig. 15b) were created using the results of this macro and then measured in ImageJ to get the width. The average area of breakaway cells per image (Fig. 15f) was determined by modifying the Analyze Particle's parameters to exclude the large cell population

and identify individual cells. Individual cell tracking was done manually (Fig. 12e) using ImageJ's Manual Tracking plugin.

Statistics and Graphs

Umbrella plots in Fig. 12b and GFP intensity over distance in Fig. 9b and 9d were created in Microsoft Excel. All other plots and statistical analyses were produced using the free, open-source statistics language R (r-project.org) [75]. Box and whisker plots were made using R's boxplot command (boxplot {graphics}). The box shows the 25th, 50th (median), and 75th percentiles, and the whiskers extend to the most extreme data point, which is no more than 1.5 times the interquartile distance. Individual data points were overlaid on the boxplots using the stripchart command (stripchart {graphics}) to visually show the number of replicates for each experiment and any outliers. P-values were determined using all replicates in an experiment with the R implementation of the Welch Two Sample t-test (t.test {stats}). Asterisks were used to demonstrate significance: * for p-values ≤ 0.05, ** for p-values ≤ 0.01, and *** for p-values ≤ 0.001. Datasets comparing voids created with scratches and MAts were screened for trends caused by user error. For the data on intra-experiment reproducibility with A549 cells (Fig. 8e), the direction of scratching was found to influence the initial width of the void. This source of user-error was eliminated by restricting the dataset to scratches made by pulling toward the user rather than pushing the pipette tip away from the user. Interaction plots in Fig. 13 display means $\pm$ standard deviation.

Supplemental Material

Fig. C3 shows dimensions of Star, Microwell, and Dot MAts. Fig. C4 shows current fabrication and usage of MAts in 6-well plate format. Fig. C5 shows how submicron tool-

marks on the MAt contact surface enable cell protrusions into the void. Fig. C6 shows the maintenance of FITC gelatin substrates using MAt and scratch assays with A549 cells. Video C1 animates the steps of the standard MAt assay. Video C2 shows void-filling migration of HEp3 cells patterned with MAts on collagen-coated glass. Video C3 shows wound healing migration of HEp3 cells on collagen-coated glass that was scratched. Video C4 shows void-filling migration of HEp3 cells when MAts are attached before coating with collagen.

Results

MAt Production

Mat development was driven by the need for a migration assay in which the contribution of the underlying matrix can be defined by the investigator. The basic requirements of such an assay include 1) the deposition of a defined matrix, 2) plating cells adjacent to the defined substrate, 3) creating reproducible cell-free voids for accurate quantitation of cell migration, 4) avoiding damage to the substrate during the creation of the void, 5) adaptability to a variety of cell culture surfaces, and 6) ease of use. MAt assays are the first method to meet each of these requirements. MAts were designed to reproducibly create a void width similar to the typical void width of an in vitro traditional scratch assay [13]. Four different designs were created: 1) a general purpose, star-shaped MAt with four individual arms 650 μm wide, where each arm represents an individual void, 2) a microwell MAt composed of 4 small chambers separated by thin sidewalls designed to create voids of 200, 400, and 800 μm, 3) a dot MAt with an 800 μm radius created for use in high-throughput, 96-well format, and 4) a 2 mm wide block MAt that enables parallel coating of different matrixes (Fig. C3). Because of our prevalent use of the star-shaped pattern, hereafter "MAt" refers to that design unless otherwise specified.

MAts are molded in a one-step process from a mixture of magnetite and PDMS pre-polymer. A two-tiered mold was needed to eliminate tool marks and achieve a crisp transition from contact surface to sidewalls (Fig. C4 and Methods). The bottom tier consists of a flat brass base polished to a flat, mirror finish. The top tier consists of an outer frame and inner cubes with tapered sidewalls positioned so that the void or empty space between cubes creates the desired star design (Fig. C4).

Patterning Cells with Microscale Precision

Because MAts have a mirror finish on their contact surface and square edges at the transition from contact surface to sidewall, they can pattern cells with micron precision. After coating matrix protein onto a culture surface (Fig. 6b), we place the dish directly on top of an array of magnets and gently lower the MAts onto the culture surface (Fig. 6c). The magnetite-containing MAts are held to the culture surface during cell plating (Fig. 6d) and adhesion by means of the magnetic force generated by the underlying magnets. The field of the magnets is constant, but the force they apply on the MAt is readily adjusted by adjusting the distance of the magnets from the surface, such that the force between the MAt and protein-coated surface excludes cells during adhesion and subsequent culture. Removal of the MAt creates a void in the monolayer which is imaged at the start, during, and/or after completion of the assay in order to quantify migration (Fig. 6e). Star MAts (Fig. 7a) create cell-free voids even with aggressive cancer cells, such as the human epidermoid carcinoma cell line HEp3 (Fig. 7b,c). To confirm the ability of a MAt to exclude submicron cell protrusions, confocal imaging was used to visualize the contact area between the MAt, the culture surface, and the adjacent cells. Three-dimensional reconstruction of this interface revealed complete exclusion of the GFP-expressing cells (green, Fig. 7c). In contrast, MAts generated

with an unfinished surface containing submicron tool marks are unable to exclude invasive cells protrusions (Fig. C5b-d).

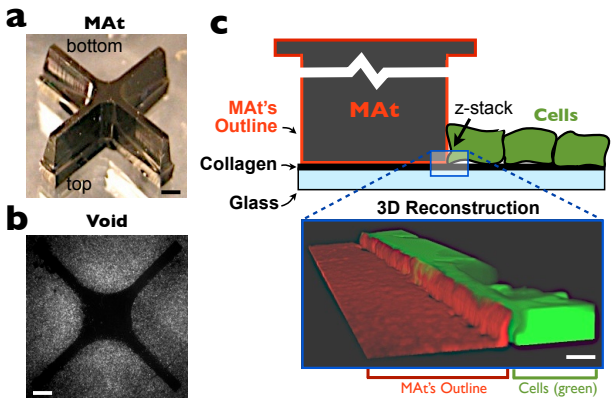

Figure 7. MAts prevent cell protrusions into the void. **(a)** A Star MAt, inverted to show the surface that is pressed against the substrate, and **(b)** corresponding void created in a monolayer of GFP-expressing cancer cells (HEp3) on t.c. plastic. Scale bars = 1 mm. Image acquired on a Lumar stereomicroscope using the 0.8x objective at 12.5x total magnification. **(c)** GFP-expressing HEp3 cells (green) were plated on collagen-coated glass coverslips adjacent to a MAt labeled with Alexa-549. Confocal imaging was used to visualize the interaction between the MAt, the culture surface, and the adjacent cell monolayer. With the MAt in place, a z-stack of images was captured with the shared spinning disk confocal (see Methods) and reconstructed in 3D. Scale bar, 50 μm.

Protection of the Underlying Substrate

The ability of MAts to prevent damage to the underlying substrate and disruption of the adjacent cells was evaluated by comparing the integrity of the void in a MAt assay with the integrity of the void in a standard scratch assay [13]. For both assays the A549 cells (Fig. 8a-b and Fig. C6) or fibronectin (Fig. 8c-d) were allowed to bind to a collagen or FITC gelatin-coated surface. In the scratch assay, mechanical surface abrasion removed the cells and most, but not all, of the collagen substrate underlying the cells. This partial removal of the matrix left an irregular void (Fig. 8a, inset a´) where cellular debris (arrowhead) and disrupted matrix (arrow) were clearly visible. The matrix disruption was very evident when

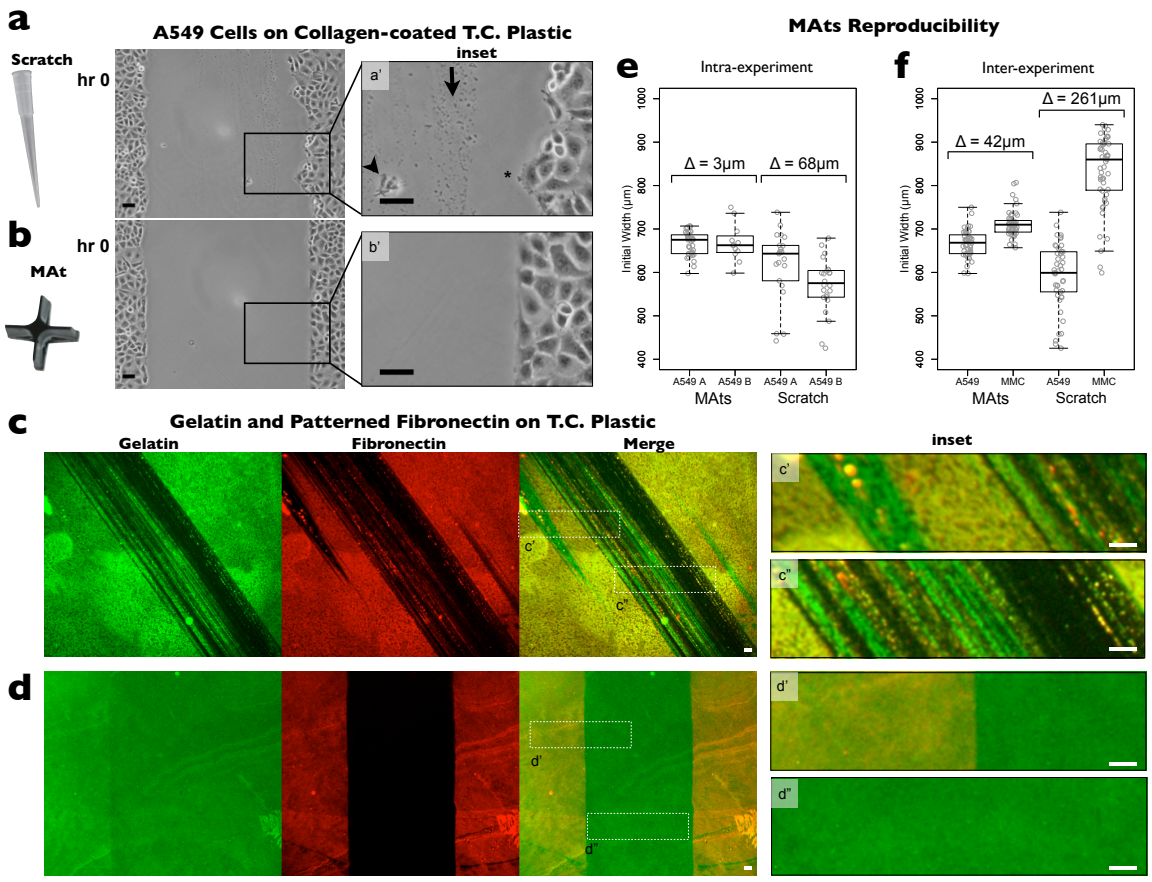

Figure 8. MAts protect the matrix and improve reproducibility. A scratch was used to mechanically create a void in a monolayer of A549 cells **(a)** or a matrix composed of fibronectin to collagen adsorbed to a glass surface **(c + insets)**. Similarly a MAt was used to create a void in a monolayer of A549 cells **(b)** or a fibronectin matrix (red) bound to a layer collagen (green) after placement of the MAt **(d + insets)**. Magnified inset a´ reveals the cell debris (arrowhead), disrupted matrix (arrow), and irregularities along the cell front (asterisk) that are created by the mechanical removal of the cells in the scratch assay but which are absent in a void created by the MAt **(b´)**.The ability of a MAt to protect the underlying matrix while providing a high-precision seal is shown through the detection of a fibronectin-free void when fibronectin (red) is adhered to the collagen after placing the MAt **(d)**. **(e)** The intra-experimental variability of void formation for MAt and scratch assays was quantified for independent repeat experiments (A549 A vs. A549 B) with ≥ 12 void measurements each. **(f)** The inter-experimental variability of void formation for MAt and scratch assays was quantified using a parallel analysis of A549 and mouse mammary epithelial cells (MMC) with ≥ 45 void measurements each. For boxplot details and microscopy, see Methods. Scale bars, 50 μm.

scratching surfaces coated with both fluorescently labeled collagen and fibronectin (Fig. 8c). The disruption of the matrix was irregular across the "wound" with streaks of matrix remaining perpendicular to the void. Upon close examination the non-uniform disruption is

particularly apparent in places where the fibronectin, but not the underlying collagen, were removed (insets c´ and c˝). In contrast, the voids created by MAts are uniform, without evidence of a disrupted matrix or dislodged cells (Fig. 8b,d). The uniformity of fibronectin patterned on the collagen surface is particularly striking (Fig. 8d and insets d´, d˝). Similar observations were made with collagen-coated surfaces covered with A549 cells (Fig. C6). These results demonstrate the unique ability of MAts to provide a defined void with intact matrix for migration of densely organized cells.

Intra- and Inter-Assay Reproducibility in MAt and Scratch Migration Assays

The intra-experimental reproducibility of MAts was determined by evaluating the average void width in 92 images from two independent experiments (Fig. 8e). The median initial width for repeated MAt experiments with A549 cells (Fig. 8e) was highly reproducible (MAt experiment A: 665.5 ± 4.7 μm and B: 668.1 ± 12.3 μm; values are given as mean ± SEM), while manual scratching was highly variable (scratch experiment A: 617.6 ± 17.8 μm and B: 570.5 ± 12.8 μm) despite active precaution against user-induced error (see Methods).

The inter-experimental reproducibility of MAts was determined by evaluating initial void widths (Fig. 8f) in parallel experiments of A549 and murine mammary carcinoma cells (MMC). Both cell types display epithelial, pre-EMT (epithelial-to-mesenchymal transition) characteristics [76], but MMC cells exhibit greater cell-cell adhesion. This cell-cell adhesion can disrupt cells adjacent to the wound during void formation. Indeed, in scratch assays the initial void width for MMC cells was 300 μm greater than the void for A549 cells, compared to a mere 50 μm difference when using MAts (Fig. 8f). Considering the 600 μm width of the pipette tip, the action of scraping MMCs removed an additional 150 μm swath on each side of the scratched surface. This was also observed in Fig. C6b, where the area devoid of cells cells due to scratching was much wider than the area of disrupted matrix. In contrast, MAts

created a consistent 650 μm void width with minimal (≤ 25 μm) removal of cells adjacent to the stencil. Thus MAts significantly improve intra- and inter-experimental reproducibility.

Migration on Micropatterned and Microfabricated Substrates

The structural complexity experienced by cells migrating in an in vivo microenvironment has been recreated in vitro using complex protein patterns [43,77-80] and complex physical topographies [5,81]. These features approximate the complexity of an in vivo environment, but the analysis of migration on patterned and textured substrates has been restricted to single cell migration because these delicate substrates are disrupted in scratch assays. MAts make it possible to analyze migration on patterned proteins and topographies because they are positioned with a gentle, controlled magnetic force and because the elastomeric stencil can conform to the textured surface.

Analysis of Haptotaxis on Micropatterned Proteins (Fig. 9)

Parallel, 100 μm wide lanes of collagen and bovine serum albumin were printed microfluidically [82] onto a plastic culture surface using magnetically adhered channels. HEp3 cells expressing green fluorescent protein (GFP) were patterned in serum-free medium with MAts placed perpendicular to the lanes of protein (Fig. 9a). Cell culture medium was changed one hour prior to removing MAts in order to prevent HEp3 cells from detaching from the substrate. After removal of the MAts, we monitored migration into the void in the absence of serum. From the confluent populations, HEp3 cells migrated readily onto collagen-coated lanes but not onto BSA-coated lanes (Fig. 9c). Migration was quantified by tracking GFP-expressing cells in collagen vs. albumin-coated lanes. BSA-coated surfaces, that allowed for cell adhesion adjacent to the Mats, supported only limited migration when cells were given collagen as an alternate choice (Fig. 9b, d).

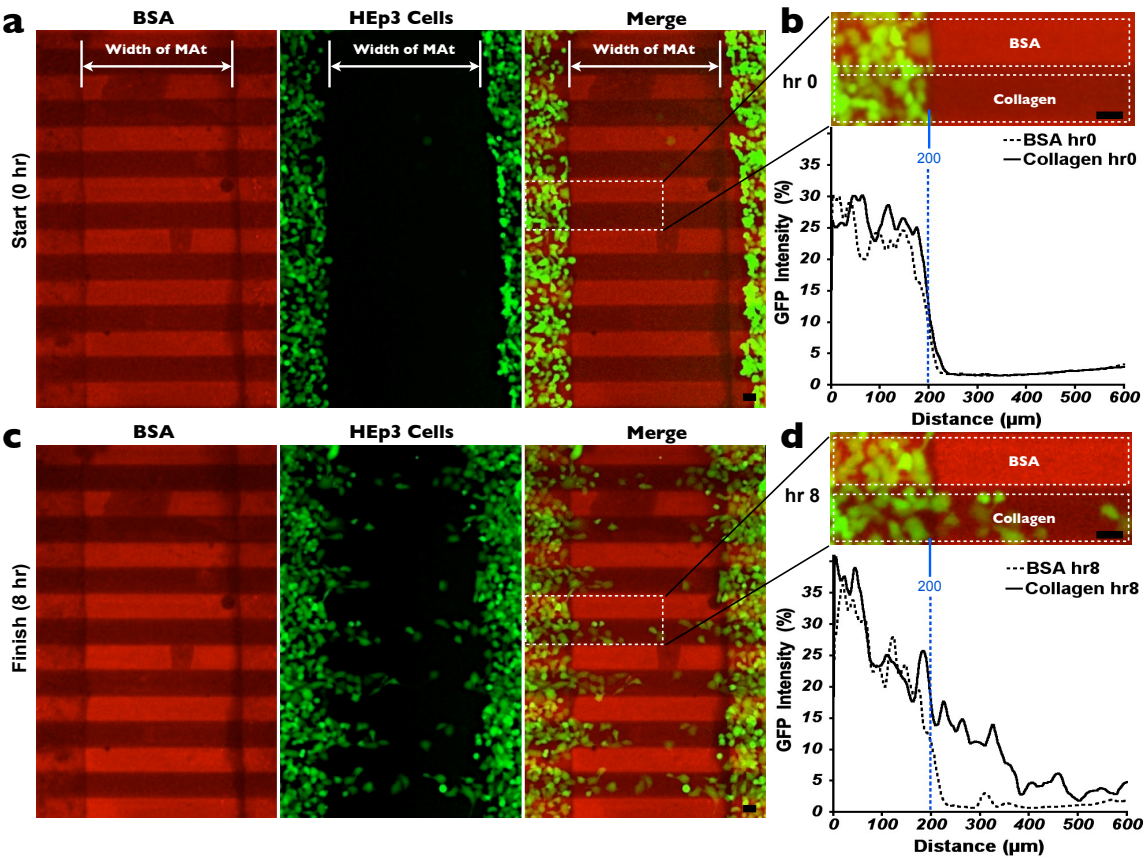

Figure 9. Micropatterned substrates reveal preferential cell migration. MAts were adhered perpendicular to 100 μm-wide alternating lanes of BSA (bright red) and collagen (weakly red) micropatterned onto the t.c. surface using a magnetically adhered microfluidic channel network. HEp3 cells (green) were cultured adjacent to the MAts and their migration across the lanes was monitored at 0 and 8 hours after removal of the MAts **(a and b, respectively)**. Motility was documented as the average cell intensity plotted over distance for both collagen-coated lanes (solid line) and BSA-coated lanes (dashed line) with the crisp cell boundary created by the MAts indicated with a blue line **(c and d)**. Despite the cells' ability to adhere to BSA-coated t.c. plastic, no cells were observed in these lanes, showing the strong preference of HEp3 cells to migrate on collagen-coated t.c. plastic. Scale bars, 50 μm.

Analysis of Topography Orientation Sensing (Fig. 10)

The response to matrix topography and its orientation was evaluated on aligned and randomly oriented poly(ε-capralactone) nanofibers, a structural model that mimics the organization of white matter of the brain [5]. Using MAts, HEp3 cells were patterned on planar sheets of collagen-coated nanofibers. In order to reduce protrusions and premature migration into the void on nanofiber substrates, MAts were removed after incubating 8 hours

rather than the normal 16 hours. The voids created by MAts were organized into three distinct configurations (Fig. 10a): 1) aligned: nanofibers = oriented perpendicular to the void and thus aligned with the direction of cell migration into the void, 2) counter-aligned: nanofibers oriented parallel to the void and thus orthogonal to the direction of cell migration, and 3) random: nanofibers oriented randomly. Migration was the greatest when the direction of migration was aligned with the nanofibers (61 ±7 μm/hr). This rate of migration was

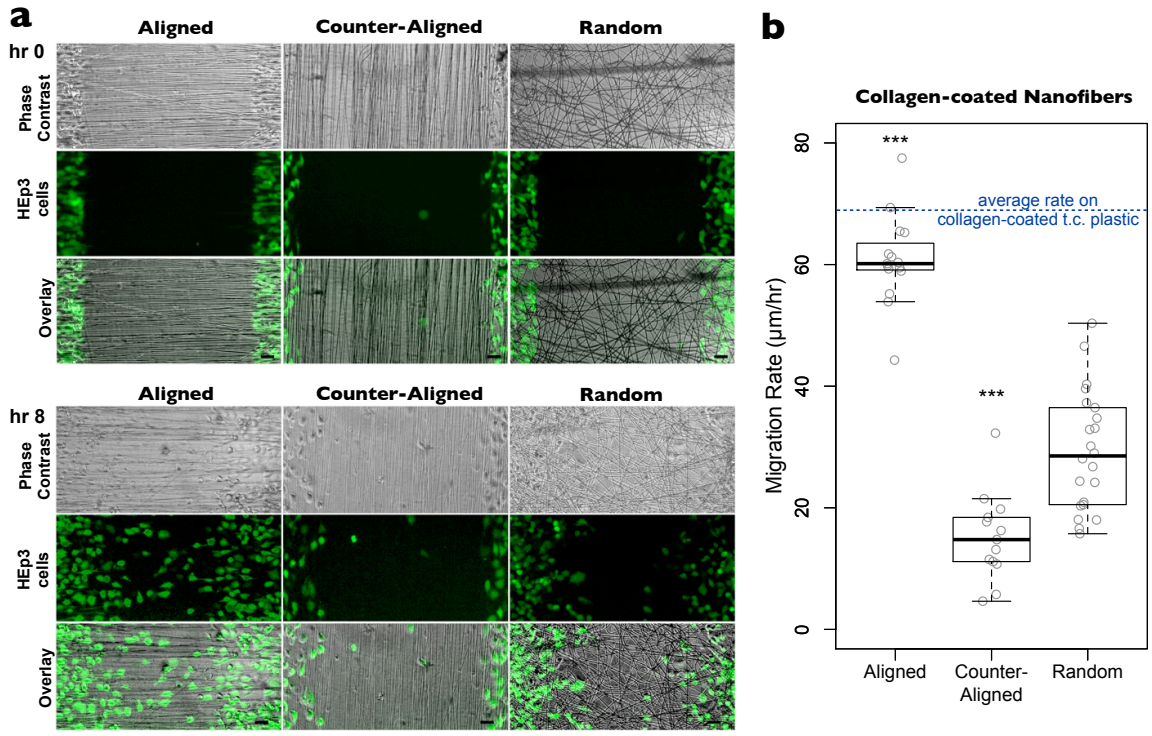

Figure 10. Oriented nanofibers increase or decrease migration. **(a)** HEp3 GFP cells (green) were patterned onto collagen-coated nanofibers using MAts. Nanofibers were either oriented perpendicular to the void and with the direction of migration (Aligned), oriented parallel to the void (Counter-aligned), or randomly distributed (Random). Migration into the void was imaged at 0 and 8 hours. **(b)** Migration rates were determined from the rate of void closure. For boxplot details, see Methods. Scale bars, 50 μm.

comparable to migration on a continuous, flat surface (not shown). Migration on random fibers was intermediate in speed (29 ±9 μm/hr) but significantly faster than in the counter-aligned configuration (15 ±7μm/hr, Fig. 10b). These observations suggest that a permissive

matrix (collagen type I) can be made non-permissive simply by organizing fibers perpendicular to the direction of migration.

Analysis of Durotaxis (Fig. 11)

Traditional in vitro cell culture surfaces such as glass are extremely rigid (elastic modulus = 1-100 GPa) compared to in vivo tissues (0.1-10 kPa, elastic modulus) [71,72,83]. Since the migratory behavior of adherent cells is strongly influenced by matrix rigidity [6,84-86] pliable hydrogels are increasingly replacing rigid surfaces for the analysis of cell migration. However, the difficulty of patterning cell populations without damaging the pliable

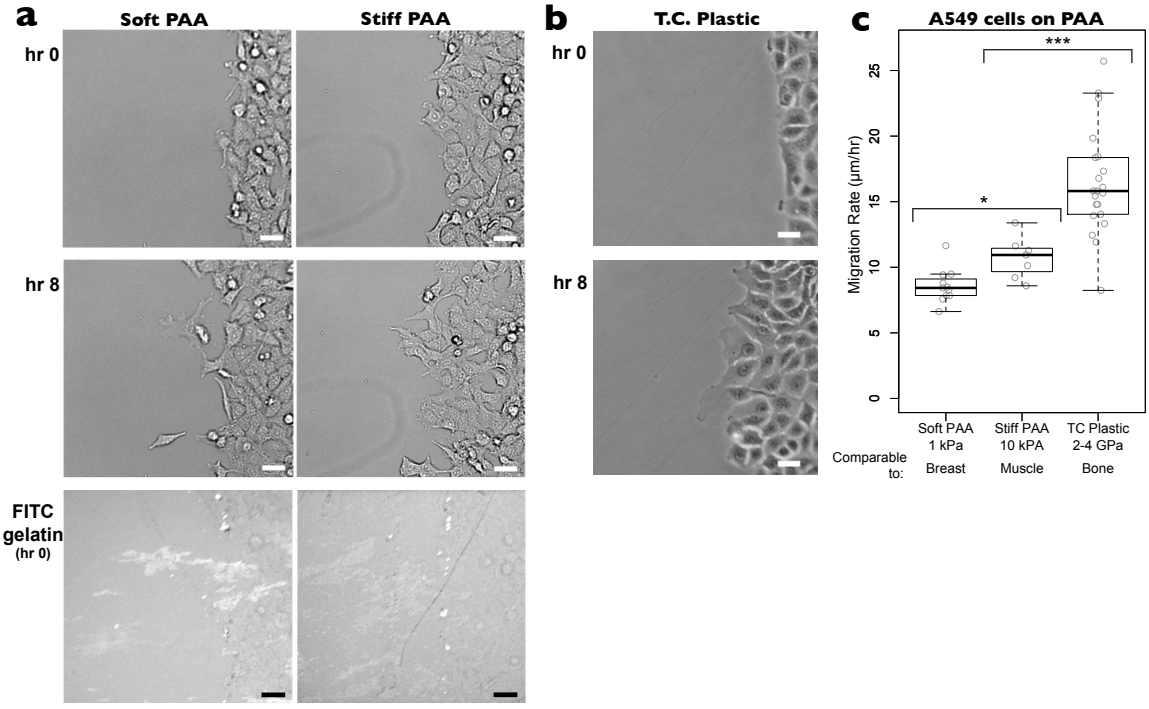

Figure 11. Substrate elasticity alters morphology and migration rate. Using MAts, the migration of A549 cells on FITC gelatin bound to polyacrylamide gels of low and high elastic modulus (**a**, 1kPa and 10kPa) was compared with migration on t.c. plastic (**b**, 2-4 gPa). **(c)** Migration rates were determined based on void closure (n≥7). Images for **(a)** were acquired via differential interference contrast on the BX61 and phase contrast for **(b)** on the TMS-F. For boxplot and microscope details, see Methods. Scale bars, 50 μm.

substrates limits their use in cell migration to the analysis of single cells. MAts overcome this limitation and enable evaluation of densely organized cell migration on pliable surfaces. MAts were placed directly onto soft (1 kPa) vs. hard (10 kPa) polyacrylamide (PAA) gels [87]. To compensate for the different elastic moduli and to prevent excessive compression of soft PAA, proportionally weaker magnets were placed underneath soft PAA gels (see Methods), enabling patterning of A549 cells on hydrogels of any stiffness (Fig. 11a). Interestingly, tumor cells displayed a more spindle-like morphology on pliable substrates than on rigid t.c. plastic (Fig. 11a-b). This spindle-like morphology is similar to the morphology of invasive cancer cells in vivo [68,77,88]. Quantitative analysis revealed that A549 cells on soft PAA exhibited significantly slower migration rates (9 $\pm$1 μm/hr) than stiff PAA (11 $\pm$1 μm/hr).

Rapid Single Cell Dissemination on an Intact, Permissive Substrate

Mechanical removal of cells during a scratch assay not only disrupts the monolayer and damages the underlying matrix but also orients the matrix orthogonal to the path of migration (Fig. 8). Orientation of the substrate can strongly impact cell migration. Consequently, we asked what specific impact matrix disruption had on cell migration. To answer this question, we used time-lapse microscopy of HEp3 tumor cells migrating in MAt and scratch assays to evaluate the impact of matrix disruption (Fig. 12). The undamaged matrix left in a void by the MAt allowed unrestricted migration on collagen-coated glass (Fig. 12a, left column and Video C2 vs. Video C4). Single cell tracking (colored lines) revealed individual cells migrating rapidly into the void. In contrast, migration across a scratch void was greatly diminished and occurred in two distinct phases (Fig. 12a, right column and Video C3). In the first 7.5 hours the cells migrated collectively into the void. In the 8th hour the cells began migrating parallel to the edge of the monolayer without moving further into the void (Fig. 12b). Repeating the experiment with a FITC gelatin substrate verified that the sec-

ond phase was due to disruption of matrix proteins (Fig. 12c). Although void closure was not significantly different between the MAt assay and the scratch assay (Fig. 12d), single-cell tracking illustrated that the productive motility of individual cells in a MAt assay was at least

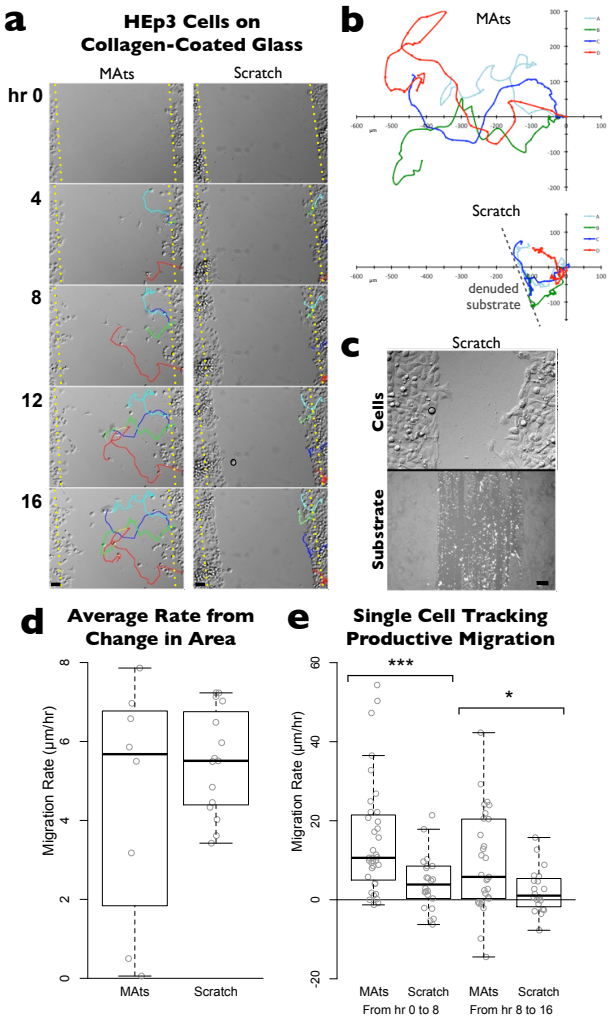

Figure 12. Consequences of matrix disruption for cell migration. **(a)** HEp3 cells plated on collagen-coated glass coverslips were imaged every 5 minutes for 16 hours as they migrated into voids created with a MAt or a scratch. **(b)** Umbrella plots showing the trajectories of individually tracked HEp3 cells. **(c)** Substrate damage responsible for the inhibition of productive cell migration (upper panel) was visualized using FITC gelatin coated glass (lower panel) after 8 hours of migration. **(d)** Average migration rates for HEp3 cells patterned with MAts or scratches on collagen-coated glass were equal using standard area-based analysis. **(e)** Migration rates as determined by individual cell tracking. Images were acquired via differential interference contrast and fluorescence microscopy using the upright microscope (see Methods). Frames were recorded every 5 minutes for 19 hours. For boxplot details, see Methods. Scale bars, 50 μm.

twice the productive motility (i.e. the component of migration perpendicular to the initial boundary of the void) of individual cells in a scratch assay (Fig. 12e). This implies that although a similar number of cells can migrate into the void for both assays, damage to both cells and substrate in the scratch assay prevents effective migration of individual cells away from the leading edge. Indeed, a detailed analysis of individual "break away" cells shows that MAts enable a far greater number of cells to escape the leading edge and migrate into the void (Fig. 15c). These observations demonstrate that even in a densely organized cell population, individual cell migration is heavily dependent upon the local matrix. Moreover, the interpretation of a migration assay can change dramatically when considering this contribution of the matrix to cellular behavior.

Cell-Autonomous Properties and the Underlying Matrix

During the progression of cancer, tumor cells frequently gain phenotypic plasticity, such as through an epithelial-to-mesenchymal transition (EMT). This transition dramatically changes the cell's adhesive properties and autonomous migration behavior. HEp3 and A549 are both epithelial cells, but HEp3 cells exhibit mesenchymal behavior while A549 cells exhibit epithelial behavior. Although HEp3 cells would be expected to migrate faster than A549 cells, the divergence between the two cells lines is very matrix-dependent (Fig. 13). The cell lines exhibit opposing behaviors in response to the availability of intact collagen matrix, and a 7-fold difference in their migration on collagen is reduced to less than 2-fold on plastic (Fig. 13a).

Similar to global phenotypic changes, the loss of a singular molecular component (specifically the collagen receptor $\alpha 2\beta 1$) can also have strong impacts on migration. MMCs that lack the $\alpha 2$ integrin subunit (MMC $\alpha 2$-/-) exhibited diminished adhesion to collagen

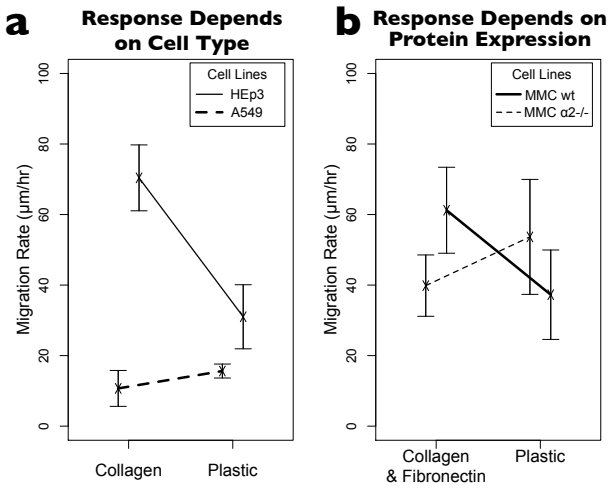

Figure 13. Correlation of cell-autonomous mechanisms and the underlying matrix. **(a)** A549 and HEp3 cells display pre- and post- EMT migratory behavior, respectively. Using MAts, the migration of these cells on t.c. plastic was contrasted with their migration on collagen-coated plastic ($n \geq 18$). **(b)** The migration of murine mammary carcinoma cells from wildtype (MMC wt) and integrin α2 knockout mice (MMC α2-/-) was similarly evaluated on a matrix of collagen + fibronectin vs. t.c. plastic ($n \geq 10$).Values of n are individual data points. Lines connect mean values. Error bars = SD.

but continued to adhere and migrate normally on fibronectin-containing matrixes [68]. Interestingly, cells lacking integrin α2 migrated faster on t.c. plastic than on the fibronectin and collagen matrix (Fig. 13b). Conversely, wildtype cells expressing endogenous α2 migrated slower on t.c. plastic than on the fibronectin and collagen matrix. While a migration deficiency on collagen-containing matrixes is not unexpected, the inverse disparity between wildtype and α2-null cells (i.e., α2-null cells migrated faster on t.c. plastic than wildtype cells) suggests that α2 can contribute to migration in a cell-autonomous, ligand-independent manner. This is consistent with our previous in vivo studies demonstrating that α2 is a metastasis suppressor [68]. These results demonstrate that the availability of a specific substrate can, in fact, strongly impact the interpretation of cell-autonomous migratory behavior.

Matrix Switching

Matrix switching during migration affects motility disproportionally. When a cell migrates away from its point of origin, it enters a new microenvironment and is exposed to new extracellular adhesive options. The nature of this new matrix can determine the rate of migration and the type of motility (i.e., collective vs. single cell motility, Fig. 12, 13, and 15). However, independent of the permissive/non-permissive nature of each individual matrix,

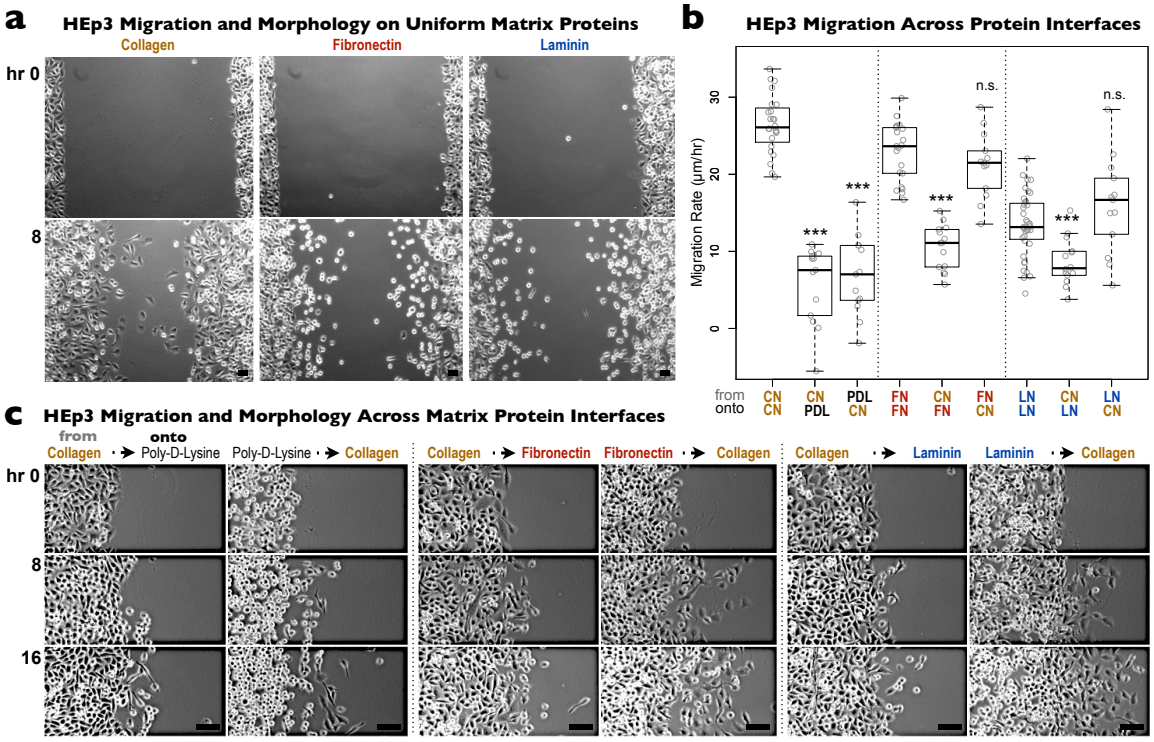

Figure 14. Matrix switching during migration affects motility disproportionally to the nature of the matrix **(a)** Using Star MAts HEp3 cell migration was analyzed on uniform substrates of collagen (CN), fibronectin (FN), and laminin (LN). The migration rates are displayed in **(b)** as from CN onto CN, from FN onto FN, and so on. **(c)** Using Block MAts, two adjacent matrixes were created as described in Methods. Cells were seeded onto one matrix, cultured to confluence, and subsequently allowed to migrate onto the adjacent matrix. Images taken at 0, 8, and 16 hours document migration and the morphological changes visible when HEp3 cells switch from CN onto adjacent poly-D-lysine (PDL), FN, and LN, or vice versa. **(b)** The quantitation of migration rates across these interfaces revealed significant matrix-specific effects and unexpected migration deficiencies that could only be contributed to matrix switching and not the matrix itself (CN vs. FN). Images were taken on the Axiovert 135 microscope. Microscope and boxplot details are described in Methods. Scale bars, 50 µm.

the act of switching from one matrix to another may affect migration. To address this possibility we created two adjacent areas coated with different matrix proteins (collagen, fibronectin, or laminin) or poly-D-lysine (PDL) using block MAts and subsequently analyzed the migration of HEp3 cells from one area to the other in a 16 hour period (Fig. 14a-c). The consequences of matrix switching were revealed by comparing it with migration on uniform collagen, PDL, and laminin (Fig. 14a).

As might be anticipated, when two adjacent areas were coated with the same matrix proteins (laminin, fibronectin, or collagen) there was no reduction in migration when compared to migration across a uniform coating of matrix protein. However, this was not true when two dissimilar coatings were coated adjacent one another.

When evaluating cells migrating to or from a PDL-coated area, we found that the cells moved at a rate similar to that seen on uniform PDL (approximately 6μm/hr, Fig. 14b) which is much less than the rate of migration on collagen (26μm/hr). It appears that the limited HEp3 cell spreading on PDL (Fig. 14c, second column) and low motility on PDL limits the ability of these cells not only when they move onto the PDL surface but also when they must leave the PDL to enter the collagen-coated surface.

In contrast to PDL, fibronectin and laminin supported rapid migration onto adjacent collagen coated areas. However, when migrating cells switched from collagen to fibronectin or laminin there was an unexpected reduction in the rate of migration. The reduced rate of migration was surprising because it was even less than the rate of migration supported by a uniform matrix of fibronectin (23.0 μm/hr) or laminin (13.4 μm/hr, Fig. 14b) which was already significantly less than the migration of collagen (26μm/hr). The reduced migration indicates that switching from collagen to fibronectin or laminin adversely affected cell migration. Conversely the same is not true for cells switching from fibronectin or laminin to collagen.

Discussion

MAts and Related Migration Assays

The creation and design of MAts was inspired by space-filling assays which exclude cells by various means such as stencils [36-38,89], stoppers [34,90], barricade gels [32], microfluidic barriers [46,91], and ligand switchable substrates [67]. After the cells have adhered, migration is initiated by removing the stencil or stopper, dissolving the barrier gel, releasing the microfluidic barrier, or switching the substrate. Unfortunately, current space-filling methods have significant limitations. Stencils and stoppers that auto-adhere to the plastic or glass culture surface cannot be applied to wet or protein-coated surfaces. Barriers that are manually forced onto the culture surface are difficult to apply without damaging an underlying matrix. Furthermore, barrier gels, microfluidic barriers, and ligand switchable substrates place restrictions on the substrate used.

By attaching MAts to a culture surface, an exclusion zone (void) is created in a cellular monolayer. Similar to a scratch assay, documenting the movement of cells into this void provides a means to quantify the rate of migration. However, MAts are unique because they protect the underlying surface in the void and thereby allow full control over the composition of the matrix onto which the cells migrate. This application is not limited to classic analysis of protein-coated plastic and glass surfaces but is readily extended to protein micropatterns, nanotextured surfaces, and pliable substrata such as hydrogels. In the past, migration on such substrates was limited to single cells or non-patterned colonies and droplets of cells [42,45]. Consequently, MAt assays are not merely an improvement over scratch assays, they provide a unique, versatile method to enable investigations into the contribution of the substrata to cell migration.

Effects of Matrix Context

In several instances, providing a new substrate resulted in unexpected changes in migration. Switching from one matrix to another during migration (Fig. 14) caused a disproportionate reduction in motility. Such matrix-dependent phenotypes have been reported for primary cells during long-term culture [92] but have not been observed in established cell lines during such short temporal and spatial dimensions. Our observations suggest that at microscopic dimensions a change in the available matrix can influence migration in a dynamic manner that requires accounting for more than just the molecular identity and the supportive nature of the matrix, but also accounting for the time prior to and after matrix switching. We expect further analysis of the effect of matrix switching on migration to reveal an unappreciated form of biological hysteresis [93-96].

Furthermore a single matrix protein (collagen) can mediate very different rates of migration depending on the context of its presentation to the cell. When provided collagen as a choice adjacent to a non-permissive matrix such as BSA (Fig. 9), cells migrated rapidly on collagen ($\geq$50 μm/hr) and were not observed migrating on BSA. Similar rates of migration were achieved by physically aligning nanofibers (coated with collagen) with the direction of migration into the void ("Aligned" Fig. 10). In contrast, orienting the nanofiber surface, and thereby the matrix, parallel to the void causes cells to migrate along, rather than into the void ("Counter-aligned" Fig. 10). These experiments show the rate of productive motility depends upon the organization of the extracellular matrix.as well as the molecular composition.

MAts and Migratory Companion Cells

Migration on a non-permissive matrix or adversely organized substrate can be facilitated by companion cells. For this reason (and others) the role of tumor-associated cells is

under intense investigation. While it is generally accepted that fibroblast and immune cells can modify the tumor-associated matrix, MAts enables the analysis of this modification and its contribution to migration in vitro. Fig. 15 displays proof of this concept, HEp3 cells were sparsely interspersed within a monolayer of A549 cells and allowed to migrate collectively

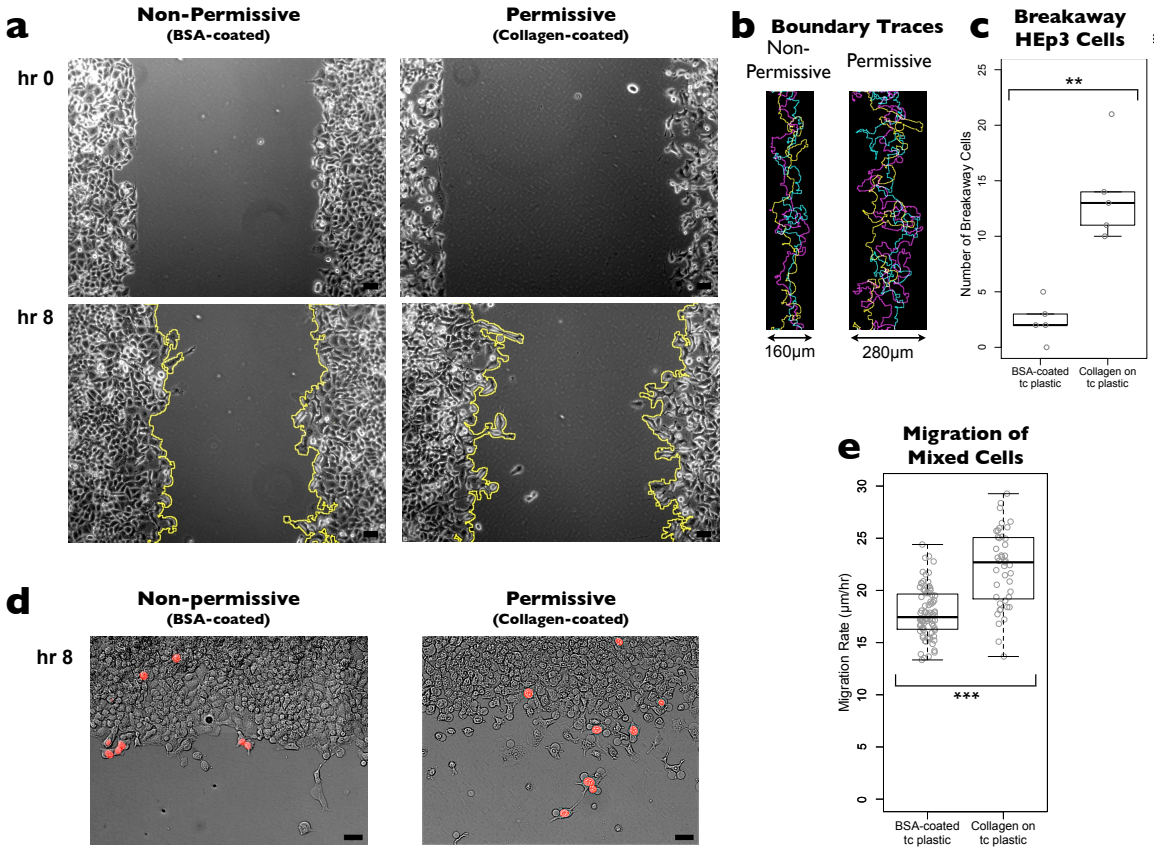

Figure 15. Inhibition of tumor cell dissemination on non-permissive substrates. **(a)** Representative images of mixed cell populations (A549:HEp3 at 100:1) on BSA-coated and collagen-coated t.c. plastic. BSA is non-permissive to HEp3 migration but not A549 migration, whereas migration on collagen-coated t.c. plastic is permissive to HEp3 migration. Boundary tracing highlights the extent to which the cells migrate uniformly (yellow). **(b)** Multiple boundary traces are overlaid and aligned to determine the average ruffling wdith for the mixed cells on HEp3-non-permissive and HEp3-permissive substrates. **(c)** HEp3 dissemination is quantified displaying a significant increase in dissemination on the collagen-coated substrate. **(d)** Representative images of HEp3 dissemination. HEp3 cells express mCherry-H1 enabling fluorescent detectiong. **(e)** Migration of the collective mixed cells is only moderately increased on a permissive matrix (1.3 fold). Images were acquired on the inverted microscope (a) and upright microscope (d) as described in Methods. Scale bars, 50 μm.

with the A549 cells into a void containing a BSA-coated surface ("Non-permissive" Fig. 15) or a collagen-coated surface ("Permissive"). HEp3 cells migrated across the BSA-coated surface because of the A549 cells. When presented with collagen numerous HEp3 cells disseminated away from the edge of the monolayer of cells. Similar future studies will illuminate the role of such cell-cell interactions in development, normal physiology, and disease.

Conclusion

MAts provide experimental accuracy and versatility. The use of magnetic force to attach a stencil onto a substrate represents a new strategy in the arena of space-filling assays. This strategy works well on wet and dry surfaces, on simple and complex protein coatings, on rigid and pliable substrates, and on microfabricated textures. The strategy is applicable to standard culture wares, high-throughput plates, and microculture models by simply using different shapes of MAts (Fig. C3). Such versatility is crucial in the early stages of discovery when experimental conditions and parameters are routinely refined and must be controlled fully by the investigator.

MAts open up exciting new approaches to analyzing the migration of densely organized cells. These studies can range from the analysis of migration on defined, intact substrates to the evaluation on complex engineered substrata such as protein-coated hydrogels. Using MAts we identified specific migratory responses contributed by matrix modifications including inadvertent damage and specific matrix orientation, and by matrix switching. MAts can be customized to meet a wide variety of applications (Fig. C3). MAts readily incorporate microfluidic designs and microfabrication techniques, creating opportunities for protein patterns and interfaces that enable innovative investigations of cellular behavior. Unique problems that can be addressed with MAts include: a) determining the contribution of complex protein patterns and protein complexes to migration, b) evaluating the migration of densely

organized cells on pliable substrata with defined matrix adhesions, c) determining the contribution of tumor-associated cells to migration onto substrate not permissive to tumor cells, d) deciphering how cells choose among the adhesive substrata available during migration, and e) evaluating the cryptic epitopes in the extracellular matrix. Most important, MAts allow the experimenter to define the composition of the substrate onto which the cells migrate. This control makes it possible to quantitatively determine the contribution that a defined matrix makes to cell migration in the context of complex microenvironment.

Acknowledgements

We thank Kevin Branch, John Fellenstein, Philip Samson, and David K. Schaffer for technical support. The Vanderbilt Institute for Integrative Biosystems Research and Education (VIIBRE) provided microfabrication resources. Aron Parekh provided key insight into the production of polyacrylamide gels. We thank Allison Price for a critical review of the writing and Mary Zutter for extending the use of the wildtype and integrin α2 deficient MMC. Andries Zijlstra and William Ashby were supported by CA120711-01A1, CA143081-01 and the Ronnie James Breast Cancer Discovery award.

CHAPTER IV

MAGNETICALLY SEALED LIVE CELL IMAGING CHAMBERS (MSLICs)

Introduction

Various platforms have been developed to facilitate live-cell imaging, especially of mammalian cells. Mammalian cells have some of the strictest environmental requirements and are generally maintained at 37 ºC in a culture medium having a pH of 7.2-7.4 in equilibrium with an atmosphere of 5% CO_2 in air [97]. Consequently, most live-cell imaging platforms consist of a chamber to hold and image the cells and control systems to maintain 37 ºC, 5% CO_2 levels, and high humidity to avoid evaporation. Successful live-cell imaging requires expertise in microscopy, the live-cell imaging platform, and the biology of interest in order to recognize and eliminate artifacts due to improper conditions and analyze clearly the biology of interest. To facilitate maintenance of successful cell culture conditions on the microscope, we present magnetically sealed live-cell imaging chambers (MSLICs). MSLICs fit in multi-well plate microscope stage mounts and can be sealed quickly by hand without dirtying the imaging windows. Furthermore, MSLICs are versatile, enabling static or dynamic fluidic investigations such as cell migration assays, analysis of the effects of pulsed delivery of treatments, 3D culture of acini, and so on.

Table 3. Live-cell imaging chambers.

Chambers		Example	Pros	Cons
Open		glass-bottomed dish	direct access to cells and medium	requires CO_2 control system
		multi-well plate	lower volume	requires CO2 control system
Closed	Permanently	bonded glass and PDMS microfluidics	unlikely to leak	must flow cells into position
	Temporarily	auto-adhesive	low physical profile, versatile	prone to leak or drift if glass is protein- or cell-coated
		clamped	large variety, commercially available	bulky clamps may interfere with microscope movement
		magnetically sealed	low physical profile, versatile, seals wet protein- or cell-coated glass	magnetic fields may disturb electronics in close proximity

Live-cell imaging platforms vary according to the type of chamber used (see Table 3). Live-Cell imaging chambers are either open to the surrounding environment or closed. However, some closed chambers, including the MSLICs presented herein, can be operated in the open configuration. Each requires certain control systems in order to maintain appropriate culture conditions (Fig. 16).

Open chambers require greater control of the surrounding environment in order to maintain conditions appropriate for living cells (Fig. 16a). Consequently, they are combined with temperature, CO_2, and often humidity control systems in order to maintain 37 ºC and 5% CO_2 levels, and minimize evaporation and the resulting change in osmolarity [97-99]. These control systems are costly, yet crucial to experiments requiring direct access to cells and medium such as patch clamp and chemotaxis studies using micropipettes.

Many experiments do not require direct access to the cells and medium. For such experiments, closed chambers can be used. By preventing contact between the surrounding atmosphere and contents of the chamber, closed chambers eliminate the need for CO_2 and humidity control systems (Fig. 16b) [99]. Generally, the cell culture medium is incubated in

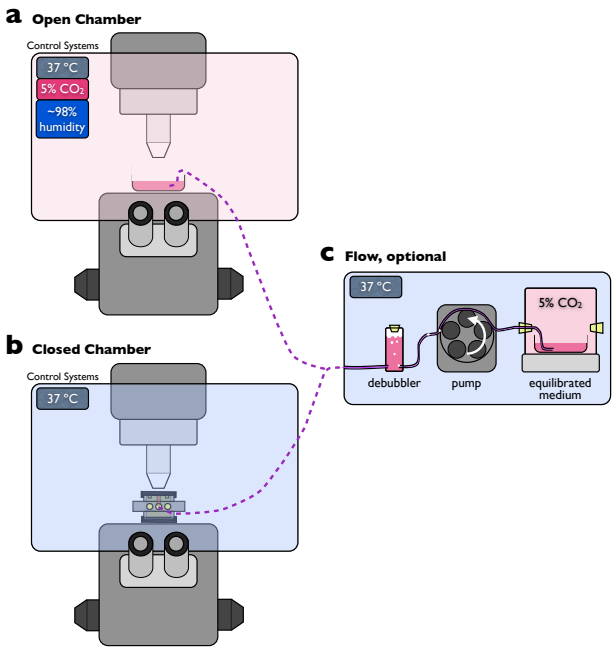

Figure 16. Strategies for maintaining an appropriate environment for live-cell imaging. Live-Cell imaging can be performed with **(a)** open chambers or **(b)** closed chambers. **(a)** Open chambers require control of temperature, CO_2 levels and humidity. **(b)** Closed chambers are usually equilibrated to 5% CO_2 before being sealed and thus require only temperature regulation by heating a microscope enclosure (shown) or alternatively a small area of the stage (not shown). **(c)** Flow is best suited for closed chambers but can also be used with open chambers. Incorporating flow into live-cell imaging systems generally requires a reservoir of equilibrated medium such as the dish of medium in a sealed jar containing 5% CO_2 shown; a

the laboratory's cell culture incubator until its CO_2 levels reach equilibrium with the 5% CO_2 in the atmosphere of the incubator. Then the MSLIC is sealed in order to maintain appropriate CO_2 levels and osmolarity.

Closed chambers are either permanently closed such that cells must be introduced through ports and channels or temporarily sealed (see Table 3). The most common permanently closed chambers are glass or PDMS microfluidic devices. Being permanently sealed the chance of leaking is extremely low; however, fluidic connections may be prone to leak if poorly made [100]. Temporarily closed chambers vary in their sealing mechanism. Chambers can be temporarily sealed via adhesion. Often the auto-adhesive nature of silicone and glass are used to close the chamber. Two examples of this are auto-adhesion of PDMS microflu-

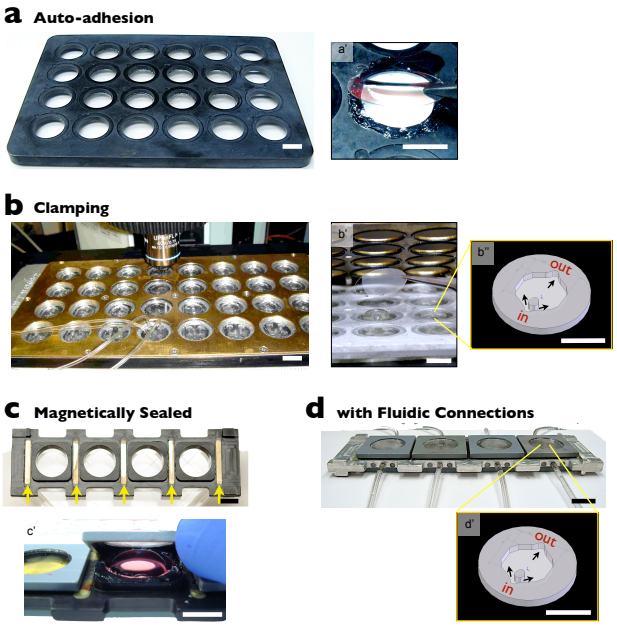

Figure 17. Various temporarily closed live-cell imaging chambers. **(a)** Auto-adhesive materials such as glass and silicone can be used to form closed chambers. The aluminum base shown enables creation of 24 live-cell imaging chambers. **(a´)** Silicone vacuum grease is used to seal glass cover slips against the aluminum base. **(b)** Clamping provides force to counter pressure from fluidic systems. **(b´)** Glass cover slips were sealed with silicone vacuum grease and then clamped onto the aluminum base by bolting on a brass lid containing rubber o-rings. **(b˝)** A fluidic chamber cast into the aluminum base using PDMS facilitates the introduction and removal of fluids by reducing the volume from 1.5 to 0.2 mL. **(c-d)** Magnetically sealed live-cell imaging chambers (MSLICs) provide force using magnets (c, arrows). **(c´)** Static magnetically sealed live-cell imaging chambers (MSLICs) compress glass cover slips against auto-adhesive materials using magnetic force in order to form a sealed chamber. **(d)** Side holes enable fluidic connections. **(d´)** Fluidic chambers can be cast in the MSLIC using PDMS. Scale bars, 1 cm.

idic devices onto glass and sealing glass cover slips onto silicone vacuum grease as in Fig. 17a and a´. Unfortunately, these strategies are prone to leak or drift if the glass cover slips have been completely coated with cells or hydrophilic proteins making them slippery. Alternatively, many chambers are temporarily closed via a clamping mechanism. These mechanisms are difficult to create in a low profile so as to avoid interfering with the microscope while moving positions. We fabricated a clamped array of fluidic live-cell imaging chambers (see Fig. 17b) with a low profile for simultaneously imaging multiple chambers. However, tightening the fifteen screws was a time-consuming process.

Magnetically sealed live-cell imaging chambers (MSLICs, Fig. 17c-d) overcome several limitations of closed live-cell imaging chambers. Utilizing magnetism, MSLICs provide force similar to standard clamping mechanisms but without being obtrusive or time-consuming. This is accomplished by gluing magnets into the aluminum frame of the chambers (Fig. 17c, yellow arrows). Then glass cover slips are placed into thin ferromagnetic steel lids which are attracted to the magnets held into the frame (see Fig. 19). Currently, silicone vacuum grease is used to ensure a leak free seal (Fig. 17c´). However, o-rings or gaskets could also be used. This combination of clamping via magnetic force and auto-adhesion overcomes the primary limitation of auto-adhesive devices and enables successful imaging of glass cover slips even when they are completely coated with cells or proteins. Furthermore, MSLICs can be outfitted with fluidic systems (Fig. 16c and 17d), millifluidic chambers (Fig. 17d´) and potentially microfluidic devices.

Only a few other magnetically sealed chambers have been developed and to the best of our knowledge, none of them provide the versatility of MSLICs. Tkachenko *et al.* developed a magnetically sealed perfusion chamber used to investigate effects of hydrodynamic stresses [101]. Rafat *et al.* demonstrated successful sealing of microfluidic devices using magnetic force [102]. However, neither present a versatile chamber readily compatible with microscopes equipped to hold a multi-well plate. MSLICs fit into multi-well plate microscope stage mounts, are versatile, can be connected to fluidic control systems, and customized by casting various PDMS chambers including microfluidics into the aluminum MSLIC base. In this publication, we present initial proofs of concept for the MSLICs, specifically pulsed treatment of cells on glass cover slips and 3D culture of acinar structures.

Fabrication of MSLICs

MSLICs were designed to be assembled by hand and fit into common multiwell stage inserts. Their basic dimensions are 5″ by 1.5″ by 5/16″ as shown in Fig. 18 which gives dimensions in millimeters. For details on MSLIC lid dimensions refer to Fig. C7. As currently designed, MSLICs accommodate 22 mm diameter cover slips. CNC milling was used to create the final shape of the base in aluminum which was then anodized or coated with a continuous 0.0005″ layer of parylene-C (Paratronix, Inc. Attleboro, MA) to prevent adverse reactions with cell culture medium. After anodizing or coating the base, neodymium-iron-boron

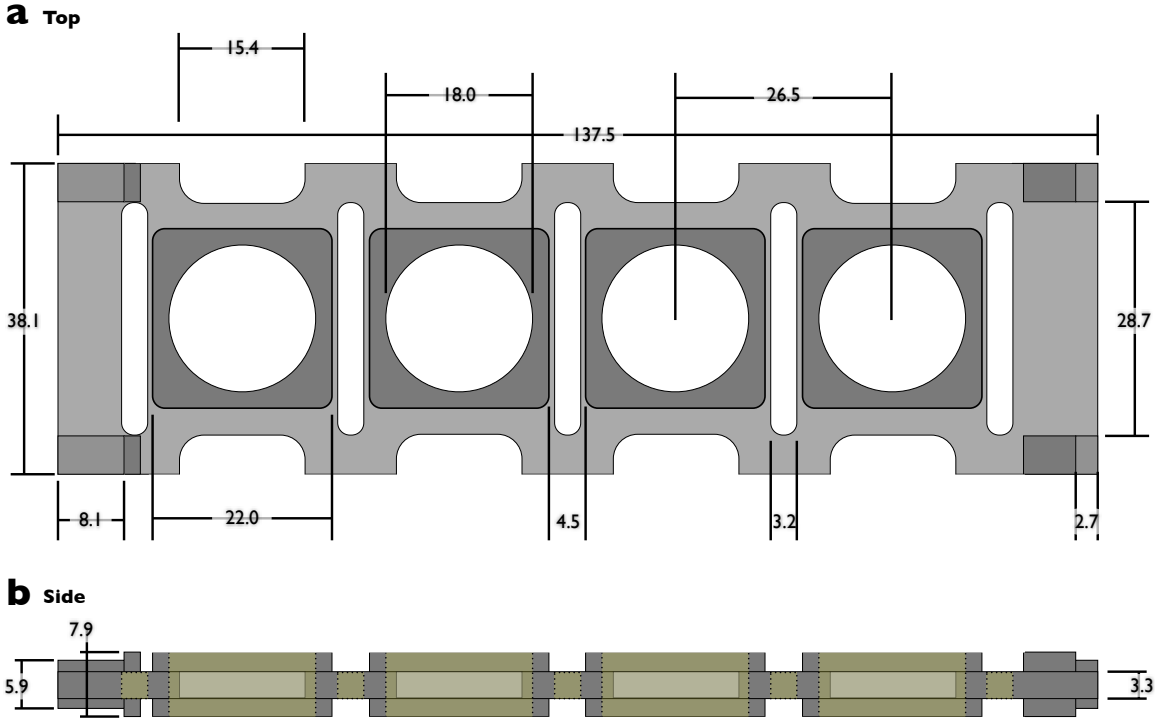

Figure 18. MSLIC dimensions. **(a)** Top view shows dimensions of through holes for magnets and MSLIC chambers as well as recesses along the edge designed to facilitate manually attaching MSLIC lids. **(b)** Side view reveals thickness of original stock (7.9 mm) and reduced size to accomodate lids (3.3 mm) and our microscope stage (5.9 mm). All dimensions are in millimeters. Tolerances are 0.1 mm.

magnets 1″ by 1/8″ by 1/8″ (BX022, K&J Magnetics) were glued (DP460, 3M) into the five narrow slots adjacent to the holes of the chambers (Fig. 18). For fluidic MSLICs three 0.09″ diameter holes were drilled through the sides into each of the four chambers (Fig. C7). The hole diameter was chosen to enable pressure fitting of 3/32″ outer diameter Tygon® tubing as described in "Fluidic Setup" below.

To seal the MSLIC, eight lids per array were machined from ferromagnetic steel. The lids consist of a rectangle with both an 18 mm diameter hole cut through the center for viewing and a 22.2 mm square recess into which standard cover slips (#1.5, 22 mm diameter) can be seated (Fig. 17c and Fig. C7). To make the inside of the lids compatible with cell culture and prevent corrosion, the outside of the lids were painted with high-temperature paint (7832T1, McMaster-Carr) and heated twice from room temperature to 65-70 ºC according to the manufacturer's instructions. Then the lids and fluidic MSLIC base were coated with a 0.0005" layer of parylene-C (Paratronix, Inc. Attleboro, MA) in order to prevent adverse reactions with the cell culture medium. Parylene-C coating creates a continuous protective layer except in areas of contact necessary for fixturing. During the coating MSLIC lids lay on a metal grate with the inside facing up so that the inside would receive a continuous paylene-c coating and any breaks due to contact would occur on the protected, painted outside.

Sterilization

After each use glass cover slips and silicone vacuum grease were removed from the MSLIC base and ferromagnetic lids. The base and lids were wiped clean with wet paper towels and soaked in distilled water for at least one hour. Immediately prior to an experiment the needed parts were soaked for 30 minutes or more in 70% ethanol and then dried in a 150 mm culture dish (351058, BD Falcon) in the cell culture hood. Aproximately, every sixth use

or after contamination with yeast, the MSLICs were soaked in dilute bleach (1:1000 dilution of a 6.3% stock) for at least 1 hour and then rinsed by immersion 7-8 times in pure distilled water.

Assembly

After sterilizating the MSLIC base and lids, two glass cover slips for each MSLIC chamber being used were rubbed with 70% ethanol using a Kimwipe (34155, Kimberly-Clark) and then dried with another Kimwipe. As shown in Fig. 19a The MSLIC base and lids were coated with a thin (<1 mm) layer of silicone high vacuum grease (1597418, Dow

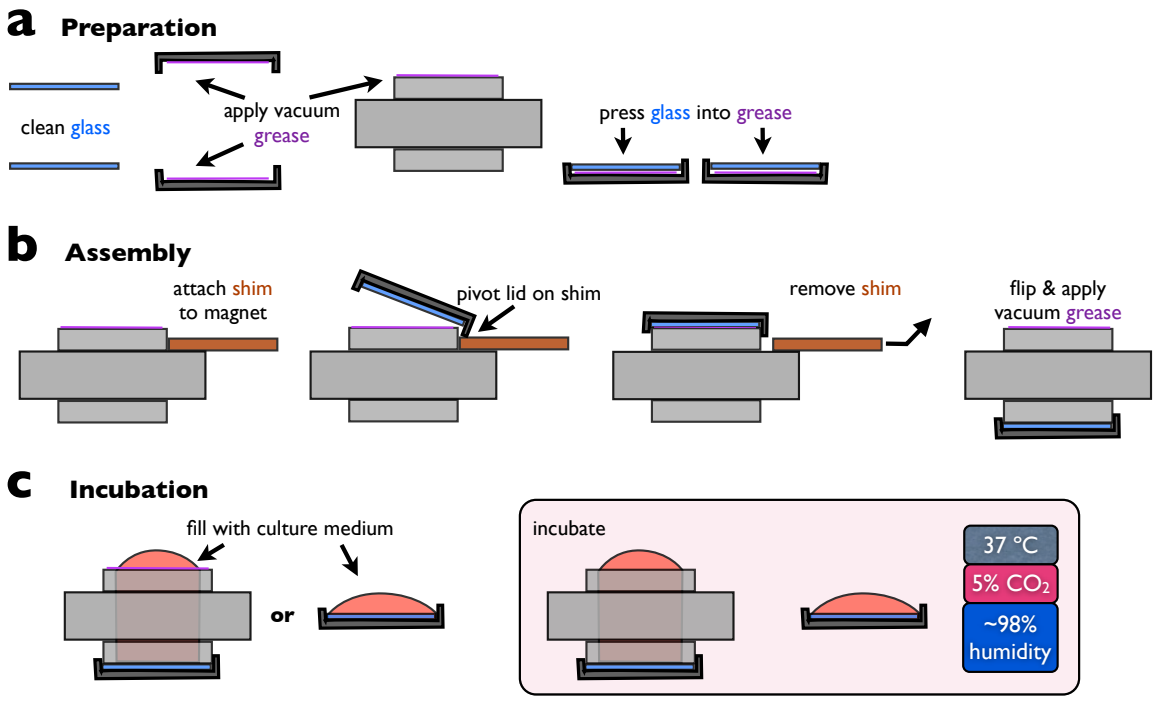

Figure 19. MSLIC assembly. **(a)** Prior to assembly glass cover slips are cleaned and the MSLIC base and lids are coated with a thin (<1 mm) layer of silicone vacuum grease. **(b)** To avoid cracking glass cover slips on the MSLIC, a shim was placed on the base and used as a pivot point. After attaching one glass cover slip, the MSLIC is flipped over in order to coat the other side with vacuum grease prior to incubation. **(c)** Cell culture medium and/or cells (not shown) were incubated in the lid and/or the MSLIC at 37°C, 5% CO_2, and 98-99% humidity). The MSLIC is closed by repeating the first three steps in (b).

Corning). The clean glass cover slips were carefully pressed into the MSLIC lids. To avoid cracking the glass cover slip during assembly, a shim was attached. Then the lid was pivoted on the shim rather than on the glass cover slip until flush with the MSLIC base (Fig. 19b). This created a chamber that was filled with cell culture medium and cells as needed. The open MSLIC and lid were incubated at 37ºC, 5% CO_2, and 98-99% humidity in order to equilibrate the medium and/or allow cells to adhere (Fig. 19c). The MSLIC was sealed immediately after removal from the incubator by quickly aspirating medium from the MSLIC lid, but not from the chamber, and then repeating the process shown in Fig. 19b. While closing the chamber, the meniscus of medium protruding above the MSLIC base prevented air entrapment.

Cell Culture and Acini Formation

Human head and neck carcinoma HEp3 and MCF10A cells were cultured in DME medium supplemented with penn/strep, HEPES buffer, non-essential amino acids, and 10% fetal bovine serum and according to the procedures of Ramirez et al. accordingly [68]. Cells were cultured at 37ºC in a humidified 5% CO_2 incubator and passaged every 3-4 days. Acini were formed by sandwiching MCF10A cells between two layers of matrigel according to the protocol of Debnath *et al.* [103]. However, instead of exchanging medium every 4 days, cells were grown in fluidic live-cell imaging chambers (Fig. 17b) with a recirculating supply of 20 mL changed weekly.

Microfluidics

Microfluidic devices were fabricated inside MSLICs (not shown) and fluidic live-cell imaging chambers by clamping a fluidic or microfluidic master mold against the chamber,

taping over holes in the sides, and pouring degassed polydimethylsiloxane prepolymer (Sylgard 184, Dow Corning) into the chamber. The polymer was then cured in an oven at 50 or 60 ºC for at least 3 hours or at room temperature for >24 hours. After carefully removing the master mold and tape from MSLICs, holes were partially punched through the top of the PDMS and through the side holes to create an elbow channel within the cured PDMS. This elbow channel was used to connect tubing into the sides of the chamber (Fig. 17d). For 3D cultures such as acini formation, the simple millifluidic chamber shown in Fig. 17b˝ (approximately 9 mm by 9 mm x 2 mm) was cast in PDMS in the MSLIC base.

Temperature Control

Temperature controllers are required to maintain a steady 37ºC (±1 ºC or less) for live-cell imaging. To achieve this microscope boxes were created. Initial designs were created from corrugated plastic crate material. After successfully maintaining temperatures, the plastic crate material was replaced with 1/2˝ transparent acrylic. By encasing the microscope base and most of the filter wheel chamber (upright microscope) or brightfield light source (inverted microscope), the stage and objectives were maintained at 37ºC as needed to avoid focal drift. Experimentation revealed that boxes with a large area (>1 ft^3) to the side of the microscope maintain a more constant temperature since they have a larger reservoir of air to dissipate the on and off switching of the heating element.

Temperature controllers were assembled from readily available components. A fan (4840N, Ebmpapst) and matching heating element (AF20-200-120-1AD10-4.7, Farnam) were bolted together and mounted from the top of the microscope box. The fan was plugged into an electrical outlet so as to continually circulate the air. A simple temperature controller (BAH-1000-SC, Big Apple Pet Supply) was purchased locally from a hardware store and used to power the heating element whenever the temperature at the probe dropped

below 37ºC. The probe was suspended near the stage of the microscope. Blowing air directly onto the stage caused fluctuations in focal distance corresponding to the on and off switching of the heating element. Therefore, air from the fan was directed toward the side or back of the microscope box.

Fluidic Setup

Tygon® tubing of 3/32˝ OD (S-50-HL, Saint-Gobain Performance Plastics) was used to connect fluidic MSLICs. The stainless steel tubing from 18G needles (305195, Becton Dickinson) was seperated from the Luer connector and blunted using a Dremel® tool with a cut-off blade. To prevent leakage we pressure fitted Tygon® tubing into the side holes of the MSLIC by first inserting 4-6 mm pieces of tubing into the side hole and then pressing 18G stainless steel tubing into the tubing causing it to expand and seal tightly against the hole. The excess stainless steel tubing protruding from the sides of the MSLIC was connected to long (~3´) pieces of Tygon® tubing in order to connect the MSLIC to a debubbler, an IPC tubing pump (Ismatec, Glattbrugg, Switzerland), and a cell culture medium reservoir (Fig. 17b-c).

Image Analysis

Analysis of the localization of fluorescent antibodies to membrane proteins was designed to include a human in the loop of analysis. First batch, automatic thresholding of the fluorescent images identified bright spots of antibody (see Appendix B the ImageJ macro entiteld "HILParticleAnalysis MeFirst"). After automatically identifying spots of antibody localization, manual screening was performed with the assistance of a second ImageJ macro "HILParticleAnalysis MeLast" (see Appendix B) in order to put a human in the loop of

analysis. This macro overlaid the bright spots onto the original DIC images allowing quick visualization and selection of specific spots. By running this second macro twice, we selected spots corresponding to areas of cell-cell contact and spots free of cell-cell contact. The bright spots corresponding to the cell-cell contact areas were divided by the sum of all the manually selected spots and multiplied by 100 in order to achieve a percentage (Fig. 20b-c). Average fluorescent intensity measurements were recorded for each image ImageJ and then converted into percentages by dividing each fluorescent intensity measurement by the brightest average measurement in the time series and multiplying by 100 (Fig. 20a,c).

Results and Discussion

Avoiding exposure to atmosphere and room temperature is key to successful assembly and analysis of cell phenomenon using closed live-cell imaging chambers. Fluidic chambers are more forgiving than closed non-fluidic chambers because improperly equilibrated medium due to atmosphere exposure can be replaced. In both cases exposure to room temperature should be minimized. To avoid such exposure MSLICs were designed to be quickly sealed after removal from the incubator and if properly handled require no cleaning. As shown in Fig. 19, glass cover slips can be cleaned, lids and the MSLIC base can be greased, MSLIC chambers can be sealed via magnetic force, cells can be incubated in this chamber or the MSLIC lid, and after incubation the MSLIC can be sealed quickly without breaking or dirtying glass cover slips. By carefully handling the ferromagnetic lids, the glass cover slips remained clean eliminating the need for cleaning after assembly and thus reducing assembly time and exposure to room environment. Furthermore the MSLIC can be filled with culture medium and incubated 60 minutes or more in order to achieve proper CO_2 concentrations in the medium. By sealing the chamber within a couple minutes of removal from the incuba-

tor the medium's pH remained equilibrated as observed via the phenol red pH indicator in the medium.

MSLICs facilitated time-lapse microscopy by stabilizing the cover slips, an unexpected result of sealing cover slips with magnetic force. Wet, slippery cover slips (e.g. cover slips covered densely with matrix proteins or cells) are difficult to seal against silicone vacuum grease and prone to drift in temporarily closed, auto-adhesive live-cell imaging chambers (as an example see Fig. 17a and a´). Magnetic force helped seal and stabilize slippery, wet cover slips on the MSLIC reducing drift in x, y, and z (data not shown).

MSLICs are adaptable to fluidic and 3D culture applications on the microscope. We fabricated MSLICs with holes through the side in order to connect tubing horizontally rather than vertically which would potentially interfere with maneuvering the microscope. (Fig. 17d). Three-dimensional cell culture experiments were performed after casting millifluidic chambers (Fig. 17d´) into the MSLIC base. Fluid flow helped maintain stable and viable 3D cultures for experiments such as the acini assay.

Cell Migration

MSLICs are compatible with MAts assays and single cell migration assays. The use of MSLICs with MAts enabled individual cell tracking as reported in Chapter 3, Fig. 12. Briefly, HEp3 cell migration was recorded in 5 minute intervals for 16 hours in MSLICs for both scratch assays and MAt migration assays (Fig. 12a-b). Quantifying migration via area analysis resulted in equal migration rates for MAts and scratches (Fig. 12d). However, the time-lapse images showed distinct differences (Fig. 12a-b). Individual cells in the MAts assay migrated very rapidly or very little, whereas the cells in the scratch assay migrated up to a certain point and then turned 90 degrees. Quantifying these differences required tracking individual cells and calculating their productive migration, i.e. migration directed into the void (Fig. 12e).

This single-cell level of migration analysis was possible because of the combination of MAts, MSLICs, and video-microscopy.

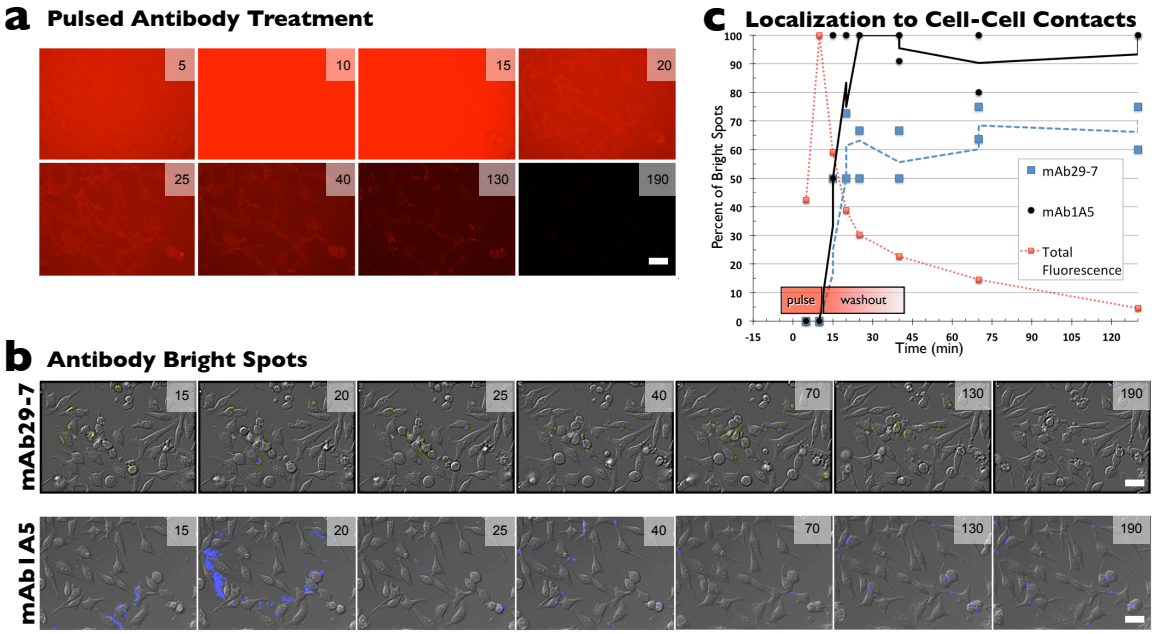

Figure 20. MSLICs deliver pulsed treatment of fluorescent antibodies. **(a)** Fluorescently labelled antibodies produce a strong signal while treating cells and being washed out over a 190 minute period. **(b)** Automated thresholding identifies bright spots of antibody clusters of the control antibody mAb29-7 and mAb1A5 which binds to membrane protein CD-151 causing increased clustering at areas of cell-cell contact compared to mAb29-7. **(c)** Plot of the percentage of antibody overall intensity and antibody bright spots in areas of cell-cell contact over time. Scale bars, 50 μm.

Pulsed Treatment

Using MSLICs, we also observed the dynamic cellular response to a pulse of solution containing an antibody mAb1A5 against membrane protein CD-151 versus a control antibody mAb29-7 which binds a membrane protein (CD44) without impacting cellular behavior (Fig. 20) [88]. The pulse of antibody was visualized via fluorescence (Fig. 20a and c, red line). After the intensity rose to its maximum level, we stopped the flow for 5 minutes. Then the medium containing treatment was replaced with fresh medium as seen by the de-

crease in intensity in Fig 18a and c, red line. Clustering of the antibody was observed within 15 minutes (Fig. 20a-b) and continued throughout the three hours of observation.

We anticipated that mAb1A5 would cluster in areas of cell-cell contact because it is known to inhibit cell migration in vitro and prevent metastasis in vivo [88,104]. This is currently thought to occur through the cell-cell adhesion molecule ALCAM. Using a human in the loop algorithm (see Appendix B), antibody clusters occurring in areas of cell-cell contact were analyzed for mAb1A5 and mAb29-7 (Fig. 20b-c). Conditions were observed in duplicate for each antibody. The resulting percentages for each set of images are shown in Fig. 20c. During the roughly 30 minute period in which excess antibody was being washed out, trends were not clear. This may be due to noise and improper detection of antibody clusters (Fig. 20b, mAb1A5 at 20 min.). During the second hour mAb1A5 clustering in areas of cell-cell contact was nearly 100% whereas mAb29-7 was only 60-70%.

3D Culture of Acini Under Long-Term Flow

MCF-10A cells were grown in matrigel on glass cover slips and sealed via clamping in millifluidic chambers (Fig. 17b). Acini were cultured with 20 mL of medium which was continuously recirculated and replaced weekly. After 16 days of culture, time-lapse images were recorded revealing cell motion within the non-invasive acini (Fig. 21a, arrow). Such motility was also observed and published by Pearson and Hunter [105]. After recording cell motility for 4 hours, the chambers were opened. The acini were removed, fixed, sectioned, and stained with H&E. This revealed that the acini were not hollow as expected but filled with dead cells (Fig. 21b). This may be related to providing continuous replenishment of medium or other unknown factors.

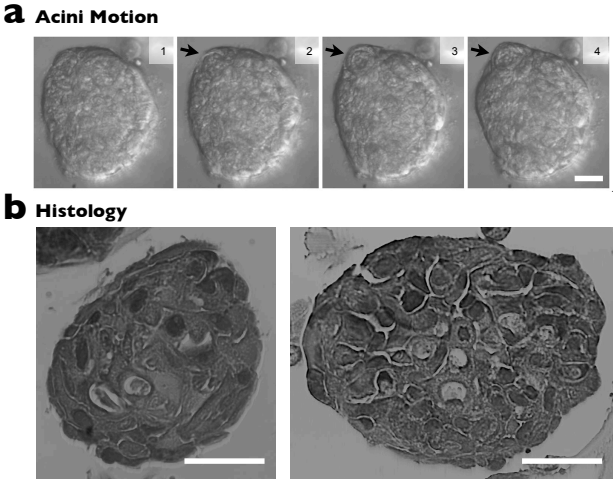

Figure 21. MCF10A acini formed solid cores in MSLICs. **(a)** After culturing MCF10A mammary epithelial cells in matrigen for 16 days, time-lapse microscopy recorded significant cell motion in the acini over a 4 hour period (arrow). **(b)** Subsequent fixation and histology revealed a solid core of dead cells whereas acini experiments in culture dishes which have their medium changed every 4 days are hollow. Scale bars, 0.1 mm.

MSLICs were designed to facilitate live-cell microscopy and provide control via fluidics over the soluble microenvironment of the cells being studied. Non-fluidic and fluidic versions were created. Both versions are compatible with MAts assays as well as other cell-based assays. Fluidic MSLICs provide dynamic control of medium conditions and are operable with a variety of pumps and handheld syringes.

Future Directions

Hands-on experience with MSLICs has uncovered two potential improvements. First, MSLICs should be designed for autoclave sterilization. Current MSLICs and fluidic MSLICs contain permanently embedded NdFeB magnets. These magnets would lose magnetization in the temperatures of autoclave sterilization. Future versions fitted with magnets in a silicone or other removable glue would enable sterilization. Magnets would be removed and sterilized with 70% ethanol or ultraviolet light while the MSLIC frame and lids were

autoclaved and afterward be reattached to the MSLIC frame. This would enable autoclave sterilization of the assembled fluidic system and greatly reduce the risk of contamination.

Second, PDMS microfluidic devices should be designed specifically for the fluidic MSLIC. Microfluidic channels and chambers were tested in MSLICs using existing PDMS microfluidic designs which are flat except for the microfluidic channels and chambers (data not shown). However, these microfluidic devices were prone to leakage presumably due to the low breakthrough pressure between the PDMS and glass cover slips. Glass cover slips were pressed against the PDMS via magnetic force (Fig. 22a) whereas conventional PDMS microfluidic devices are permanently bonded to the glass. To increase the breakthrough pressure and prevent leakage, future MSLIC microfluidic devices should contain a raised

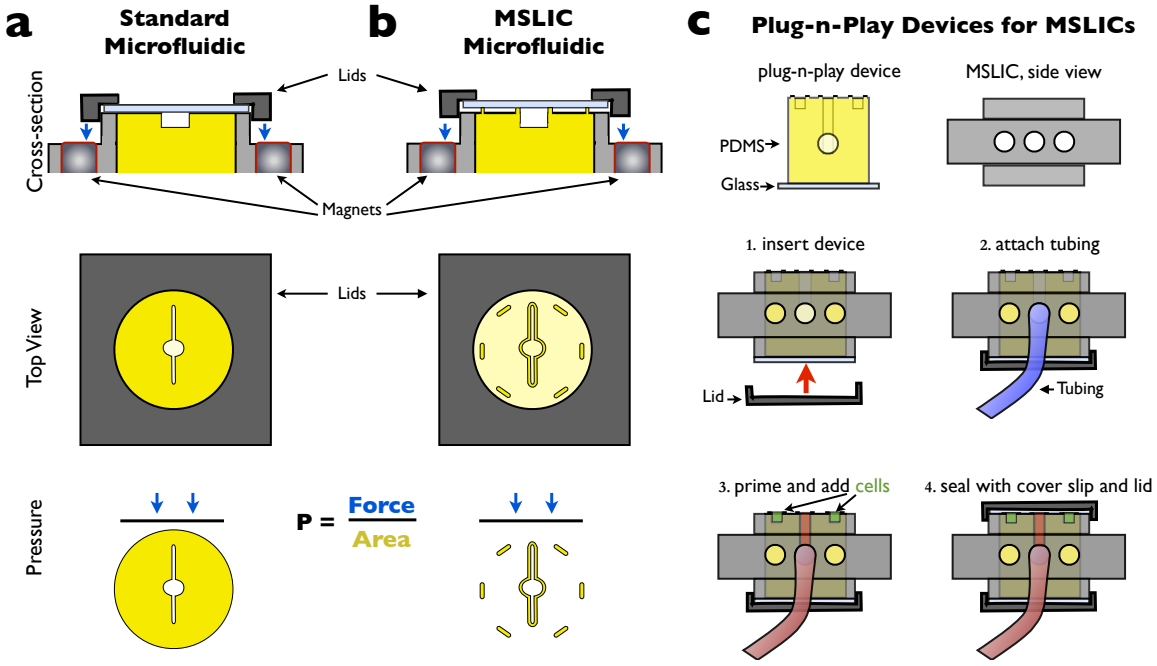

Figure 22. Incorporation of microfluidic devices into MSLICs. **(a)** PDMS Microfluidic devices are mostly flat creating a large contact area (top view, bright yellow). Magnetic attraction between the lids and magnets creates force (blue arrows). The pressure between the glass and PDMS microfluidic device is this force divided by the contact area. **(b)** Microfluidics can be designed with a raised ridge around the channels and chambers and ridges near the edge of the glass as needed to avoid cracking. The reduced contact area results in higher pressure. **(c)** Microfluidic and other devices can be prefabricated to the dimensions of the MSLIC enabling plug-n-play capability.

PDMS ridge around the fluidic passageways (Fig. 22b). By reducing the direct contact area, this ridge will experience a significantly higher pressure and thus raise the breakthrough pressure eliminating leaks between the PDMS and glass. Furthermore, these microfluidic devices can be fabricated independently to the dimensions of the MSLIC and then pressed into place, plumbed, and used (Fig. 22c). This "plug-n-play" approach eliminates the need to mix and cast PDMS in the MSLIC and the challenge of removing cast PDMS in order to switch to another device. Furthermore, the concept promotes MSLIC use with a wider variety of devices since third parties could fabricate their devices to the dimensions of the MSLIC.

With or without these design improvements, MSLICs enable control of the soluble environment surrounding cells which includes nutrients, cellular waste, stimulatory factors, and even dissolved gases such as oxygen and carbon dioxide. Cells in vivo may experience various conditions such as acidity, hypoxia, and nutrient deprivation which often fluctuate. For example, intermittent hypoxia occurs in the tumor microenvironment in vivo and has been shown to have significant effects on cells in vitro [106,107]. Fluidic MSLICs can recreate such fluctuations. For example, by switching between normoxic and hypoxic medium, intermittent or cyclic hypoxia can be simulated enabling nearly immediate observation of biological effects via live-cell microscopy. Because MSLICs are completely sealed, oxygen and other gases cannot escape even though PDMS itself is gas-permeable. Studying the biological effects of switching soluble conditions is an important future direction for fluidic MSLICs, and we have already shown that medium can be switched to antibody containing medium within 5 minutes and washed out within 45 minutes using a millimeter scale chamber (Fig. 16). With a microfluidic chamber delivery and washout times should be reduced by a few orders of magnitude. Regardless of chamber size washout is expected to take longer than delivery for medium containing soluble factors including oxygen [107].

Conclusion

MSLICs enable rapid assembly of cell-based assays with the advantage of being a closed chamber and only require temperature regulation on the microscope. With MSLICs the pulsed delivery and subsequent clustering of antibodies targeting two cell-membrane proteins were investigated. Additionally, 3D cultures of acini were grown for 16 days after which cell motility on the surface of the acinar structure was observed via video-microscopy. MSLICs provide significant versatility by functioning as static or dynamic fluidic devices. Furthermore, millifluidic and microfluidic chambers can be fabricated into the large opening of the MSLIC enabling a wide variety of 2D and 3D assays. A promising direction for MSLIC research is the investigation of cellular responses to dynamically controlled medium fluctuations of oxygen levels and/or acidity. The clever use of magnetic force to seal a live-cell imaging chamber combines the benefits of both clamping and auto-adhesive temporarily closed chambers. Using MSLICs drift was reduced without sacrificing ease of assembly. Consequently, MSLICs represent a highly versatile base for numerous static and fluidic cell-based experiments.

Acknowledgements

We thank John Fellenstein for his significant contribution to the final design of MSLICs as well as machining all the MSLIC components. The Vanderbilt Institute for Integrative Biosystems Research and Education (VIIBRE) provided microfabrication resources. Funding was provided through R01 CA143081-01 and P01 CA040035.

CHAPTER V

CONCLUSION

When tools for biological studies are designed to compliment and integrate with each other, the range of complexity controlled by the user can be increased in a stepwise or scalable manner without sacrificing significant analytical ability. Such tools constitute systems of scalable complexity and are greatly needed in order to fill the gap between simple in vitro and in vivo models. The development and implementation of systems of scalable complexity will facilitate discovery, accelerate translational research, and ultimately improve prevention, detection, and treatment of disease. The overarching goal of this dissertation research has been the development and implementation of an easy-to-use system of scalable complexity. Pursuit of this goal resulted in the complimentary and synergistic MAts and MSLIC tools.

Impact of this Work

On their own, MAts and MSLICs have already made significant contributions to the fields of cell migration, microfluidics, and live-cell microscopy. As a system their impact is still in its infancy but is expected to greatly surpass all current accomplishments. This expectation is justifiable. MAts have already been implemented in over six Vanderbilt laboratories. At the time of writing, the laboratories of Dr. Coffey, Dr. Kaverina, Dr. Moses, Dr. Pietenpol, Dr. Zijlstra, and Dr. Zutter have utilized MAts in place of scratch and other cell migration assays. Additionally, MAts are patent pending and have attracted the attention of various suppliers of biological materials and assays.

Nevertheless, if MAts and MSLICs only inspire development of other systems of scalable complexity, their impact will have been significant and important. Technology has provided the capability to create scalable complexity and fill the gap between in vitro and in vivo models. With creativity, research, and development; more easy-to-use systems of scalable complexity will be developed filling the gap and improving the relevance of basic biological research to clinical disease.

2D Migration

MAts enable studies normally carried out with single cells such as chemotaxis, haptotaxis, and durotaxis to be executed with densely organized cells. Using a dense cancer cell population and MAts we revealed an unexpected chemotactic inhibition of migration. Block MAts placed side-by-side created areas of collagen and fibronectin forming an interface. Cells patterned around block MAts adhered to one protein and were allowed to migrate onto the other protein when the MAts were removed. On either collagen or fibronectin alone, the cells migrated robustly (Fig. 14a-b). Surprisingly, migration was significantly inhibited when cells adhere to collagen and were allowed to migrate onto fibronectin. This study demonstrates not only that the collagen-fibronectin interface can act as a chemotactic inhibitor of migration in only one direction but also that using MAts common single cell migration studies such as chemotaxis can be extended to dense or confluent cells.

Furthermore, MAts and MSLICs together have revealed significant differences between "wound healing" assays such as the scratch assay and "space-filling" assays such as the MAts migration assay. Initial widths were more reproducible using MAts than scratches (Fig. 8e-f); however, the migration rate of MAts was more varied than for scratches (Fig. 12d-e). This increased variation corresponds directly to the less-damaging and less-stimulating process of removing MAts versus scratching and is currently attributed to the naturally-occurring

heterogeneity within a cell population. Scratching appears to mask this heterogeneity by damaging the cells, orienting the substrate, or possibly both. Understanding this heterogeneity is important to our understanding of therapeutic efficacy or failure and represents a form of biological complexity of great relevance to in vivo biology [108,109].

3D Culture

MSLICs on their own revealed motility of non-invasive epithelial cells on acini in matrigel (Fig. 21a). This was also observed by Pearson and Hunter and published only months ahead of our discovery [105]. Consequently, out investigations were not pursued further. Nevertheless, these observations demonstrate the high spatial and temporal resolution possible in 3D assays using MSLICs.

Future Directions

The System: MAts and MSLICs together

Various areas of biological research will benefit from systems of scalable complexity such as the system presented in this dissertation. Several areas revolve around simulating fluctuations that occur in vivo. For example the effect of intermittent hypoxia on cell migration, angiogenesis, and cancer are being intensely investigated [106,107,110,111]. However, most of these studies focus on large-scale effects rather than direct cellular responses to fluctuations. Observing these cellular responses requires making observations at or above the Nyquist frequency, which is twice the frequency of the fluctuation. For example, fluctuations in oxygen partial pressure in vivo have been observed to cycle once to thrice per hour [106]. Observing such phenomenon generally requires live-cell microscopy. MSLICs enable

live-cell microscopy while controlling fluid conditions in order to create the desired fluctuations. This can be achieved on any microscope with a temperature controlled environment. MSLICs and MAts are ideal tools for in vitro investigations of the cellular effects of fluctuations because they are easily implemented and enable high temporal resolution of the related cellular processes as well as a functional measure of cell behavior: migration.

Another promising area of research for MAts and MSLICs is heterogeneity within cell populations. Although it is well-documented that a population of cells from a single cell type will display heterogeneous properties and behavior in 2D culture, these studies need to be extended into 3D [107,112,113]. MSLICs may help answer questions such as, "Will cell-to-cell phenotypic heterogeneity increase or decrease in 3D?" Because MSLICs enable perfusion of 3D culture, the 3D environment can be controlled precisely, fluorescently labelled, and even fixed in place on the microscope. These capabilities will facilitate studies of cellular heterogeneity in 3D. Additionally, MAts can provide a needed functional readout: cell migration.

MAts Alone

Some promising future directions for MAts independent of MSLICs are protein printing and bead or 3D matrix overlays. Various approaches using PDMS stamps have been developed for the purpose of printing or transferring via contact a pattern of proteins onto a substrate such as glass or plastic [79,114-116]. Since MAts are made of PDMS, standard microcontact printing techniques should be readily implementable with MAts. The result would enable simultaneous protein printing and cell adhesion. While proteins were printed by the MAt, cells could be plated and allowed to adhere around the MAt. Preliminary investigations by Eric Bankaitis revealed the ability of MAts to print proteins with existing MAts. The printed proteins patterns were irregular. Developing a homogenous protein print using

MAts would greatly simplify the process of creating matrix protein interfaces. Currently, creating matrix protein interfaces requires multiple steps and involves moving block MAts manually as done for Fig. 14.

Though MAts are designed for 2D surfaces, they can also be overlaid to create a quasi 3D environment which is sometimes referred to as 2.5D. After removing MAts, we overlaid cells with collagen which subsequently polymerized forming a 3D matrix. However, the jostling involved in moving the cells from incubator to microscope caused the 3D collagen to detach. MAts successfully pattern cells on textured 2D surfaces such as nanofibers (Fig. 10). In order to avoid 3D matrix detachment in future studies, the cells could be patterned on a textured surface around which the collagen would polymerize and thus anchor itself preventing detachment. A more interesting potential approach to overlaying cells involves magnetic beads. Magnetic beads large enough to avoid being endocytosed could be overlaid in place of MAts utilizing the same magnets that originally secured the MAts. Magnetic beads completely coated with polystyrene are currently used to bind a variety of important biological proteins and are compatible with living cells. By attaching cell-cell adhesion molecules to these beads and overlaying them on MAts migration assays, the role of cell-cell contacts could be investigated while still providing a standard substrate for cell migration. Essentially, overlaying MAts migration assays with collagen on textured surfaces and with magnetic beads adds to the range of complexity achievable with MAts 3D migration and simulated cell-cell interactions respectively.

MAts have also found application in the field of microfabrication. Common, readily accessible microfabrication techniques create micrometer and even sub-micrometer features. However, these features must be integrated with larger ones in order to connect to the larger, centimeter and meter scale world of humans. Common microfabrication techniques are unable to create the large required features. By sealing MAts against a microfabricated surface,

MAts can exclude polymers and resins as they cure and thus create interfaces between the micro- and macro-scales (see Appendix D). These MAts-made interfaces represent a significant improvement over the common practice of punching holes through PDMS microfluidic devices (Fig. D3). The use of MAts in microfabrication should overcome many current limitations of interfacing microscale features with the macroscale features needed for manual handling.

Build Bridges: The need for systems of scalable complexity

The system of scalable complexity presented herein represents a bridge that begins with in vitro models and extends towards in vivo models. In engineering terminology this system represents a bottom-up approach. However, the top-down approach is also applicable to the creation of systems of scalable complexity. Certain model organisms are readily amenable to integration with microfluidics and even-high throughput analysis. For example microfluidic devices have been developed for studying both the nematode Caenorhabditis elegans and zebrafish Danio rerio [117-120]. Similarly, we have incorporated simple microfabricated structures on the chick embryo for analysis of angiogenesis and tumor-host interactions. This device, called the angiogenesis disk, improves analytical capacity for angiogenesis studies on the chick embryo by orienting the interaction between tumor and host into the optical plane of the microscope (Fig. 23). Because the angiodisk is thin (0.5-1.5 mm) analysis can be performed on common fluorescent microscopes. The angiodisk and fish and worm microfluidic devices represent important steps towards a top-down system of scalable complexity.

Regardless of the engineering approach taken, the development of systems of scalable complexity is crucial to improving biomedical research. Systems of scalable complexity provide versatility and reduce barriers to translating research from simple to more complex

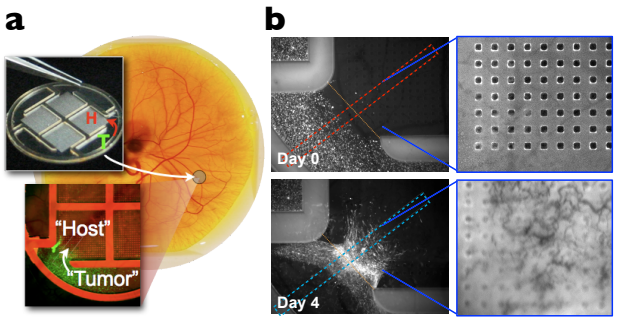

Figure 23. The angiodisk aligns the tumor-host interaction enabling simple image aquisition and analysis. **(a)** The angiodisk rests on the highly vascularized chorioallantoic membrane of the *ex ovo* chick embryo and contains tumor cells initially in a chamber separate from the host chamber into which new vessels form. **(b)** At day 0 tumor cells are visible via fluorescence (left image) in the tumor chamber (lower left) and the host chamber is void of blood vessels (magnified right image). After 4 days the tumor cells have migrated into the host chamber (left image) and blood vessels have also formed there (right image).

studies or vice versa. They represent bridges across the great divide between in vitro and in vivo models. Unfortunately, too often research and development of new tools and techniques only serves to place stepping stones in this great divide. Great effort is given to achieving a technological advancement. Unfortunately, less effort is given to integration and broad implementation. As a result many incredible tools become orphaned remaining unimplemented in biological research. Transforming stepping stones into bridges requires the effort of both engineers and biologists and their willingness to reach across the differences between their respective fields. Technology has given us the possibility of creating systems of scalable complexity providing the versatility and ease of use essential to enable more groundbreaking research. It is now up to us to put forth the effort, find the necessary creativity, and make these bridges a reality. The building of bridges across the in vitro to in vivo divide will accelerate biological research and discovery and ultimately improve society's ability to prevent, diagnose, and treat disease.

APPENDIX

A. PROTOCOL FOR THE BASIC MAGNETICALLY ATTACHABLE STENCIL MIGRATION ASSAY

Materials

Magnetically Attachable Stencils (MAts)

Magnet arrangements

Spray bottle with 70% ethanol

Extra-cellular matrix (ECM) proteins

Cell culture medium

Phosphate Buffered Saline (PBS)

Growth factors, inhibitors, or other treatments

Procedure

Preparation of MAtS

1| MAtS need to be primed for 24 hours by immersion in deionized water. Clean and sterilize MAtS with 70% ethanol. Spray ethanol directly against the contact surface of the MAtS to remove unwanted dust or debris. Then soak the MAtS in 70% ethanol for 10 minutes. Dry the MAtS in an oven (~60 ºC) or under vacuum (-20 mm Hg) to remove any ethanol that may have been absorbed into the MAtS.

▲ CRITICAL STEP If simply removed from soaking in Ethanol and left at room temperature, MAtS may look dry and still retain ethanol within which will slowly diffuse out into the cell culture medium altering normal cell behavior. For this reason it is important to use a

source of heat or vacuum or combination of the two such as a vacuum oven. However, high temperatures (>70ºC) may create distortions in the MAtS as the elastomer shrinks.

Coating of cell culture dishes

2| Coat 6 (or 12 well plates) with proper ECM substrates (generally Collagen at 100 μg/ml in PBS) by incubating the dishes overnight at 4 ºC or for 2 h at 37 ºC without rotation or shaking.

3| Remove the unbound ECM substrate. (Optional, block the coated dishes with PBS containing 0.5% bovine serum albumin for 1 h at 37 ºC.) Then, wash twice with PBS and refill the wells with 1.5 ml or more (750 μl or more for 12-well plates) of media before plating the cells. (It is recommended to either use a lower percentage of serum than that used in the growth media to minimize cell proliferation or plate cells in full growth medium until they adhere to the dish, usually 5-6 hours, followed by overnight serum starvation.)

▲ CRITICAL STEP Apart from the serum, if the assay is to study the effects of growth factors or other compounds, these soluble factors may need to be included in the media before addition of cells or added to the serum free medium during serum starvation.

Applying the cells

4| Attach the multi-well plate to the magnet arrangement and place the MAtS into the multi-well plate. Incubate at 37 ºC and 5% CO_2 in order to maintain proper pH in the medium while preparing the cells.

5| Resuspend subconfluent growing cells in a tissue culture dish by washing cells twice with PBS, adding trypsin, and incubating until cells have detached. Then mix cells with medium containing serum. Gently pipette the solution and rock the dish to disperse the cells

equally. Take an aliquot from the cell suspension and determine the cell count using a hemocytometer.

6| Plate sufficient cells onto the prepared 6 or 12-well plate to create a confluent monolayer (for 6-well plate: 0.8 M actively growing HEp3 cells, 1 M A549 cells). The required number of cells for a confluent monolayer depends on both the particular cell type and the size of the dish and should be adjusted accordingly. Incubate the dishes properly for 5-16 hr at 37 ºC and 5% CO_2, allowing cells to adhere and spread across the substrate. (Optional, cells may be subjected to serum starvation or other conditions for multiple days prior to the initiating the assay)

Initiating the MAtS assay (and optional simultaneous scratch assay)

7| Remove magnets from the multiwall plate being careful to lift the multiwall plate straight up until it is away from the magnets. Then remove MATs by carefully lifting the attached plastic tag fastener or an arm of the MAtS so as to avoid any twisting or sliding of the MAtS that would remove cells from the substrate. When grabbing the arm of the MAtS a broad-tipped tweezer seem to work better than fine-tipped tweezers. (Optional, scrape the cell monolayer in a straight line to create a "scratch" with a p200 pipet tip. Remove the debris and smooth the edge of the scratch by washing the cells once with 2 ml of medium or PBS and then replace with 2-3 ml of medium specific for the assay.)

▲ CRITICAL STEP Proper removal of the MAtS results in precise widths between cell monolayers. Wider than normal (>700 μm wide) cell-free areas especially near the tips of the star MAtS or on only one or two arms suggest that the MAtS were not removed properly and scraped some cells away.

8| Acquire the initial images. To repeatedly obtain the same field of view during image acquisition, start from either the end of an arm or the center of the MAtS and capture images of adjacent areas. Using a 10x objective, capture 3 or 4 adjacent pictures on each of the 4 arms of the MAtS. Always start from either the ends or the center and capture adjacent images in a specific order, for example top, left, right, and bottom arm. (Optional, scratches can similarly be referenced from the end of the scratch or the intersection of two scratches that cross in order to ensure that the same area is imaged for each timepoint.)

9| Place the dish in a tissue culture incubator at 37 ºC until the next timepoint, (generally 8-18 hours). The time frame for incubation should be determined empirically for the particular cell type used. Multiple timepoints can be taken as needed.

▲ CRITICAL STEP Allowing cells to completely close the open area (or scratch) creates imprecise data since it cannot be determined what timepoint the open area closed. For this reason it is best to choose a final timepoint that allows the cells under the fastest migrating condition to close between 60% and 80% of the original open area.

10| Acquire additional images following the same order as before. Incubate and repeat steps 9 and 11 until all timepoints have been imaged.

Analysis of Images

11| Analysis of the images can be performed with a variety of software. Our lab uses TScratch for quantification [57]. Images should be placed in subfolders for each timepoint and then renamed so that corresponding images in each timepoint have the same name. For each image, TScratch determines what area are covered with cells and then calculates the percent of the total pixels that are not covered. This is the percent open area. Each image can be manually adjusted, though having to adjust the majority of the images manually sug-

gests that the analysis parameters need to be modified. For more details on analysis see the Calculations section.

▲ CRITICAL STEP MAtS enable powerful statistical analysis of collective cell migration with the ability to resolve fine differences in cell conditions. This requires capturing clean images suitable for automated analysis from multiple points (8-12) on each MAtS.

Timing

Step 1: 40 min

Step 2: 2 h or overnight

Step 3: 1.5 h

Step 4: 5 min

Step 5: 30 min

Step 6: 5-16 h (as needed)

Step 7: 10 min

Step 8: 30 min

Step 9: 8–18 h (as needed)

Step 10: 30 min

Step 11: 30-60 min (as needed)

Calculations

Calculating rate of migration in μm/hr

Since, scratches vary widely in initial size, a comparison of the actual microns traveled per unit time may be more informative. The open areas determined by TScratch can be

used for this calculation providing that the following assumption is true: the height of the wound area equals the height of the image. This being true it is easy to go from

$$\%area = \frac{width_{wound} * height_{wound}}{width_{image} * height_{image}} * 100$$

to

$$\%area = \frac{width_{wound}}{width_{image}} * 100$$

to

$$width_{wound} = width_{image} * \frac{\%area}{100}$$

Now take the difference of the widths of the wounds and divide by time to get your rate. Use the appropriate calibration to get μm/hr rather than pixels/hr.

Rotating the camera so that the boundary between cells and wound area is often necessary, especially when dealing with scratches, in order to keep the height of the wound equal to the height of the image.

It is also important to note that the width of the wound closes twice as fast as the cells migration rate because there are two monolayers of cells migrating towards each other to close the wound.

Calculating Percent Closure

The % wound closure is calculated using the percent open area of two different timepoints as follows.

$$\%closure = \frac{\%area_{initial} - \%area_{final}}{\%area_{initial}} * 100$$

Acknowledgements

Much of the above content was adapted from the publication of Liang et al. entitled "In vitro scratch assay: a convenient and inexpensive method for analysis of cell migration in vitro"[13]. Numerous MAts' users have also contributed to the development of this protocol. Among them the most notable contributors were Katie Hebron, Tara Fox, and Eric Bankaitis.

B. IMAGEJ MACROS TO FACILITATE IMAGE ANALYSIS

Scratch Assay Analysis Macro

This macro has two highly similar variations. One method uses ImageJ's edge detection algorithms to help create the contrast needed to successfully run ImageJ's particle analyzer. The second method uses a background subtraction instead. [121]

Code for Edge Detection and Thresholding Method

```
//This macro was designed to measure the size of the scratch wound in a wound scratch assay. It uses an edge-detection and thresholding technique.
// It will batch process all images in a directory. Images captured by time-lapse should be compiled into stacks using a tool similar to "Metamorph nd & ROI files importer (nd stack builder)" by Fabrice P. Cordelières
//Images to be analyzed should be placed in one directory (Source Directory)
//A second directory should be created to save results files and images (Destination Directory)
//Setting correct Lower and Upper thresholds is important to obtain a good result.

// Developed by: Stuart J Gallagher; William J Ashby; Fabrice P Cordeliéres; Lionel Larue.
//Institut Curie; Vanderbilt University.

//This program is free software; you can redistribute it and/or modify it under the terms of the GNU General Public License as published by the Free Software Foundation; either version 3 of the License, or (at your option) any later version. This program is distributed in the hope that it will be useful, but WITHOUT ANY WARRANTY; without even the implied warranty of MERCHANTABILITY or FITNESS FOR A PARTICULAR PURPOSE. See the GNU General Public License for more details. You should have received a copy of the GNU General Public License along with this program. If not, see http://www.gnu.org/licenses/.

dir1 = getDirectory("Choose Source Directory ");
dir2 = getDirectory("Choose Destination Directory");
list = getFileList(dir1);
x = getNumber("Input lower threshold", 0);
y = getNumber("Input upper threshold", 80);
```

```
//This generates a message box to generate the lower (x) and upper (y) bounds for thresholding later on.

setBatchMode(true);    //use this to save time by not displaying images

 for (i=0; i<list.length; i++){
        showProgress(i+1, list.length);
        open(dir1+list[i]);

        run("8-bit");   //my experience is that I get better results in 8-bit.
        run("Duplicate...", "title=copy duplicate");
        selectWindow(list[i]);
        run("Sharpen", "stack");  //this step really helps a lot for thin cells with thin lamellopodia
        run("Find Edges", "stack");

        setThreshold(x,y);

//very important to get an appropriate threshold

        run("Convert to Mask", " ");
        run("Analyze Particles...", "size=12000-Infinity circularity=0.00-1.00 show=Outlines summarize stack");
        selectWindow("Summary of "+list[i]);
        saveAs("Text", dir2+list[i]);
        run("Close"); //This saves and closes the Analyze Particles results

        selectWindow("Drawing of "+list[i]);
        run("Red");
        run("Invert LUT");
        run("RGB Color");
        selectWindow("copy");
        run("RGB Color");
        imageCalculator("Add stack", "copy", "Drawing of "+list[i]);
        run("Size...", "width=600 constrain interpolate");
        saveAs("Tiff", dir2+"Drawing "+list[i]);
 //The above makes and saves an file containing the original image overlaid with the outline of the wound that was fitted by the program.


        close();
        close();
        close();
 }
```

Code for Background Subtraction and Thresholding Method

```
//This macro was designed to measure the size of the scratch wound in a wound scratch assay. It uses a back-ground subtraction technique.
// It will batch process all images in a directory. Images captured by time-lapse should be compiled into stacks using a tool similar to "Metamorph nd & ROI files importer (nd stack builder)" by Fabrice P. Cordelières
//Images to be analyzed should be placed in one directory (Source Directory)
//A second directory should be created to save results files and images (Destination Directory)
//Setting correct Lower and Upper thresholds is important to obtain a good result.

// Creator: Stuart J Gallagher; William J Ashby; Fabrice P Cordeliéres; Lionel Larue.
//Institut Curie; Vanderbilt University.

//This program is free software; you can redistribute it and/or modify it under the terms of the GNU General Public License as published by the Free Software Foundation; either version 3 of the License, or (at your option) any later version. This program is distributed in the hope that it will be useful, but WITHOUT ANY WARRANTY; without even the implied warranty of MERCHANTABILITY or FITNESS FOR A PARTICULAR PURPOSE. See the GNU General Public License for more details.

dir1 = getDirectory("Choose Source Directory ");
dir2 = getDirectory("Choose Destination Directory");
list = getFileList(dir1);

x = getNumber("Input lower threshold", 0);
y = getNumber("Input upper threshold", 80);
//This generates a message box to generate the lower (x) and upper (y) bounds for thresholding later on.
setBatchMode(true);    //use this to save time by not displaying images

 for (i=0; i<list.length; i++){
        showProgress(i+1, list.length);
        open(dir1+list[i]);
        run("8-bit");   //my experience is that I get better results in 8-bit.
        run("Duplicate...", "title=copy duplicate");
        selectWindow(list[i]);

        run("Subtract Background...", "rolling=30 light stack");
        run("Enhance Contrast", "saturated=5");
        run("Invert", "stack");

        setThreshold(x,y);

        run("Convert to Mask", " ");
        run("Analyze Particles...", "size=12000-Infinity circularity=0.00-1.00 show=Outlines
summarize stack");
        selectWindow("Summary of "+list[i]);
```

```
        saveAs("Text", dir2+list[i]);
        run("Close");  //This saves and closes the Analyze Particles results

        selectWindow("Drawing of "+list[i]);
        run("Red");
        run("Invert LUT");
        run("RGB Color");
        selectWindow("copy");
        run("RGB Color");
        imageCalculator("Add stack", "copy", "Drawing of "+list[i]);
        run("Size...", "width=600 constrain interpolate");
        saveAs("Tiff", dir2+"Drawing "+list[i]);

//The above makes and saves an file containing the original image overlaid with the outline
of the wound that was fitted by the program.

        close();
        close();
        close();
}
```

Human-in-the-Loop Particle Analysis

Features

This pair of macros runs FIJI's particle analysis algorithm on a batch of images and then enables a user to screen through the automatic analysis and select the relevant images [122]. The first macro performs batch particle analysis and requires user input of the source directory and results directory and enables modification of parameters for the analysis. The second macro enables the user to click on particles which are then boxed in red and included in the text file containing the filename, number in the list, and particle area. Right clicking essentially undoes the selection and turns the surrounding box to black. The selected particles are output in a text file containing the filename, list number which is used to keep track of the individual particle, and area of the particle. Additionally the original spreadsheet "ZZ Results.xls" found in the results folder is amended to contain a column with the heading "Focused" and saved as "Results With Focus Info.xls" in the parent directory. A value of 1

in this "Focused" column indicates that the particle was selected. Simply sorting the spreadsheet using this list will facilitate elimination of the unselected particles. This pair of macros greatly improves automated analysis by efficiently putting a human in the loop of automated image analysis. I recommend testing the macros against a small dataset to verify proper functionality before moving to a large dataset.

Code for the Automated Analysis

```
 //HumanInLoop ParticleAnalysis MeFirst.ijm
 //This macro was designed to facilitate particle analysis of a folder of images by automating the processing of the images in the folder. It is designed to work with the HumanInLoop ParticleAnalysis MeLast.ijm macro which then facilitates manual selection of desired particles by the user.
//Images to be analyzed should be placed in one directory (Source Directory)
//A second directory should be created to save results files and images (Destination Directory)
//Setting correct Lower and Upper thresholds is important to obtain a good result.

// Developed by William J Ashby.
// Vanderbilt University.

//This program is free software; you can redistribute it and/or modify it under the terms of the GNU General Public License as published by the Free Software Foundation; either version 3 of the License, or (at your option) any later version. This program is distributed in the hope that it will be useful, but WITHOUT ANY WARRANTY; without even the implied warranty of MERCHANTABILITY or FITNESS FOR A PARTICULAR PURPOSE. See the GNU General Public License for more details.

 //get appropriate directories from user
 dir1 = getDirectory("Choose Source Directory ");
 dir2 = getDirectory("Choose Destination directory");
 list = getFileList(dir1);

        //give user an opportunity to adjust default parameters to better fit their application
        Dialog.create("Adjust for objective magnification");
        Dialog.addNumber("Objective Magnification (use 10 if unknown)", 10);
        Dialog.addMessage("\tIf needed particle size limits can be adjusted below \nLeave mag. at 10 if customizing particle size limits\n");
        Dialog.addNumber("Minimum particle size (pixels^2)",10000);
        Dialog.addNumber("Maximum particle size (pixels^2)",1000000);
        Dialog.addMessage("\tIn the following dialogs select \n first the Source Directory, \nthen a Destinaion directory for Results");
        Dialog.show();
```

```
	//Assigning the entered values to variables
	magnification=Dialog.getNumber();
	userMin=Dialog.getNumber();
	userMax=Dialog.getNumber();
	sMin=magnification*magnification/100*userMin;
	sMax=magnification*magnification/100*userMax;

setBatchMode(true);

for (i=0; i<list.length; i++){
	//print (list[i]);
	open(dir1+list[i]);
	name=File.nameWithoutExtension;
	//Prepare the image by removing any scale and making 8-bit
	run("Set Scale...", "distance=0 known=0 pixel=1 unit=pixel");
	run("8-bit");
	saveAs("Tiff", dir2+i+" Original "+name);//Saving with this naming scheme is re-
quired for the MeLast macro to function
	//Threshold
	setAutoThreshold("Default");
	run("Convert to Mask");
	//Dilate to close little openings in spheres
	run("Dilate");
	run("Dilate");
	//Analyze particles
	run("Analyze Particles...", "size="+sMin+"-"+sMax+" circularity=0.00-1.00
show=[Count Masks] display exclude include summarize");
	//Save the masks file
	saveAs("Tiff", dir2+i+" CountMask "+name);//Saving with this naming scheme is
required for the MeLast macro to function
	close();
	//Save the thresholded image
	saveAs("Tiff", dir2+i+" Thresholded "+name);//Saving with this naming scheme is
required for the MeLast macro to function

}
//Save the results
selectWindow("Results");
saveAs("Results", dir2+"ZZ Results.xls");

//Save the summary
selectWindow("Summary");
saveAs("Text", dir2+"Z Summary.txt");
```

Code for the Human-in-the-Loop Analysis

```
//HumanInLoop ParticleAnalysis MeLast.ijm
```

```
  //This macro was designed to facilitate particle analysis of a folder of images by being run after automatically processing  the images in a folder using the HumanInLoop ParticleAnalysis MeFirst.ijm macro. It facilitates manual selection of desired particles by the user. Selected images are surrounded by a red box. Right-clicking removes the particle from those selected and turns the box black.
//The results directory needs to be the same as the results directory used with HumanInLoop ParticleAnalysis MeFirst.ijm
//The macro also asks for the parent directory which contains both the original data directory and the results directory.
//A brief text file will be saved with only the selected particles, their areas, and their filenames. The original spreadsheet of all the particles will be amended and saved as "Results With Focus Info.xls". This spreadsheet indicates selected particles by a value of 1 in the column labelled "Focused".

// Developed by William J Ashby.
// Vanderbilt University.

//This program is free software; you can redistribute it and/or modify it under the terms of the GNU General Public License as published by the Free Software Foundation; either version 3 of the License, or (at your option) any later version. This program is distributed in the hope that it will be useful, but WITHOUT ANY WARRANTY; without even the implied warranty of MERCHANTABILITY or FITNESS FOR A PARTICULAR PURPOSE. See the GNU General Public License for more details.

//Values for different Cursor Loc input
     shift=1;
     ctrl=2;
     rightButton=4;
     alt=8;
     leftButton=16;

//Ask user for the previous Results directory
  dir1 = getDirectory("Choose Results Directory ");
//Ask user for the parent directory which should contain both the original data folder and results folder
  dir2 = getDirectory("Choose Parent Directory ");

  list = getFileList(dir1);
//This Text window creates the list matching the numbers to filenames and is essential to making sense of the excel data file
  run("Text Window...","name=Filenames");
  print("[Filenames]","Filename\tNumber\tArea\n");

//check that a results list is included
  open(dir1+"ZZ Results.xls");

  print("Number of items in list "+list.length);

for (i=0; i<list.length-2; i=i+3){
```

```
        print("Now on list number "+i);
        open(dir1+list[i+1]);
        myImage=File.name;
        run("8-bit");
        open(dir1+list[i]);
        print(File.name);
        rename("CountMask");


//Crop image using the mask
        //duplicate the count mask then
        run("Duplicate...","title=cropMask");
        //make regular mask from count masks
        run("8-bit");
        run("Auto Threshold", "method=Default white");
        //Create extra space in order to see the edges
        for(ii=0; ii<30; ii++)
                run("Erode");
        run("Divide...", "value=255");
        setMinAndMax(0, 1);
        //Crop the original image
        imageCalculator("Multiply", myImage, "cropMask");

        rename("2Display");
        run("RGB Color");
        //Show the cropped image

//Ask for user to select focused spheres
    x2=-1; y2=-1; z2=-1; flags2=-1;
    setLineWidth(6);
    xNew=0;
    yNew=0;
    logOpened = false;

    print("Click particles you want to keep in your analysis\nClose Log Window to Move to
NEXT IMAGE");
    selectWindow("2Display");
    if (getVersion>="1.37r")
       setOption("DisablePopupMenu", true);
    while (!logOpened || isOpen("Log")) {
       getCursorLoc(x, y, z, flags);
       if (x!=x2 || y!=y2 || z!=z2 || flags!=flags2) {
                //lookup the value at x,y, in the count mask
                if (flags&leftButton!=0) {
                        selectWindow("CountMask");
                        xyVal=getPixel(x,y);
                        //If non-zero the get the related data
                        if(xyVal!=0){
                                xNew=x;
```

```
                                yNew=y;
                                valNew=xyVal-1;
                                selectWindow("2Display");
                                setColor(255,0,0);
                                drawRect(getResult("BX", valNew),getResult("BY", valNew),
getResult("Width", valNew), getResult("Height", valNew));
///                             //Get the data
                                setResult("Focused",valNew, 1);
                                print("Getting "+xyVal);

print("[Filenames]",myImage+"\t"+xyVal+"\t"+getResult("Area",valNew)+"\n");

                        }
                        selectWindow("2Display");
                        print("Close Log Window to Move to NEXT IMAGE");
                }
                if (flags&rightButton!=0) {
                        selectWindow("CountMask");
                        print("Close Log Window to Move to NEXT IMAGE");
                        xyVal=getPixel(x,y);
                        valNew=xyVal-1;
                        selectWindow("2Display");
                        setColor(0,0,0);
                        drawRect(getResult("BX", valNew),getResult("BY", valNew), getRe-
sult("Width", valNew), getResult("Height", valNew));
///                     //Remove xyVal from data list
                        setResult("Focused",valNew, 0);
                        print("Removing "+xyVal);
                }
                logOpened = true;
                startTime = getTime();
        }
        x2=x; y2=y; z2=z; flags2=flags;
        wait(5);
    } //Closing the log window proceeds to next image

    run("Close All");

}//end of for loop for processing images in directory

selectWindow("Results");
saveAs("Results", dir2+"Results With Focus Info.xls");

selectWindow("Filenames");
saveAs("Text",dir2+"Filenames and numbers");
```

Hyper with Stacks: An ImageJ Toolset

Features

This toolset was created to facilitate extraction of in focus time series from five dimensional (x,y,z,t,color) microscope datasets [123]. The toolset provides buttons on the ImageJ or FIJI toolbar to do the following: 1) Convert a stack to hyperstack (In order to save time, the default values can be adjusted in the code). 2) Set the focus point F1 (i.e. index your z position) for all the timepoints in between the previously indexed (or first) timepoint and the current timepoint. 3) Split out the currently selected channel from your hyperstack using the index of focused z positions. 4) Re-initialize F2, which sets the entire z index to the current z position and resets the previous timepoint to 0.

Installation

Simply save the code as a text file in the >Macros>Toolsets folder and restart ImageJ or FIJI. It will show up in the toolsets dropdown under the name of the text file, i.e. Hyper with Stacks or whatever you named it. Using FIJI on a Mac this folder is found by selecting show package contents on the FIJI application.

Code

```
// Hyper with Stacks.txt --version--1.5  2011-09-23
// Initial Toolset for manually extracting focused time series from hyperstacks by William J. Ashby, Vanderbilt University, Chemical and Physical Biology
//
 var v=versionCheck();
function versionCheck() {
   requires("1.41f");
   return 1;
}
```

```
var stackOrder = newArray("xyzct", "xyczt(default)", "xyctz", "xyztc", "xytcz","xytzc");
var displayMode = newArray("Color", "Composite", "Grayscale");
var zNum=0; var cNum=0; var tNum=0; var zz=0; var cc=0; var tt=0;
var zArray; var width;  var height;
var initialize = true;
var t0=0;

macro "Blank Action Tool - "{
}

macro "Stack to Hyperstack Action Tool -
C000D00D01D02D03D04D05D06D07D08D09D0aD0bD0cD0dD0eD0fD10D11D12D13
D15D16D1bD1cD1dD1eD1fD20D21D22D23D2bD2cD2dD2eD2fD30D31D32D33D34
D38D39D3aD3bD3dD3eD3fD40D41D42D43D44D48D49D4aD4dD4eD4fD50D51D52
D53D54D57D58D59D5aD5dD5eD5fD60D61D62D63D64D67D68D69D6aD6dD6eD6f
D77D78D79D85D86D87D88D89D8aD8bD96D97D98D99D9aDa7Da8Da9Db0Db8Cfff
D14D17D18D19D1aD24D2aD3cD47D70D71D80D81D82D8fD90Da0Da1Da2Da3Da4
DadDaeDafDb1Db2Db3Db4Db5DbcDbdDbeDbfDc0DccDcdDd0DdaDdcDddDe0De8
De9DeaDecDedDf0Df8Df9DfaDfcDfdCf00D91D92D93Dc1Dc2Dc3Dc4Dc5Dc6Dd1Dd
2Dd3Dd4Dd5Dd6Dd7De1De2De3De4De5De6De7Df1Df2Df3Df4Df5Df6Df7C00fD29
D8cD9eD9fDcbDceDcfDdbDdeDdfDebDeeDefDfbDfeDffC0f0D25D26D27D28D35D3
6D37D45D46D4bD4cD55D56D5bD5cD65D66D6bD6cD72D73D74D75D76D7aD7bD7
cD7dD7eD7fD83D84D8dD8eD94D95D9bD9cD9dDa5Da6DaaDabDacDb6Db7Db9Dba
DbbDc7Dc8Dc9DcaDd8Dd9"{

// In order to make my personal defaults automatically appear in the "Stack to Hyperstack" command, the following recreates the dialog window allowing user to modify the values as necessary without having to change the macro code
//  The defaults should be customized to match common numbers of channels, z-slices, and timepoints in your data
        Dialog.create("Convert to Hyperstack");
        Dialog.addChoice("Order", stackOrder);  //the stackorder is found a few lines above and can be rearranged in order to put your default order first

        // To make this macro use your default number of channels, slices, and time frames
        // simply change the numbers 2, 5, and 1 in the following 3 lines of code.
        Dialog.addNumber("Channels (c):", 2);
        Dialog.addNumber("Slices (z):", 5);
        Dialog.addNumber("Frames (t):", 1);

        Dialog.addChoice("Display Mode:", displayMode);
        Dialog.show(); //Displays the dialog box in order to get user input for the conversion from stack to hyperstack
                        //or hyperstack to hyperstack if you already have the data in a hyperstack

        //Assigning the entered values to variables
        ans1=Dialog.getChoice();
        cNum=Dialog.getNumber();
```

```
	zNum=Dialog.getNumber();
	tNum=Dialog.getNumber();
	ans2=Dialog.getChoice();

	zArray = newArray(tNum); //Initializing zArray which stores the index of in-focus z values over time

	run("8-bit");  //This line could possibly be omitted after testing for compatibility with other size stacks
	run("Stack to Hyperstack...", "order="+ans1+" channels="+cNum+" slices="+zNum+" frames="+tNum+" display="+ans2+"");
//End of dialog section

	initialize=true;
	print("\nInitialized");
}


macro "F1 Set Focus Action Tool - C000C111C222D34D35D36D37D38D39D3aD3bD3cD44D48D54D58D64D68D74Da4Da5Da6Da7Da8Da9DaaDabDacC222C333C444C555C666C777C888C999CaaaCbbbCcccCddCeeeCfffD00D01D02D03D04D05D06D07D08D09D0aD0bD0cD0dD0eD0fD10D11D12D13D14D15D16D17D18D19D1aD1bD1cD1dD1eD1fD20D21D22D23D24D25D26D27D28D29D2aD2bD2cD2dD2eD2fD30D31D32D33D3dD3eD3fD40D41D42D43D45D46D47D49D4aD4bD4cD4dD4eD4fD50D51D52D53D55D56D57D59D5aD5bD5cD5dD5eD5fD60D61D62D63D65D66D67D69D6aD6bD6cD6dD6eD6fD70D71D72D73D75D76D77D78D79D7aD7bD7cD7dD7eD7fD80D81D82D83D84D85D86D87D88D89D8aD8bD8cD8dD8eD8fD90D91D92D93D94D95D96D97D98D99D9aD9bD9cD9dD9eD9fDa0Da1Da2Da3DadDaeDafDb0Db1Db2Db3Db4Db5Db6Db7Db8Db9DbaDbbDbcDbdDbeDbfDc0Dc1Dc2Dc3Dc4Dc5Dc6Dc7Dc8Dc9DcaDcbDccDcdDceDcfDd0Dd1Dd2Dd3Dd4Dd5Dd6Dd7Dd8Dd9DdaDdbDdcDddDdeDdfDe0De1De2De3De4De5De6De7De8De9DeaDebDecDedDeeDefDf0Df1Df2Df3Df4Df5Df6Df7Df8Df9DfaDfbDfcDfdDfeDff"{
	run("Set Focus [F1]");
}


macro "Set Focus [F1]" {
	Stack.getPosition(cc,zz,tt);
	if(initialize){
		initialize=false;
		if (zArray==0){
			if (Stack.isHyperstack) {
				Stack.getDimensions(width, height, cNum, zNum, tNum);
				zArray=newArray(tNum);
				print("\nInitialized");
			} else {
				print("Close the error window and click the Run Stack to Hyperstack button");
			}
```

```
                }

                Array.fill(zArray, zz);
                t0=0;
        }
        for (i=t0; i<tt; i++){
                zArray[i]=zz;
        }
        if (t0<tt)
                print("z is set to: "+zz+"  for t: "+t0+" through "+tt);
        if (t0>=tt)
                print("current t="+tt+"  Proceed to t>"+t0+" or re-initialize");
        else
                t0=tt;
}


macro "Split Stack Action Tool - R9077C888R9977R0977"{
   if (nSlices==1)
                exit("Stack required");
   setBatchMode(true);
   stack1 = getImageID;
   w = getWidth; h = getHeight;  title = getTitle;
   stack2 = 0;
   n = zArray.length+1;
   Stack.getPosition(c,z,t);
   for (i=1; i<n; i++) {
      showProgress(i, n);
      selectImage(stack1);
      Stack.setPosition(c,zArray[i-1],i);
      run("Copy");
      if (stack2==0) {
         newImage("Focused_C"+c+"_"+title, "8-bit", w, h, 1);
         stack2 = getImageID;
      } else {
         selectImage(stack2);
         run("Add Slice");
      }
      run("Paste");
   }
   setSlice(1);
   setBatchMode(false);
   print("Successfully split out channel "+c+"\nTo split out a different channel using this z-
index, \nsimply change the channel in the hyperstack and repeat");
}

macro "F2 ReInitialize Action Tool -
C000C111C222D14D15D16D17D18D19D1aD1bD1cD24D28D34D38D44D48D54D85D
86D8bD8cD94D9aD9cDa4Da9DacDb4Db8DbcDc5Dc6Dc7DccC222C333C444C555C66
```

```
6C777C888C999CaaaCbbbCcccCdddCeeeCfffD00D01D02D03D04D05D06D07D08D09D
0aD0bD0cD0dD0eD0fD10D11D12D13D1dD1eD1fD20D21D22D23D25D26D27D29D2
aD2bD2cD2dD2eD2fD30D31D32D33D35D36D37D39D3aD3bD3cD3dD3eD3fD40D41
D42D43D45D46D47D49D4aD4bD4cD4dD4eD4fD50D51D52D53D55D56D57D58D59
D5aD5bD5cD5dD5eD5fD60D61D62D63D64D65D66D67D68D69D6aD6bD6cD6dD6e
D6fD70D71D72D73D74D75D76D77D78D79D7aD7bD7cD7dD7eD7fD80D81D82D83
D84D87D88D89D8aD8dD8eD8fD90D91D92D93D95D96D97D98D99D9bD9dD9eD9f
Da0Da1Da2Da3Da5Da6Da7Da8DaaDabDadDaeDafDb0Db1Db2Db3Db5Db6Db7Db9D
baDbbDbdDbeDbfDc0Dc1Dc2Dc3Dc4Dc8Dc9DcaDcbDcdDceDcfDd0Dd1Dd2Dd3Dd
4Dd5Dd6Dd7Dd8Dd9DdaDdbDdcDddDdeDdfDe0De1De2De3De4De5De6De7De8De9
DeaDebDecDedDeeDefDf0Df1Df2Df3Df4Df5Df6Df7Df8Df9DfaDfbDfcDfdDfeDff"{
        run("Re-Initialize [F2]");
}

macro "Re-Initialize [F2]" {
        initialize=true;
        print("Re-initialized, proceed with selection of focused z slices");
}


var pmCmds = newMenu("Popup Menu",
      newArray("Set Focus [F1]", "Re-Initialize [F2]","-","Copy", "Paste","Rename...")
        );

macro "Popup Menu" {
   cmd = getArgument;
   run(cmd);
}
```

Boundary Tracing and Analysis

Features

This toolset was created to determine the linearity of the cell boundary of cell migrating in a MAts or scratch assay. After thresholding an image, the area identified as containing cells is dilated in order to connect individual cells or groups close to the boundary. The resulting traces are easily aligned by rotating and translating in order to compare the total displacement along the boundary between control and experimental conditions. Visual depictions of multiple traces overlaid in different colors can also be very powerful (see Fig. 15b).

Installation

Simply save the code of the two macros as separate text file on you computer and open it with ImageJ or FIJI. It will ask for source and results directories then process the images.

Code for Boundary Tracing

```
//Batch Boundary Analysis draw trace.ijm

dirData = getDirectory("Select directory of data to process")
dirSave = getDirectory("Select location to save data")

list = getFileList(dirData);
setBatchMode(true);    //use this to save time by not displaying images

run("Set Measurements...", "area mean standard modal perimeter bounding shape median
skewness kurtosis redirect=None decimal=3");
print("lengthTotal,"+list.length);

for (i=0; i<list.length; i++){
        showProgress(i+1, list.length);
        open(dirData+list[i]);
        title = getTitle();
        print((i+1)+","+title);
        name = File.nameWithoutExtension;
        //print(name+"   That's the name");

run("8-bit");
run("Enhance Contrast", "saturated=0.35");
//setMinAndMax(40, 140);

//call("ij.ImagePlus.setDefault16bitRange", 0);
//run("Find Edges");
run("Apply LUT", "stack");
run("Find Edges", "stack");

//setTool("zoom");
//setAutoThreshold("Default");
//run("Threshold...");
//setAutoThreshold("Default");
setAutoThreshold("Default dark stack");
setThreshold(60, 255);  //USE 60,255 for XY 40
run("Convert to Mask", " ");
//setAutoThreshold("Default dark");
```

```
//run("Convert to Mask");

run("Smooth", "stack");
run("Despeckle", "stack");
run("Invert LUT");

//run("8-bit");

//run("Threshold...");
setAutoThreshold("Default dark stack");
//setThreshold(5, 255);
run("Convert to Mask", " ");
run("Dilate", "stack");
run("Dilate", "stack");
run("Dilate", "stack");
run("Dilate", "stack");
run("Dilate", "stack");

run("Analyze Particles...", "size=30001-Infinity circularity=0.00-1.00 show=Outlines summarize stack");
saveAs("Tiff", dirSave + name + "_Boundary.tif");
doWand(32, 86);
run("Measure");

run("Close All");

}

selectWindow("Results");
saveAs("Results", dirSave+"/Boundary Stats.xls");

selectWindow("Log");
saveAs("Text", dirSave+"/Boundary Name Log.txt");
```

Code for Analysis

```
//Batch Boundary Analysis STATSonly.ijm

dirData = getDirectory("Slect directory of data to process")
dirSave = getDirectory("Select location to save data")

list = getFileList(dirData);
setBatchMode(true);    //use this to save time by not displaying images

run("Set Measurements...", "area mean standard modal perimeter bounding shape median skewness kurtosis redirect=None decimal=3");
print("lengthTotal,"+list.length);
```

```
for (i=0; i<list.length; i++){
        showProgress(i+1, list.length);
        open(dirData+list[i]);
        title = getTitle();
        print((i+1)+","+title);
        name = File.nameWithoutExtension;
        //print(name+"   That's the name");

run("8-bit");
run("Enhance Contrast", "saturated=0.35");
//setMinAndMax(40, 140);

//call("ij.ImagePlus.setDefault16bitRange", 0);
//run("Find Edges");
run("Apply LUT", "stack");
run("Find Edges", "stack");

//setTool("zoom");
//setAutoThreshold("Default");
//run("Threshold...");
//setAutoThreshold("Default");
setAutoThreshold("Default dark stack");
setThreshold(60, 255);  //USE 60,255 for XY 40
run("Convert to Mask", " ");
//setAutoThreshold("Default dark");
//run("Convert to Mask");

run("Smooth", "stack");
run("Despeckle", "stack");
run("Invert LUT");

//run("8-bit");

//run("Threshold...");
setAutoThreshold("Default dark stack");
//setThreshold(5, 255);
run("Convert to Mask", " ");
run("Dilate", "stack");
run("Dilate", "stack");
run("Dilate", "stack");
run("Dilate", "stack");
run("Dilate", "stack");

//run("Analyze Particles...", "size=30001-Infinity circularity=0.00-1.00 show=Outlines
summarize stack");
//saveAs("Tiff", dirSave + name + "_Boundary.tif");
doWand(50, 286);
run("Measure");
```

```
run("Close All");

}

selectWindow("Results");
saveAs("Results", dirSave+"/Boundary Stats.xls");

selectWindow("Log");
saveAs("Text", dirSave+"/Boundary Name Log.txt");
```

C. SUPPLEMENTAL FIGURES AND TABLES

Figures

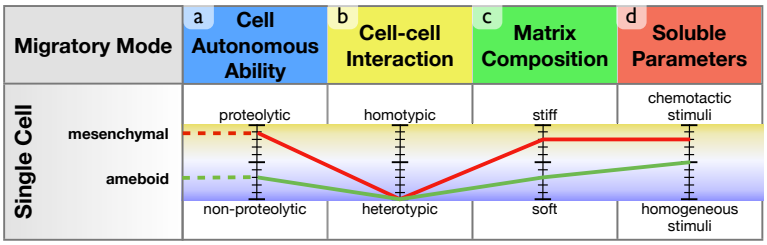

Figure C1. The multi-scale tuning model. A multi-scale model presents multiple interdependent parameters classified under four distinct categories (cell autonomous ability, cell-cell interaction, matrix composition and soluble parameters). Individual migratory parameters are displayed in a tuning model in which the tuner (🎚) represents the continuous range between two opposing properties for the same parameter. The magnitude of any parameter influences its impact on the mode and means of migration as well as the influence of related parameters. This example demonstrates the utility of the tuning model: **(a)** Proteolytic modification of the microenvironment promotes mesenchymal migration while non-proteolytic properties perpetuate ameboid movement. **(b)** Heterotypic interactions with adjacent cells facilitate the movement of individual cells while homotypic interactions generally suppress single cell movement and are associated with collective movement. **(c)** Stiff substrates promote movement in a mesenchymal fashion while soft substrates facilitate ameboid movement. **(d)** Mesenchymal motility benefits greatly from a chemotactic stimulus while ameboid movement is supported by both chemotactic and homogeneous stimuli.

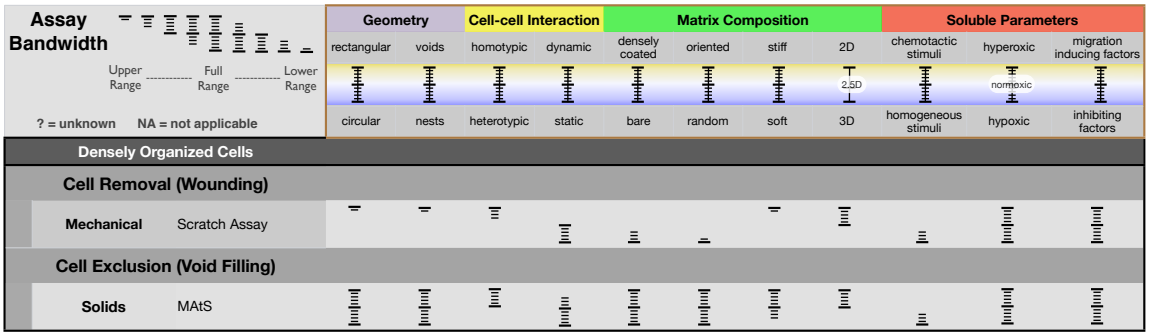

Figure C2. Assay bandwidth. In Table 1 a panel of assays is represented with the respective ability to assay across different geometries, and assess the contributions of cell-cell interactions, matrix composition, and soluble stimuli. The tuning model introduced in Figure 1 is used to represent the continuous range between two opposing properties for each parameter. The ability of each assay to assess a given parameter is represented as a tuner where the visible range represents the bandwidth associated with that assay. In this example the scratch assay and the MAtS assay are shown. The display of tuners for each assay readily reveal the limited range of the scratch assay: Scratch assays provide only rectangular voids which allow for analysis of migration of cells experiencing homotypic interactions under relatively static conditions. The matrix underlying the cells is damaged and largely removed by the act of scratching. Consequently, the matrix composition during this migration is "bare" and mostly "random". This assay also requires either glass or plastic as a culture surface thereby limiting the analysis of migration of "stiff" substrates. Like most assays described herein, the scratch assay is limited to 2D arrangements of cells responding to a homogeneous stimulus of soluble factors. In contrast, the MAtS assay uses a non-destructive stencil to exclude cells rather than remove them. Consequently this assay distinguishes itself from the scratch assay primarily by the geometries that are possible and the ability to evaluate the contribution of the underlying matrix (outlined in red).

MAts	Star	Block	Dot	Microwell
Length	12 mm	6 mm	1.6 / 2.0 mm (bottom/top)	20 mm
Width	12 mm	2.5 mm	1.6 / 2.0 mm (bottom/top)	15 mm
Height	5.5 mm	5 mm	5 mm	2 mm
Initial Width for Migration	0.7 mm	2.5 mm	1.63 mm (diameter)	0.8, 0.4, & 0.2 mm
Purpose	general use	matrix switching	high-throughput	low cell-quantities

Figure C3. Dimensions of different MAts for migration assays. Images are at the same scale and were acquired using the stereomicroscope and a Neolumar 0.8x objective at 6.4x magnification.

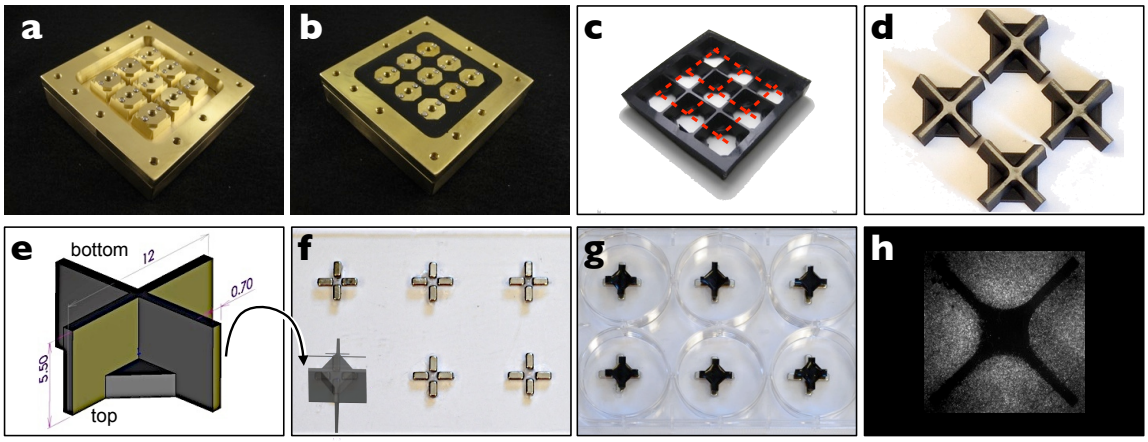

Figure C4. Fabrication and basic usage of MAts. **(a)** Polished brass was machined to create a two-tier mold consisting of a mirror-finish base onto which the outer dike and the 3 by 3 of individual squares were fastened.The squares were precisely positioned with steel dowels pressed into the base.The sides of the squares and dike were tapered by 5o to facilitate removal of the MAts. **(b)** PDMS prepolymer was mixed with magnetite (33% magnetite by weight), poured into the mold, and cured at 60oC for 3 hours. **(c)** The resulting MAts were removed as a single unit and cut with a razor blade along the dotted red lines. **(d)** This created 4 individual MAts shown with their contact surface up. **(e)** Basic dimensions are given on a 3D model of the MAt (inverted).The stars fit in a 12 x 12 mm square, are 5.5 mm tall, and have a contact surface that is 650 μm wide in order to create a 650 μm void for cell migration. **(f)** Rare earth magnets were arranged on a 1/8˝ thick sheet of acrylic in order to **(g)** attach MAts to a 6-well plate. **(h)** After incubating HEp3 GFP cells overnight, MAts were removed, resulting in a star-shaped void in the confluent cells, as seen by fluorescent stereomicroscopy (see Methods). Widths between cell populations averaged 650 μm along the 4 arms of the MAt.

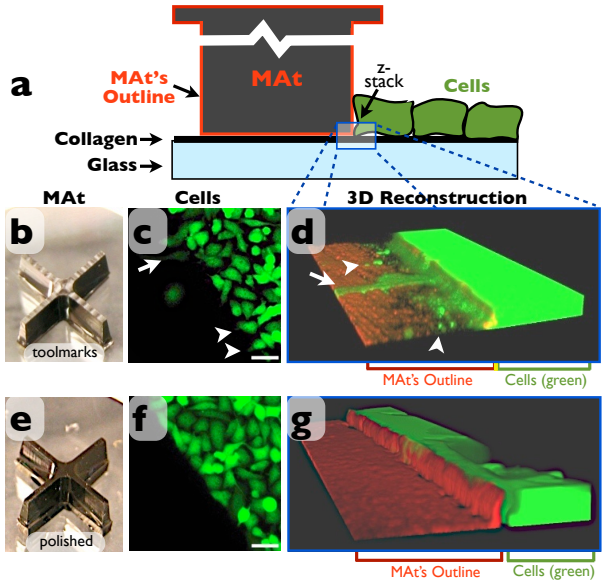

Figure C5. Tooling marks permit cell protrusions. **(a)** Schematic of a MAt coated with Alexa 546-conjugated IgG attached to a collagen-coated glass coverslip with adjacent GFP-expressing HEp3 cells (green). A MAt **(b)**, inverted to show the surface that seals against the substrate, with submicron toolmarks from CNC milling is compared to **(e)** a MAt with a mirror-finish contact surface. HEp3 cells were used because they are an aggressive human epidermoid carcinoma capable of penetrating into submicron cracks and crevices. Confocal z-stacks of the contact area between the HEp3 cells, the MAt, and the culture surface were acquired for 60 μm with 1 μm spacing using the spinning disk confocal (see Methods). **(d & g)** 3D reconstruction of the interface was created using Volocity in order to provide a 3D perspective of this crucial intersection of the MAt, cells and substrate. **(b-d)** Submicron tool marks allowed HEp3 cells to penetrate underneath the MAt on collagen-coated glass, creating long, full body extensions (arrow) or small cell protrusions (arrowheads). **(e-g)** The polished contact surface and crisp edge of the finished MAt successfully excluded HEp3 cells. Scale bars, 50 μm.

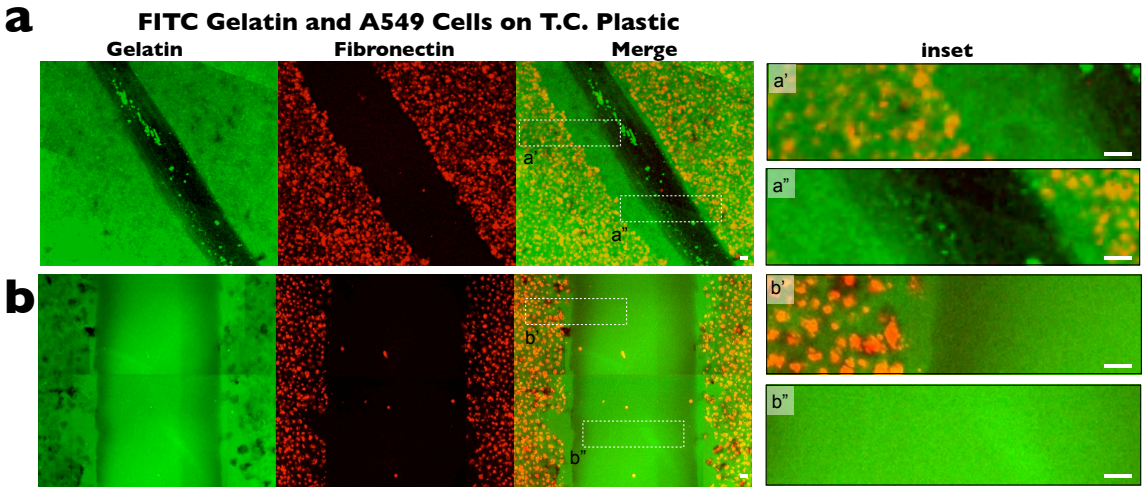

Figure C6. MAts maintain protein-coated substrates during void formation. Voids were created in a confluent A549 monolayer by means of mechanical scratching with a plastic pipette tip **(a)** or formed without substrate damage with MAts **(b)**. To visualize aberrations in the matrix and cell monolayer, representative images of collagen matrix (green) and A549 cells (red, CellTracker) were taken on the fluorescent stereomicroscope at the periphery and in the center of the void **(**insets **a′**, **a″**, **b′** and **b″)**. In contrast to voids created by mechanical scratching, voids created with MAts retained a uniform collagen-coated surface without undo disruption of cells at the edge of the void. Scale bars, 50 μm.

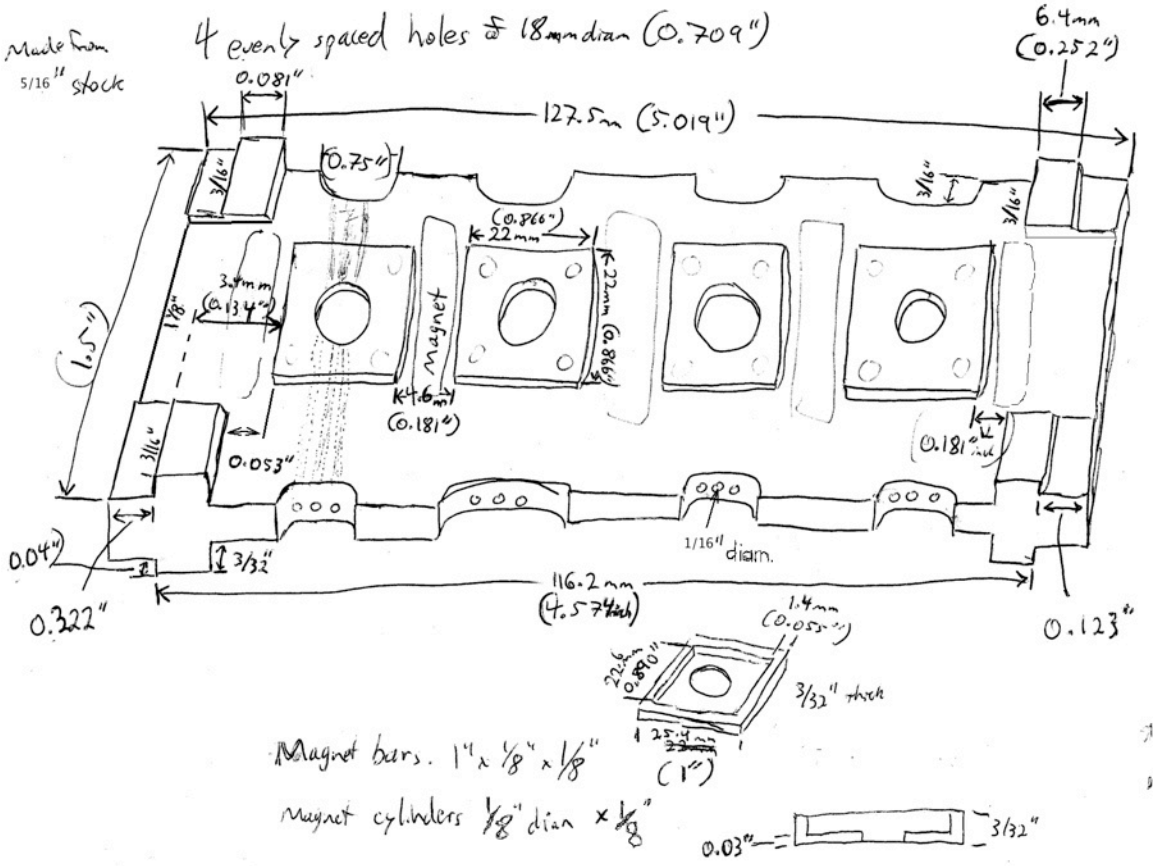

Figure C7. Dimensions of MSLIC lids and fluidic MSLICs.

Tables

Table C1. Terms and definitions.

Term	**Definition** (in relation to morphology and migration.)
Ameboid	Cells that exhibit an asymmetric morphology with poorly discernible leading front. These cells are generally poorly adherent to the matrix and other cells. Their migration is exclusively as isolated, individual cells.
Cell autonomous ability	The intrinsic ability of a cell to move independent of external stimuli.
Cell-cell interaction	Direct contact between adjacent cells
Densely Organized	Refers to the migration of a group of cells engaged in continuous-to-intermittent cell-cell contact.
Epithelial	Cells that exhibit a broad and flat morphology often seen as cuboidal when cells are confluent. These cell migrate with a broad leading front. These cells are typified by strong cell-cell adhesions and exhibit collective migration in sheets and strands.
Matrix composition	The composition of the extracellular matrix and substrate onto which the cells are adherent.
Mesenchymal	Cells that exhibit an elongated fibroblast-like appearance with a discernible leading front and trailing back. These cells possess weaker cell-cell adhesions and do not exhibit the collective migration than might be seen in epithelial cells.
Migration	Refers to the movement adherent cells use to mobilize themselves.
Nest	Refers to the formation of a cell population with defined dimensions in order to monitor migration from this “nest” onto adjacent cell-free surface.
Single Cell	Refers to the migration of an individual, isolated cell free of cell-cell adhesions.
Soluble Parameters	The condition and composition of the soluble environment surrounding the cell. This includes the traditional growth factors and their presentation (e.g. chemotactic gradient vs homogeneous availability) as well as gases (oxygen) and nutrients (glucose).
Void	Refers to an area on the culture surface that is left devoid of cells for the purpose of of creating an empty space into which adjacent cells can migrate.

Videos

Notice: Videos may not display in some applications.

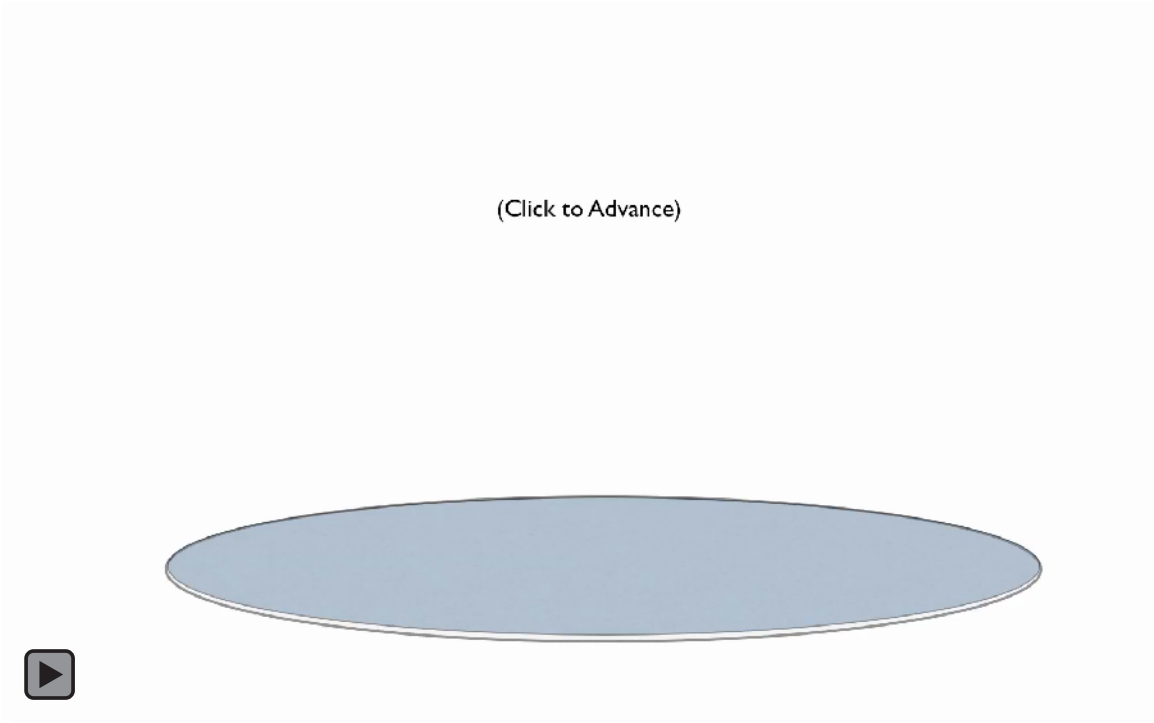

Video C1. Animation of MAtS space-filling assay. MAtS attach to protein-coated surfaces via magnetic force, pattern cells, and are removed. Images are acquired immediately and at defined time-points. Migration rates or percent closure are quantified from the captured images.

Video C2. HEp3 migration on intact collagen. MAtS were used to pattern HEp3 cells on collagen-coated glass. Cells migrated freely across the substrate after removal of MAtS. This 16-second video shows 16 hours of migration.

Video C3. HEp3 migration across scratched collagen on glass. HEp3 cells plated on collagen-coated glass were scratched. After migrating 7.5 hours, cell migration was inhibited by the lack of matrix caused by scratching. This 16-second video shows 16 hours of migration.

Video C4. Lack of collagen-coating inhibits HEp3 cell migration onto glass. MAtS were used to pattern first collagen and then HEp3 cells on glass cover slips creating a void that lacked collagen. HEp3 cells were unable to migrate into this uncoated void. Images were captured every 10 minutes for 16 hours which are presented here in a 16-second video.

D. MAGNETICALLY ATTACHABLE TEMPLATES FOR FABRICATING PDMS MICROFLUIDIC INTERCONNECTS

Summary

Magnetically Attachable Templates (MATs) provide a simple, reliable method to create the large (mm or cm) features necessary for manual loading and operation of microfluidic devices, and can be readily customized to meet specific applications. By combining a smooth surface, conformal contact, and magnetic force, MATs prevent polydimethylsiloxane (PDMS) from seeping between the mold and the MAT. MATs are fabricated by machining an initial mold, casting a set of toolmarked MATs, and then casting a second mold around these toolmarked MATs thus removing the toolmarks from the MATs' contact surface. The resulting smooth contact surface is critical to formation of seemless interconnects between microscopic features of microfluidic molds and the macroscopic features of MATs. MATs enable reproducible fabrication of microscopic-to-macroscopic interconnects, reduce the risk of tearing or introducing debris compared to punching, and are readily implementable in laboratories currently fabricating PDMS microfluidic devices.

Introduction

As microfluidic devices become increasingly important to biomedical research, there is an increasing need for a simple, reliable method of macroscopic, through-chip penetrations, such as covered fluidic reservoirs, open wells, interconnects and large vias that operate in conjunction with microfabricated features. Simple, cost effective, and efficient methods for creating polydimethylsiloxane (PDMS) microfluidic devices have been developed [124,125], primarily using SU-8 or other photoactivated epoxies. Unfortunately, using these techniques, it is difficult to create the large (>1 mm) interconnects and reservoirs that are necessary for manual loading and operation of the microfluidic devices, primarily because

the scattering and absorption of the UV light required for photolithograpy limits the thickness of an SU-8 layer that can be accurately patterned. Thick SU-8 structures require multiple layers of SU-8 that have to be exposed individually, presenting serious problems in aspect ratio, alignment, exposure, development, and mold robustness. Creating such large structures in SU-8 is challenging, time consuming and generally requires specialized equipment [126-128]. For these reasons large microfluidic structures are often made by punching or coring already-cast PDMS microfluidic devices. Repeatedly obtaining high-quality punched or cored interconnects requires significant skill. The punched or cored interconnects are often fluted, tapered, and irregular sizes. They vary greatly in quality and functionality and can be difficult to position accurately [129]. We show that punching interconnects can be avoided by simply casting PDMS around magnetically attached templates (MATs). Using magnetic force, these templates seal against the microfabricated structures of molds and create smooth, precise interconnects as the PDMS cures around them.

Few methods exist for creating interconnects during the casting of PDMS over microfluidic molds because of the difficulty of preventing PDMS from seeping into cracks or forming thin films between components. To overcome these problems John Wikswo and his colleagues have developed a method for machining small screw holes through or around SU-8 patterns on brass (which can be more readily drilled than a silicon wafer) and then attaching large, plastic posts and other features to the micropatterned brass mold with screws (personal communication with Dr. John Wikswo). The screws provide the needed force to seal the plastic posts against the SU-8 micropatterns. However, such machining is technically challenging and time-consuming, and SU-8 may fracture or chip away during the process. Alternatively, NdFeB magnets have been attracted to molds to successfully create interconnects [130], and excluding PDMS has also been achieved by clamping 30-100 μm tall microstructures in a press [37]. From these approaches it is clear that creating successful intercon-

nects while curing PDMS requires smooth surfaces, conformal contact, and force to prevent PDMS from seeping into cracks or forming thin films between parts.

In order to integrate the formation of interconnects and reservoirs into the casting step of PDMS microfluidic fabrication, we developed Magnetically Attachable Templates (MATs). MATs are created by mixing PDMS prepolymer with magnetite powder and then curing it in molds. The molds can be created with standard machining, and the resulting toolmarked MATs used to create molds with smooth bottom surfaces (see Materials and Methods). By combining a smooth contact surface and the conformal or compliant properties of PDMS with magnetic force, MATs successfully seal against molds and thus prevent films of PDMS from forming in the interconnects. Laboratories currently fabricating PDMS microfluidic devices can readily implement MATs because only two new materials are required: magnetite and polyvinyl alcohol. MATs provide a simple, versatile, and reusable method to successfully integrate macro features into the casting process of PDMS microfluidic fabrication.

Materials and Methods

Materials.

NdFeB magnets (K&J Magnets), PDMS (Sylgard 184, Dow Corning), magnetite (Pyrox200HP, Pyrox LLC), polyvinyl alcohol (PVA, PartAll Film #10, RexCo), polyurethane two-part resin (Crystal Clear 200, Smooth-On), brass, SU-8 (Microchem), SU-8 developer (Microchem), silicon wafer, mirror-finish stainless steel (Type 304 #8 Finish, McMaster-Carr).

Polydimethylsiloxane Formulations.

We use polydimethylsiloxane (PDMS) from the Sylgard 184 Silicone Elastomer Kit (Dow Corning). PDMS prepolymer is made by mixing 10 parts base to 1 part curing agent by weight as recommended by the manufacturer. This PDMS prepolymer may be degassed at this point by vacuum or centrifugation or used as is. To make MATs, this prepolymer is immediately mixed with magnetite powder at a 2 to 1 ratio, resulting in a mixture that is 33% magnetite by weight. The PDMS-magnetite mixture (PDMS-M) can be mixed by hand, but a more homogenous mixture is achieved by using a rotary mixer (AR-100, Thinky). When cured, the PDMS-M is noticeably stiffer than plain PDMS. The PDMS or PDMS-M is cured according to the manufacturer's recommendations.

Removing Toolmarks from Custom-Made MATs' Contact Surfaces Using a Sacrificial PVA Layer

It is possible to cast PDMS in molds fabricated by computer numerical control (CNC) milling in brass, wax or acrylic. We use brass molds to create the positive relief of the desired MAT (Fig. D1a). After carefully coating non-critical areas of the brass with PVA, polyurethane resin was cast into the brass relief to create a negative mold (Fig. D1b). From the polyurethane mold an initial set (≥ 6) of MATs with toolmarks was created (Fig. D1c). These MATs had tooling marks on all surfaces. (The MATs were not treated with PVA because such treatments resulted in strong polyurethane-to-PDMS adhesion.) To remove tooling marks from the contact surfaces, PVA was poured onto mirror-finish stainless steel and spread into a thin film via a stream of air, and then dried. The toolmark-bearing MATs were subsequently sealed against the PVA film with magnets underneath the mirror-finish stainless steel (Fig. D1d). Then the assembly was washed for 2-3 minutes in slowly running distilled water to remove any uncovered PVA. After drying, the assembly was cast in polyure-

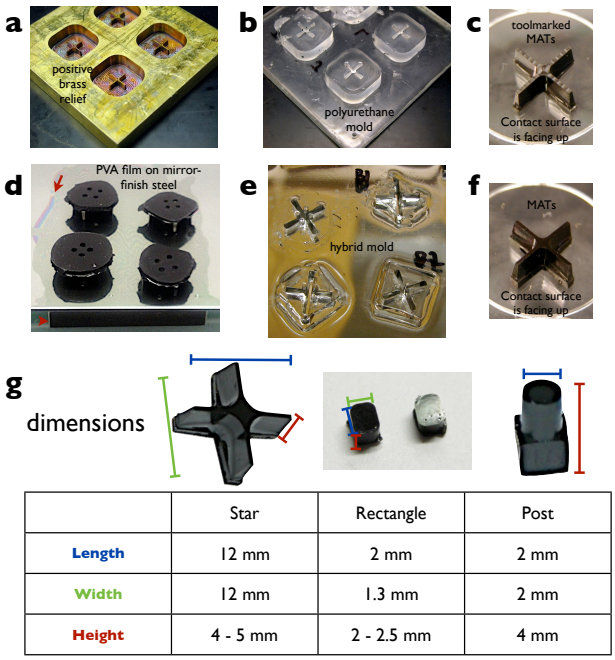

	Star	Rectangle	Post
Length	12 mm	2 mm	2 mm
Width	12 mm	1.3 mm	2 mm
Height	4 - 5 mm	2 - 2.5 mm	4 mm

Figure D1. Hybrid mold using sacrificial PVA layer on mirror-finish stainless steel. **(a)** CNC milling in brass created the positive relief of the desired star shape. Polyurethane resin cast over the brass relief creates **(b)** a negative mold. From this negative, polyurethane mold **(c)** toolmarked MATs were created. **(d)** To remove tooling marks from the criti- cal contact surface, a thin film of PVA (arrow) was poured onto mirror-finish stainless steel and then dried. MATs were subsequently sealed against the PVA film via magnetic force provided by magnets (arrowhead) underneath the non-magnetic stainless steel. Then the assembly was washed for 2 minutes in slowly-running distilled water to remove all the exposed PVA. Excessive water was genlty blown off the surface, and the assembly was left to air dry. **(e)** A hybrid, stainless steel and polyurethane, mold was created by casting polyurethane over the stainless steel and around the MATs. After the polyurethane cured. the MATs were removed and water was introduced into the voids left by the MATs in order to dissolve the PVA film on the stainless steel. **(f)** PDMS-magnetite cast into the hybrid molds produced MATs with mirror-finish contact surfaces.

thane resin, the MATs were subsequently removed, and the remaining PVA was rinsed away. These molds replaced the toolmarked contact surface with a mirror-finish contact surface (Fig. D1e-f). The downside was that after several cycles of heating and cooling, the polyurethane began separating from the stainless steel, destroying the mold, so the initial toolmark-free MATs cast in the mold were recast in polyurethane to create entirely polyurethane molds. To facilitate removal and storage of MATs, glass microscope slides were laid on top

of the mold using ~1 mm spacers in such a way that the PDMS-M cured onto the glass (not shown).

Microfluidic Masters

We often use macroscopic MATs in conjunction with SU-8 photolithographic microfluidic masters on silicon wafers. For this study, we utilize masters with 100 μm wide and 100 μm tall microfluidic channels that were obtained from the Vanderbilt Institute for Integrative Biosystems Research and Education (VIIBRE). Desired heights of SU-8 were created on silicon wafers or glass slides by spinning a certain formulation, for example, SU-8 2100 at 3000 RPM to achieve 100 μm features. The desired pattern was applied to the film of SU-8 by placing a mask or stencil over the SU-8 and then exposing it to UV light at an exposure dose appropriate to the thickness. The UV-activated SU-8 was then baked resulting in polymerization of the exposed SU-8. The desired 3-D structures were "developed" by placing the wafer in a special solvent called "developer" which dissolved all the unexposed SU-8. A detailed protocol for SU-8 photolithography can be found in References [131,132]. Frequently, low-profile SU-8 structures would mark the location where the larger MATs were to be positioned prior to PDMS casting.

Design and Dimensions

MATs can be fabricated in numerous shapes and sizes (Fig. D1g). Star MATs are 10 mm in diameter and have 4 arms that are 4 mm long. The contact surface of each arm is 700 μm wide, creating 700 μm spaces between the two cell monolayers. This spacing is similar to the mean width of scratches made with a 200 μl capacity pipette tip and visible with 10x ob-

jectives on most microscopes. Rectangle MATs are 20 mm long, 13 mm wide, and 2-2.5 mm tall. Dot MATs are 2 mm diameter and 4 mm tall.

Preventing PDMS-PDMS Bonding

In order to prevent the PDMS-M of MATs from bonding to the PDMS of microfluidic devices, MATs are oxygen plasma treated for about 20-40 seconds, as is commonly done to irreversibly bond PDMS to glass, then immediately immersed in PVA for at least 2 hours [133,134]. Excess PVA is aspirated, and the treated MATs are dried. PVA-treated MATs are then used to create posts, interconnects, or reservoirs on microfluidic devices.

Results and Conclusions

MATs can create interconnects in various shapes by sealing against a microfluidic mold via magnetic force, after which the PDMS microfluidic device is cast. This is accomplished with the following steps. First the desired MATs are fabricated with a mirror-finish contact surface as described in Methods (Fig. D1). After acquiring or creating replica molds containing microfluidic patterns on glass, silicon wafers, or other suitable substrates, magnets are positioned underneath the areas of the master to which MATs will be attached. MATs are subsequently placed onto these areas (Fig. D2a). The magnetic force attaches the magnetic template to the micropatterns and/or substrate, creating a seal that prevents PDMS seepage into the space between the MATs and the underlying microfluidic master. PDMS prepolymer is cast around and/or over this assembly, which is subsequently placed in an oven at 60ºC for 3-4 hours until cured (Fig. D2b). After the PDMS has cured, the MATs are removed with the PDMS of the device (Fig. D2c). Then the MATs are carefully removed from the PDMS device, resulting in a well-defined interconnect and/or macroscopic feature in the PDMS device which can now be sealed to glass or PDMS (Fig. D2d). This process can

be used to make various shapes of interconnects and reservoirs in PDMS microfluidic devices, eliminating the need for punching.

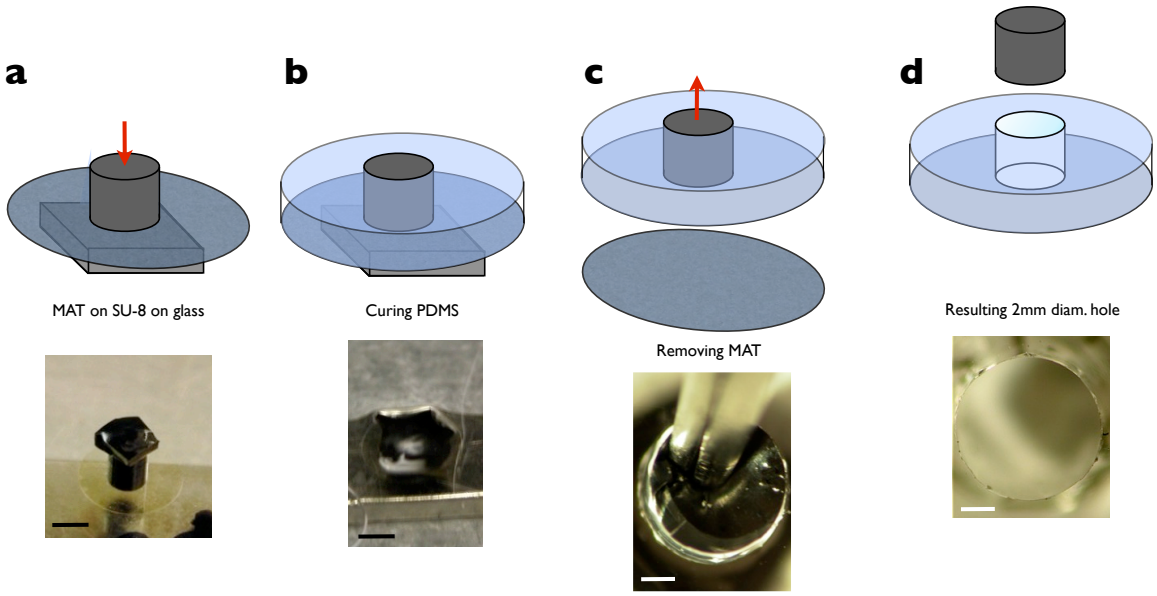

Figure D2. Interconnect fabrication. **(a)** MATs are attached via magnetic force to micropatterns. **(b)** PDMS is cast around the MATs. **(c)** After PDMS has cured and been removed from the mold, the MATs are gently removed. **(d)** The resulting interconnect has precise dimen- sions as defined by the MAT. Scale bars, **a-b** 2 mm , **c-d** 0.5 mm.

The quality of MAT-made interconnects was compared to interconnects punched with sharpened stainless steel tubing (Fig. D3a). Punching can introduce debris which may fall into and obstruct part of the device (arrows, Fig. D3a and b). Punching can also cause tearing that results in misshaped, dysfunctional interconnects (not shown), particularly after inserting tubing into punched holes. In contrast, MATs are not prone to tearing, create interconnects free of debris, and produce sidewalls that are square to the contact surface (Fig. D3d-f). Furthermore, analysis of the cross-sections of these interconnects reveals the tapering and rough vertical fluting created by punching (Fig. D3c and c´). In contrast, the MAT-created interconnects have smooth sidewalls with only subtle horizontal striations and are free of taper (Fig. D3f and f´). MATs' horizontal striations result from machining of the

original molds and may not be present in MATs created using 96-well plates or other means. Regardless, the reproducibility, smoother sidewalls, and control of dimensions make MAT's interconnects superior to common punching techniques.

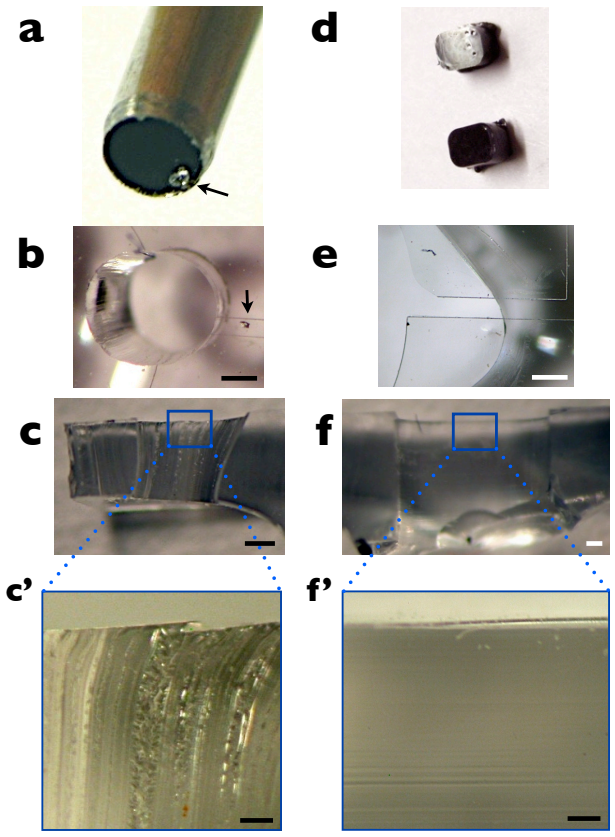

Figure D3. Comparison of punched and MATs' interconnects. **(a-b)** Punching often creates debris (arrowheads). **(c)** Punches also cause fluting and often tapered holes. **(d-f)** On the other hand, MATs' interconnects are reproducible, smooth, and have only subtle horizontal striations compared to punching. Scale bars 0.2 mm, except **c′** and **f′** which are 0.05 mm.

The primary difference between MAT-made and punched interconnects is that PDMS wicks up MATs. This wicking may be beneficial when interconnects taller than their surroundings are desired. However, curvature due to wicking can be detrimental to bright-field imaging such as phase contrast or differential interference contrast. To avoid meniscus-related imaging effects, microfluidic devices should be designed so that either the intercon-

nects are sufficiently far away from MATs (~5 mm) or so that the imaging area is kept flat by designing MATs to be nearly the same height as the PDMS device itself.

MATs are superior to other methods of creating interconnects in several ways. First, MATs can be reused. Second, they are attached directly to the mold before casting the device rather than being attached to a cast device. Third, the resulting interconnects have shapes and dimensions equal to those of the MATs. Fourth, the machining of molds that are used to cast the MATs creates subtle horizontal striations rather than harsh vertical fluting produced by punching.

Furthermore, MATs are compatible with standard PDMS microfabrication procedures. MATs can be temporarily attached to micropatterned photoresists on glass, plastic, silicon wafers, or even PDMS. Potentially, MATs could be permanently attached to SU-8 using the nitrogen plasma cleaning technique of Zhang et al. [135]. Standard oxygen plasma cleaning is utilized to attach polyvinyl alcohol to the PDMS surface and prevent PDMS-PDMS bonding as the microfluidic device is cast [134]. Laboratories already fabricating PDMS microfluidic devices can readily implement MATs by simply acquiring the needed magnetite and PVA and suitable molds for creating MATs.

The design and implementation of MATs is flexible enabling creativity. Functional star, cylinders, and rectangular posts have been created. Currently, we are focused on reusable, broadly-applicable designs such as cylinders for interconnects. However, single-use designs are possible. By omitting the PVA-treatment, MATs containing interconnects or reservoirs in themselves would bond to the cast PDMS microfluidic device. This would eliminate the time and effort required to remove MATs while still providing a reproducible, high quality interconnect. A highly reliable design for such an interconnect was recently characterized by Chang et al. and represents a good candidate for a single use MAT [136]. MATs can also be used to create reservoirs or large chambers not suitable for fabrication on microfluidic

molds using microfabrication techniques. Though generally MATs create an interface perpendicular to the mold surface, designs with various angles could also be created and used to reproducibly create interconnects at precise angles. Complex shapes are possible with MATs that are either difficult or impossible to create by punching such as a star shape. MATs not only improve reproducibility and reliability but also enable greater creativity while taking the punch out of PDMS microfluidic fabrication.

Acknowledgements

Andries Zijlstra and William Ashby were supported by CA120711 and CA143081. This research was funded in part by the Ronnie James Breast Cancer Discovery Award, the Vanderbilt Institute for Integrative Biosystems Research and Education (VIIBRE), and U.S. Defense Threat Reduction Agency grant HDTRA-09-1-0013. We thank Phil Samson, Dmitry Markov, Ron Reiserer, and David Schaffer for useful technical comments and suggestions, and Allison Price for her editorial assistance.

REFERENCES

[1] A. Ootani, X. Li, E. Sangiorgi, Q.T. Ho, H. Ueno, S. Toda, H. Sugihara, K. Fujimoto, I.L. Weissman, M.R. Capecchi, and C.J. Kuo, "Sustained in vitro intestinal epithelial culture within a Wnt-dependent stem cell niche," *Nature Medicine*, vol. 15, Apr. 2009, p. 701.

[2] L.G. Griffith and M.A. Swartz, "Capturing complex 3D tissue physiology in vitro," *Nature Reviews Molecular Cell Biology*, vol. 7, Mar. 2006, pp. 211–224.

[3] T.-H. Chen, J.J. Hsu, X. Zhao, C. Guo, M.N. Wong, Y. Huang, Z. Li, A. Garfinkel, C.-M. Ho, Y. Tintut, and L.L. Demer, "Left-Right Symmetry Breaking in Tissue Morphogenesis via Cytoskeletal Mechanics," *Circulation research*, vol. 110, Feb. 2012, pp. 551–559.

[4] W. Guo, M. Frey, N. Burnham, and Y. Wang, "Substrate rigidity regulates the formation and maintenance of tissues," *Biophysical journal*, vol. 90, 2006, pp. 2213–2220.

[5] J. Johnson, M.O. Nowicki, C.H. Lee, E.A. Chiocca, M.S. Viapiano, S.E. Lawler, and J.J. Lannutti, "Quantitative analysis of complex glioma cell migration on electrospun polycaprolactone using time-lapse microscopy," *Tissue engineering Part C, Methods*, vol. 15, Dec. 2009, pp. 531–540.

[6] A. Rizki, V.M. Weaver, S.-Y. Lee, G.I. Rozenberg, K. Chin, C.A. Myers, J.L. Bascom, J.D. Mott, J.R. Semeiks, L.R. Grate, I.S. Mian, A.D. Borowsky, R.A. Jensen, M.O. Idowu, F. Chen, D.J. Chen, O.W. Petersen, J.W. Gray, and M.J. Bissell, "A human breast cell model of preinvasive to invasive transition," *Cancer Research*, vol. 68, Mar. 2008, pp. 1378–1387.

[7] C. Moraes, Y. Sun, and C.A. Simmons, "(Micro)managing the mechanical microenvironment," *Integrative Biology*, vol. 3, Oct. 2011, pp. 959–971.

[8] M. Balcells, M.F. Suárez, M. Vázquez, and E.R. Edelman, "Cells in fluidic environments are sensitive to flow frequency," *Journal of Cellular Physiology*, vol. 204, Jul. 2005, pp. 329–335.

[9] R. Derda, A. Laromaine, A. Mammoto, S.K.Y. Tang, T. Mammoto, D.E. Ingber, and G.M. Whitesides, "Paper-supported 3D cell culture for tissue-based bioassays," *Proceedings Of The National Academy Of Sciences Of The United States Of America*, vol. 106, 2009, pp. 18457–18462.

[10] T.D. Palmer, W.J. Ashby, J.D. Lewis, and A. Zijlstra, "Targeting tumor cell motility to prevent metastasis," *Advanced drug delivery reviews*, vol. 63, Jul. 2011, pp. 568–581.

[11] P. Friedl and K. Wolf, “Plasticity of cell migration: a multiscale tuning model,” *The Journal of Cell Biology*, vol. 188, Jan. 2010, pp. 11–19.

[12] D.L. Nikolic, “Role of boundary conditions in an experimental model of epithelial wound healing,” *American journal of physiology Cell physiology*, vol. 291, Jan. 2006, pp. C68–C75.

[13] C.-C. Liang, A.Y. Park, and J.-L. Guan, “In vitro scratch assay: a convenient and inexpensive method for analysis of cell migration in vitro,” *Nature Protocols*, vol. 2, 2007, pp. 329–333.

[14] Y. Kam, C. Guess, L. Estrada, B. Weidow, and V. Quaranta, “A novel circular invasion assay mimics in vivo invasive behavior of cancer cell lines and distinguishes single-cell motility in vitro,” *BMC Cancer*, vol. 8, 2008, p. 198.

[15] S. Watanabe, M. Hirose, X.E. Wang, K. Maehiro, T. Murai, O. Kobayashi, H. Mikami, K. Otaka, A. Miyazaki, and N. Sato, “A new model to study repair of gastric mucosa using primary cultured rabbit gastric epithelial cells,” *Journal of clinical gastroenterology*, vol. 21 Suppl 1, 1995, pp. S40–4.

[16] Y. Kam, A. Karperien, B. Weidow, L. Estrada, A. Anderson, and V. Quaranta, “Nest expansion assay: a cancer systems biology approach to in vitro invasion measurements,” *BMC Research Notes*, vol. 2, Jul. 2009, p. 130.

[17] Justin Yarrow, Zachary Perlman, Nicholas Westwood, and Timothy Mitchison, “A high-throughput cell migration assay using scratch wound healing, a comparison of image-based readout methods,” *BMC Biotechnology*, vol. 4, Sep. 2004, p. 21.

[18] P.Y.K. Yue, E.P.Y. Leung, N.K. Mak, and R.N.S. Wong, “A Simplified Method for Quantifying Cell Migration/Wound Healing in 96-Well Plates,” *Journal of Biomolecular Screening*, vol. 15, 2010, pp. 427–433.

[19] J. Lee, Y.-L. Wang, F. Ren, and T.P. Lele, “Stamp Wound Assay for Studying Coupled Cell Migration and Cell Debris Clearance,” *Langmuir*, vol. 26, Nov. 2010, pp. 16672–16676.

[20] J. Hong, K. Kandasamy, M. Marimuthu, C.S. Choi, and S. Kim, “Electrical cell-substrate impedance sensing as a non-invasive tool for cancer cell study,” *Analyst*, vol. 136, 2010, pp. 237–245.

[21] C.R. Keese, J. Wegener, S.R. Walker, and I. Giaever, “Electrical wound-healing assay for cells in vitro,” *Proceedings Of The National Academy Of Sciences Of The United States Of America*, vol. 101, Feb. 2004, pp. 1554–1559.

[22] A.D. van der Meer, K. Vermeul, A.A. Poot, J. Feijen, and I. Vermes, “A microfluidic wound-healing assay for quantifying endothelial cell migration,” *AJP: Heart and Circulatory Physiology*, vol. 298, Feb. 2010, pp. H719–25.

[23] F.-Q. Nie, M. Yamada, J. Kobayashi, M. Yamato, A. Kikuchi, and T. Okano, “On-chip cell migration assay using microfluidic channels,” *Biomaterials*, vol. 28, Sep. 2007, pp. 4017–4022.

[24] T. Peterbauer, J. Heitz, M. Olbrich, and S. Hering, “Simple and versatile methods for the fabrication of arrays of live mammalian cells,” *Lab on a Chip*, vol. 6, 2006, p. 857.

[25] H. Tavana, A. Jovic, B. Mosadegh, Q.Y. Lee, X. Liu, K.E. Luker, G.D. Luker, S.J. Weiss, and S. Takayama, “Nanolitre liquid patterning in aqueous environments for spatially defined reagent delivery to mammalian cells,” *Nature Materials*, vol. 8, Aug. 2009, pp. 736–741.

[26] E.D. Holmstrom and D.J. Nesbitt, “Real-Time Infrared Overtone Laser Control of Temperature in Picoliter H2O Samples: ‘Nanobathtubs’ for Single Molecule Microscopy,” *Journal of Physical Chemistry Letters*, vol. 1, 2010, pp. 2264–2268.

[27] A. Bianco, M. Poukkula, A. Cliffe, J. Mathieu, C.M. Luque, T.A. Fulga, and P. Rørth, “Two distinct modes of guidance signalling during collective migration of border cells,” *Nature*, vol. 448, Jul. 2007, pp. 362–365.

[28] M.S. Hutson, “Forces for Morphogenesis Investigated with Laser Microsurgery and Quantitative Modeling,” *Science*, vol. 300, Feb. 2003, pp. 145–149.

[29] M.S. Hutson and X. Ma, “Plasma and cavitation dynamics during pulsed laser microsurgery in vivo,” *Physical review letters*, vol. 99, Oct. 2007, p. 158104.

[30] T.H. Park and M.L. Shuler, “Integration of cell culture and microfabrication technology,” *Biotechnology progress*, vol. 19, Feb. 2003, pp. 243–253.

[31] R. van Horssen and T.L.M. ten Hagen, “Crossing barriers: the new dimension of 2D cell migration assays,” *Journal of Cellular Physiology*, vol. 226, Jan. 2011, pp. 288–290.

[32] J. Leng, “RE: Request for Publications utilizing Radius Gel or Cytoselect 24-well wound healing,” *E-mail to the author*, Sep. 2010.

[33] R. van Horssen, N. Galjart, J.A.P. Rens, A.M.M. Eggermont, and T.L.M. ten Hagen, “Differential effects of matrix and growth factors on endothelial and fibroblast motility: Application of a modified cell migration assay,” *Journal of cellular biochemistry*, vol. 99, 2006, pp. 1536–1552.

[34] S. Kroening and M. Goppelt-Struebe, “Analysis of Matrix-Dependent Cell Migration with a Barrier Migration Assay,” *Science Signaling*, vol. 3, Jun. 2010, p. pl1.

[35] S. Rydholm and R. Rogers, “Parafilm Dependent Cell Patterning,” *Microscopy and Microanalysis*, vol. 11, 2005, pp. 1174–1175.

[36] E. Ostuni, R. Kane, C. Chen, D. Ingber, and G. Whitesides, “Patterning mammalian cells using elastomeric membranes,” *Langmuir*, vol. 16, 2000, pp. 7811–7819.

[37] M. Poujade, E. Grasland-Mongrain, A. Hertzog, J. Jouanneau, P. Chavrier, B. Ladoux, A. Buguin, and P. Silberzan, “Collective migration of an epithelial monolayer in response to a model wound,” *Proceedings of the National Academy of Sciences*, vol. 104, Oct. 2007, pp. 15988–15993.

[38] D. Wright, B. Rajalingam, J.M. Karp, S. Selvarasah, Y. Ling, J. Yeh, R. Langer, M.R. Dokmeci, and A. Khademhosseini, “Reusable, reversibly sealable parylene membranes for cell and protein patterning,” *Journal of Biomedical Materials Research Part A*, vol. 85A, 2008, pp. 530–538.

[39] P. Ariano, S. Dalmazzo, G. Owsianik, B. Nilius, and D. Lovisolo, “TRPC channels are involved in calcium-dependent migration and proliferation in immortalized GnRH neurons,” *Cell calcium*, vol. 49, Jun. 2011, pp. 387–394.

[40] M. Pla-Roca, R.F. Leulmi, H. Djambazian, S. Sundararajan, and D. Juncker, “Addressable Nanowell Arrays Formed Using Reversibly Sealable Hybrid Elastomer-Metal Stencils,” *Analytical Chemistry*, vol. 82, 2010, pp. 3848–3855.

[41] G. Mehta, J. Lee, W. Cha, Y.-C. Tung, J.J. Linderman, and S. Takayama, “Hard Top Soft Bottom Microfluidic Devices for Cell Culture and Chemical Analysis,” *Analytical Chemistry*, vol. 81, May. 2009, pp. 3714–3722.

[42] G. Cai, J. Lian, S.S. Shapiro, and D.A. Beacham, “Evaluation of endothelial cell migration with a novel in vitro assay system,” *Methods in cell science : an official journal of the Society for In Vitro Biology*, vol. 22, 2000, pp. 107–114.

[43] W. Georgescu, J. Jourquin, L. Estrada, A.R.A. Anderson, V. Quaranta, and J.P. Wikswo, “Model-controlled hydrodynamic focusing to generate multiple overlapping gradients of surface-immobilized proteins in microfluidic devices,” *Lab on a Chip*, vol. 8, Feb. 2008, pp. 238–244.

[44] S. Takayama, J.C. McDonald, E. Ostuni, M.N. Liang, P.J. Kenis, R.F. Ismagilov, and G.M. Whitesides, “Patterning cells and their environments using multiple laminar fluid flows in capillary networks,” *Proceedings Of The National Academy Of Sciences Of The United States Of America*, vol. 96, May. 1999, pp. 5545–5548.

[45] X. Trepat, M. Wasserman, T. Angelini, E. Millet, D. Weitz, J. Butler, and J. Fredberg, “Physical forces during collective cell migration,” *Nature Physics*, vol. 5, 2009, pp. 426–430.

[46] M.R. Doran, R.J. Mills, A.J. Parker, K.A. Landman, and J.J. Cooper-White, “A cell migration device that maintains a defined surface with no cellular damage during wound edge generation,” *Lab on a Chip*, vol. 9, 2009, pp. 2364–2369.

[47] C. Renken, “Re: Electric Fence,” *E-mail to the author*, Jun. 2011.

[48] K. Ino, A. Ito, and H. Honda, “Cell patterning using magnetite nanoparticles and magnetic force,” *Biotechnology And Bioengineering*, vol. 97, 2007, pp. 1309–1317.

[49] A. Ito, H. Akiyama, Y. Kawabe, and M. Kamihira, “Magnetic Force-Based Cell Patterning Using Arg-Gly-Asp (RGD) Peptide-Conjugated Magnetite Cationic Liposomes,” *Journal Of Bioscience And Bioengineering*, vol. 104, 2007, pp. 288–293.

[50] K. Ino, M. Okochi, and H. Honda, “Application of magnetic force-based cell patterning for controlling cell-cell interactions in angiogenesis,” *Biotechnology And Bioengineering*, vol. 102, Feb. 2009, pp. 882–890.

[51] U.D. Akavia, O. Litvin, J. Kim, F. Sanchez-Garcia, D. Kotliar, H.C. Causton, P. Pochanard, E. Mozes, L.A. Garraway, and D. Pe'er, “An integrated approach to uncover drivers of cancer,” *Cell*, vol. 143, Dec. 2010, pp. 1005–1017.

[52] J.K. Fisher, J. Cribb, K.V. Desai, L. Vicci, B. Wilde, K. Keller, R.M. Taylor, J. Haase, K. Bloom, E.T. O'Brien, and R. Superfine, “Thin-foil magnetic force system for high-numerical-aperture microscopy,” *The Review of scientific instruments*, vol. 77, Feb. 2006, pp. nihms8302–.

[53] A. Ashkin, J.M. Dziedzic, and T. Yamane, “Optical trapping and manipulation of single cells using infrared laser beams,” *Nature*, vol. 330, Nov. 1987, pp. 769–771.

[54] H.D. Ou-Yang and M.-T. Wei, “Complex fluids: probing mechanical properties of biological systems with optical tweezers,” *Annual review of physical chemistry*, vol. 61, Mar. 2010, pp. 421–440.

[55] F. Schaal, M. Warber, S. Zwick, H. van der Kuip, T. Haist, and W. Osten, “Marker-free cell discrimination by holographic optical tweezers,” *Journal of the European Optical Society: Rapid Publications*, vol. 4, 2009.

[56] M.M. Wang, E. Tu, D.E. Raymond, J.M. Yang, H. Zhang, N. Hagen, B. Dees, E.M. Mercer, A.H. Forster, I. Kariv, P.J. Marchand, and W.F. Butler, “Microfluidic

sorting of mammalian cells by optical force switching," *Nature Biotechnology*, vol. 23, Dec. 2004, pp. 83–87.

[57] T. Gebaeck, M.M.P. Schulz, P. Koumoutsakos, and M. Detmar, "TScratch: a novel and simple software tool for automated analysis of monolayer wound healing assays," *BioTechniques*, vol. 46, 2009, pp. 265–274.

[58] M.D. Abramoff, P.J. Magalhães, and S.J. Ram, "Image processing with ImageJ," *Biophotonics international*, vol. 11, 2004, pp. 36–42.

[59] A. Carpenter, A. Carpenter, T. Jones, T. Jones, M. Lamprecht, M. Lamprecht, C. Clarke, C. Clarke, I. Kang, I. Kang, O. Friman, O. Friman, D. Guertin, D. Guertin, J. Chang, J. Chang, R. Lindquist, R. Lindquist, J. Moffat, J. Moffat, P. Golland, P. Golland, D. Sabatini, and D. Sabatini, "CellProfiler: image analysis software for identifying and quantifying cell phenotypes," *Genome Biology*, vol. 7, Oct. 2006, p. R100.

[60] L. Martens, G. Monsieur, C. Ampe, K. Gevaert, and J. Vandekerckhove, "Cell_motility: a cross-platform, open source application for the study of cell motion paths," *BMC Bioinformatics*, vol. 7, Jun. 2006, p. 289.

[61] Y. Matsubayashi, W. Razzell, and P. Martin, "'White wave' analysis of epithelial scratch wound healing reveals how cells mobilise back from the leading edge in a myosin-II-dependent fashion," *Journal of cell science*, vol. 124, Mar. 2011, pp. 1017–1021.

[62] D. Wessels, S. Kuhl, and D.R. Soll, "2D and 3D quantitative analysis of cell motility and cytoskeletal dynamics," *Methods in molecular biology (Clifton, N.J.)*, vol. 586, 2009, pp. 315–335.

[63] M.R. Lamprecht, D.M. Sabatini, and A.E. Carpenter, "CellProfiler: free, versatile software for automated biological image analysis," *BioTechniques*, vol. 42, Jan. 2007, pp. 71–75.

[64] P. Friedl and D. Gilmour, "Collective cell migration in morphogenesis, regeneration and cancer," *Nature Reviews Molecular Cell Biology*, vol. 10, Jul. 2009, pp. 445–457.

[65] K.I. Hulkower and R.L. Herber, "Cell Migration and Invasion Assays as Tools for Drug Discovery," *Pharmaceutics*, vol. 3, Mar. 2011, pp. 107–124.

[66] H.-C. Chen, "Cell-scatter assay," *Methods in molecular biology (Clifton, N.J.)*, vol. 294, 2005, pp. 69–77.

[67] M.N. Yousaf, B.T. Houseman, and M. Mrksich, “Turning on cell migration with electroactive substrates,” *Angewandte Chemie-International Edition*, vol. 40, 2001, pp. 1093–.

[68] N.E. Ramirez, Z. Zhang, A. Madamanchi, K.L. Boyd, L.D. O'Rear, A. Nashabi, Z. Li, W.D. Dupont, A. Zijlstra, and M.M. Zutter, “The α2β1 integrin is a metastasis suppressor in mouse models and human cancer,” *The Journal of clinical investigation*, vol. 121, Jan. 2011, pp. 226–237.

[69] G. Sur and J. Mark, “Some reinforcing characteristics of iron-based fillers,” *Polymer Bulletin*, vol. 18, Oct. 1987, pp. 369–375.

[70] Y. Wang and R. Pelham, “Preparation of a flexible, porous polyacrylamide substrate for mechanical studies of cultured cells,” *Molecular Motors And The Cytoskeleton, Pt B*, vol. 298, 1998, pp. 489–496.

[71] N.R. Alexander, K.M. Branch, A. Parekh, E.S. Clark, S.A. Guelcher, I.C. Iwueke, and A.M. Weaver, “Extracellular matrix rigidity promotes invadopodia activity,” *Current biology : CB*, vol. 18, Sep. 2008, pp. 1295–1299.

[72] D.T. Butcher, T. Alliston, and V.M. Weaver, “A tense situation: forcing tumour progression,” *Nature Reviews Cancer*, vol. 9, Feb. 2009, pp. 108–122.

[73] S. Preibisch, S. Saalfeld, and P. Tomancak, “Globally optimal stitching of tiled 3D microscopic image acquisitions,” *Bioinformatics*, vol. 25, Jun. 2009, pp. 1463–1465.

[74] S. Preibisch, S. Saalfeld, J. Schindelin, and P. Tomancak, “Software for bead-based registration of selective plane illumination microscopy data,” *Nature Methods*, vol. 7, Jun. 2010, pp. 418–419.

[75] R. Ihaka and R. Gentleman, “R: a language for data analysis and graphics,” *Journal of computational and graphical statistics*, vol. 5, 1996, pp. 299–314.

[76] J.P. Thiery, “Epithelial-mesenchymal transitions in development and pathologies,” *Current Opinion in Cell Biology*, vol. 15, Dec. 2003, pp. 740–746.

[77] D.E. Ingber, “Can cancer be reversed by engineering the tumor microenvironment?,” *Seminars In Cancer Biology*, vol. 18, 2008, pp. 356–364.

[78] S. Jaehrling, K. Thelen, T. Wolfram, and G.E. Pollerberg, “Nanopatterns biofunctionalized with cell adhesion molecule DM-GRASP offered as cell substrate: spacing determines attachment and differentiation of neurons,” *Nano letters*, vol. 9, Dec. 2009, pp. 4115–4121.

[79] A. Quist, E. Pavlovic, and S. Oscarsson, “Recent advances in microcontact printing,” *Analytical And Bioanalytical Chemistry*, vol. 381, 2005, pp. 591–600.

[80] R.S. Kane, S. Takayama, E. Ostuni, D.E. Ingber, and G.M. Whitesides, “Patterning proteins and cells using soft lithography,” *Biomaterials*, vol. 20, Dec. 1999, pp. 2363–2376.

[81] M.J. Poellmann, P.A. Harrell, W.P. King, and A.J. Wagoner Johnson, “Geometric microenvironment directs cell morphology on topographically patterned hydrogel substrates,” *Acta biomaterialia*, vol. 6, Sep. 2010, pp. 3514–3523.

[82] A. Folch and M. Toner, “Cellular micropatterns on biocompatible materials,” *Biotechnology progress*, vol. 14, 1998, pp. 388–392.

[83] M.J. Paszek, N. Zahir, K.R. Johnson, J.N. Lakins, G.I. Rozenberg, A. Gefen, C.A. Reinhart-King, S.S. Margulies, M. Dembo, D. Boettiger, D.A. Hammer, and V.M. Weaver, “Tensional homeostasis and the malignant phenotype,” *Cancer cell*, vol. 8, Sep. 2005, pp. 241–254.

[84] C. Lo, H. Wang, M. Dembo, and Y. Wang, “Cell movement is guided by the rigidity of the substrate,” *Biophysical journal*, vol. 79, 2000, pp. 144–152.

[85] T. Ulrich, E. De Juan Pardo, and S. Kumar, “The Mechanical Rigidity of the Extracellular Matrix Regulates the Structure, Motility, and Proliferation of Glioma Cells,” *Cancer Research*, vol. 69, May. 2009, p. 4167.

[86] T. Yeung, P. Georges, L. Flanagan, B. Marg, M. Ortiz, M. Funaki, W. Ming, V. Weaver, N. Zahir, and P. Janmey, “Effects of substrate stiffness on cell morphology, cytoskeletal structure, and adhesion,” *Cell Motility and the Cytoskeleton*, vol. 60, 2005, pp. 24–34.

[87] A. Parekh, N.S. Ruppender, K.M. Branch, M.K. Sewell-Loftin, J. Lin, P.D. Boyer, J.E. Candiello, W.D. Merryman, S.A. Guelcher, and A.M. Weaver, “Sensing and modulation of invadopodia across a wide range of rigidities,” *Biophysical journal*, vol. 100, Feb. 2011, pp. 573–582.

[88] A. Zijlstra, J. Lewis, B. DeGryse, H. Stuhlmann, and J.P. Quigley, “The inhibition of tumor cell intravasation and subsequent metastasis via regulation of in vivo tumor cell motility by the tetraspanin CD151,” *Cancer cell*, vol. 13, Mar. 2008, pp. 221–234.

[89] A. Folch, B.-H. Jo, O. Hurtado, D.J. Beebe, and M. Toner, “Microfabricated elastomeric stencils for micropatterning cell cultures,” *Journal of Biomedical Materials Research Part A*, vol. 52, Nov. 2000, pp. 346–353.

[90] C. Rydberg, A. Mansson, R. Uddman, K. Riesbeck, and L.-O. Cardell, “Toll-like receptor agonists induce inflammation and cell death in a model of head and neck squamous cell carcinomas,” *Immunology*, vol. 128, 2009, pp. e600–e611.

[91] D. Majumdar, Y. Gao, D. Li, and D.J. Webb, “Co-culture of neurons and glia in a novel microfluidic platform,” *Journal Of Neuroscience Methods*, vol. 196, Mar. 2011, pp. 38–44.

[92] B.P. Nguyen, X.D. Ren, M.A. Schwartz, and W.G. Carter, “Ligation of integrin alpha 3beta 1 by laminin 5 at the wound edge activates Rho-dependent adhesion of leading keratinocytes on collagen,” *The Journal of biological chemistry*, vol. 276, Nov. 2001, pp. 43860–43870.

[93] C. Darlington, “The Internal Mechanics of the Chromosomes. I.--The Nuclear Cycle in Fritillaria,” *Proceedings of the Royal Society of London. Series B, Biological Sciences*, vol. 118, 1935, pp. 33–59.

[94] J.R. Pomerening, E.D. Sontag, and J.E. Ferrell, “Building a cell cycle oscillator: hysteresis and bistability in the activation of Cdc2,” *Nature Cell Biology*, vol. 5, Mar. 2003, pp. 346–351.

[95] D. Angeli, J.E. Ferrell, and E.D. Sontag, “Detection of multistability, bifurcations, and hysteresis in a large class of biological positive-feedback systems,” *Proceedings Of The National Academy Of Sciences Of The United States Of America*, vol. 101, Feb. 2004, pp. 1822–1827.

[96] J. Kopfová, “Hysteresis in biological models,” *Journal of Physics: Conference Series*, vol. 55, 2006, p. 130.

[97] S.A. Galdeen and A.J. North, “Live cell fluorescence microscopy techniques,” *Methods in molecular biology (Clifton, N.J.)*, vol. 769, 2011, pp. 205–222.

[98] A.J. North, “Seeing is believing? A beginners' guide to practical pitfalls in image acquisition,” *The Journal of Cell Biology*, vol. 172, Jan. 2006, pp. 9–18.

[99] George G Rose, “The Circumfusion System for Multipurpose Culture Chambers: I. Introduction to the Mechanics, Techniques, and Basic Results of a 12-Chamber (In Vitro) Closed Circulatory System,” *The Journal of Cell Biology*, vol. 32, 1967, p. 89.

[100] K. Haubert, T. Drier, and D. Beebe, “PDMS bonding by means of a portable, low-cost corona system,” *Lab on a Chip*, vol. 6, 2006, pp. 1548–1549.

[101] E. Tkachenko, E. Gutierrez, M.H. Ginsberg, and A. Groisman, “An easy to assemble microfluidic perfusion device with a magnetic clamp,” *Lab on a Chip*, vol. 9, Apr. 2009, p. 1085.

[102] M. Rafat, D.R. Raad, A.C. Rowat, and D.T. Auguste, “Fabrication of reversibly adhesive fluidic devices using magnetism,” *Lab on a Chip*, vol. 9, Oct. 2009, pp. 3016–3019.

[103] J. Debnath, S.K. Muthuswamy, and J.S. Brugge, "Morphogenesis and oncogenesis of MCF-10A mammary epithelial acini grown in three-dimensional basement membrane cultures," *Methods (San Diego, Calif.)*, vol. 30, Jul. 2003, pp. 256–268.

[104] W.J. Ashby, J.P. Wikswo, and A. Zijlstra, "Magnetically attachable stencils and the non-destructive analysis of the contribution made by the underlying matrix to cell migration," *Biomaterials*, Jul. 2012, pp. 1–50.

[105] G.W. Pearson and T. Hunter, "Real-time imaging reveals that noninvasive mammary epithelial acini can contain motile cells," *The Journal of Cell Biology*, vol. 179, Dec. 2007, pp. 1555–1567.

[106] M.W. Dewhirst, "Intermittent hypoxia furthers the rationale for hypoxia-inducible factor-1 targeting," *Cancer Research*, vol. 67, Feb. 2007, pp. 854–855.

[107] S. Toffoli, A. Roegiers, O. Feron, M. Van Steenbrugge, N. Ninane, M. Raes, and C. Michiels, "Intermittent hypoxia is an angiogenic inducer for endothelial cells: role of HIF-1," *Angiogenesis*, vol. 12, 2009, pp. 47–67.

[108] S.J. Altschuler and L.F. Wu, "Cellular heterogeneity: do differences make a difference?," *Cell*, vol. 141, May. 2010, pp. 559–563.

[109] M.D. Slack, E.D. Martinez, L.F. Wu, and S.J. Altschuler, "Characterizing heterogeneous cellular responses to perturbations," *Proceedings of the National Academy of Sciences*, vol. 105, Dec. 2008, pp. 19306–19311.

[110] I. Rosova, M. Dao, B. Capoccia, D. Link, and J.A. Nolta, "Hypoxic preconditioning results in increased motility and improved therapeutic potential of human mesenchymal stem cells," *Stem Cells*, vol. 26, 2008, pp. 2173–2182.

[111] R.A. Cairns, T. Kalliomaki, and R.P. Hill, "Acute (cyclic) hypoxia enhances spontaneous metastasis of KHT murine tumors," *Cancer Research*, vol. 61, Dec. 2001, pp. 8903–8908.

[112] M. Lacroix and G. Leclercq, "Relevance of breast cancer cell lines as models for breast tumours: an update," *Breast cancer research and treatment*, vol. 83, Feb. 2004, pp. 249–289.

[113] V. Quaranta, D.R. Tyson, S.P. Garbett, B. Weidow, M.P. Harris, and W. Georgescu, "Trait variability of cancer cells quantified by high-content automated microscopy of single cells," *Methods in enzymology*, vol. 467, 2009, pp. 23–57.

[114] C. Thibault, C. Séverac, A.-F. Mingotaud, C. Vieu, and M. Mauzac, "Poly(dimethylsiloxane) contamination in microcontact printing and its influence on patterning oligonucleotides," *Langmuir*, vol. 23, Oct. 2007, pp. 10706–10714.

[115] H. Xu, A. Gomez-Casado, Z. Liu, D.N. Reinhoudt, R.G.H. Lammertink, and J. Huskens, “Porous multilayer-coated PDMS stamps for protein printing,” *Langmuir*, vol. 25, Dec. 2009, pp. 13972–13977.

[116] K. Shen, J. Qi, and L. Kam, “Microcontact Printing of Proteins for Cell Biology,” *Journal of Visualized Experiments*, Dec. 2008.

[117] D. Wlodkowic, K. Khoshmanesh, J. Akagi, D.E. Williams, and J.M. Cooper, “Wormometry-on-a-chip: Innovative technologies for in situ analysis of small multicellular organisms,” *Cytometry. Part A*, vol. 79, Oct. 2011, pp. 799–813.

[118] S.R. Lockery, S.E. Hulme, W.M. Roberts, K.J. Robinson, A. Laromaine, T.H. Lindsay, G.M. Whitesides, and J.C. Weeks, “A microfluidic device for whole-animal drug screening using electrophysiological measures in the nematode C. elegans,” *Lab on a Chip*, vol. 12, Jun. 2012, pp. 2211–2220.

[119] S.E. Hulme and G.M. Whitesides, “Chemistry and the worm: Caenorhabditis elegans as a platform for integrating chemical and biological research,” *Angewandte Chemie (International ed in English)*, vol. 50, May. 2011, pp. 4774–4807.

[120] D. Choudhury, D. Van Noort, C. Iliescu, B. Zheng, K.-L. Poon, S. Korzh, V. Korzh, and H. Yu, “Fish and Chips: a microfluidic perfusion platform for monitoring zebrafish development,” *Lab on a Chip*, vol. 12, Mar. 2012, pp. 892–900.

[121] S.J. Gallagher, W.J. Ashby, F.P. Cordelieres, and L. Larue, “ImageJ Macro for Scratch Wound Assay Analysis,” *imagejdocu.tudor.lu* Available: http://imagejdocu.tudor.lu/doku.php?id=plugin:analysis:scratch_wound_assay_automatic_analysis_macro:start.

[122] W.J. Ashby, “Human-in-the-loop particle analysis: a FIJI macro,” *imagejdocu.tudor.lu* Available: http://imagejdocu.tudor.lu/doku.php?id=plugin:analysis:human-in-the-loop_particle_analysis_beta:start.

[123] W.J. Ashby, “Hyper With Stacks: an ImageJ Macro,” *imagejdocu.tudor.lu* Available: http://imagejdocu.tudor.lu/doku.php?id=plugin:stacks:toolset_for_manual_extraction_of_best-focused_z-slices_from_hyperstack:start.

[124] D.C. Duffy, J.C. McDonald, O.J. Schueller, and G.M. Whitesides, “Rapid Prototyping of Microfluidic Systems in Poly(dimethylsiloxane),” *Analytical Chemistry*, vol. 70, Dec. 1998, pp. 4974–4984.

[125] J. McDonald, D. Duffy, J. Anderson, D. Chiu, W. Hongkai, O. Schueller, and G. Whitesides, “Fabrication of microfluidic systems in poly (dimethylsiloxane),” *Electrophoresis*, vol. 21, 2000, pp. 27–40.

[126] L.E. Schmidt, S. Yi, Y.-H. Jin, Y. Leterrier, Y.-H. Cho, and J.-A.E. Manson, "Acrylated hyperbranched polymer photoresist for ultra-thick and low-stress high aspect ratio micropatterns," *Journal of Micromechanics and Microengineering*, vol. 18, 2008, p. 045022.

[127] P. Vulto, N. Glade, L. Altomare, J. Bablet, L.D. Tin, G. Medoro, I. Chartier, N. Manaresi, M. Tartagni, and R. Guerrieri, "Microfluidic channel fabrication in dry film resist for production and prototyping of hybrid chips," *Lab on a Chip*, vol. 5, Feb. 2005, pp. 158–162.

[128] V. Auzelyte, M. Elfrnan, P. Kristiansson, C. Nilsson, J. Pallon, N.A. Marrero, and M. Wegden, "Exposure parameters for MeV proton beam writing on SU-8," *Microelectronic Engineering*, vol. 83, 2006, pp. 2015–2020.

[129] A. Christensen, D. Chang-Yen, and B. Gale, "Characterization of interconnects used in PDMS microfluidic systems," *Journal Of Micromechanics And Microengineering*, vol. 15, 2005, pp. 928–934.

[130] C. Koch, J. Ingle, and V. Remcho, "Magnets for facile molding of via holes in PDMS," *RSC Blogs: Chips and Tips* Available: http://blogs.rsc.org/chipsandtips/2008/02/02/magnets-for-facile-molding-of-via-holes-in-pdms/.

[131] Y. Xia and G. Whitesides, "Soft lithography," *Angewandte Chemie-International Edition*, vol. 37, 1998, pp. 551–575.

[132] D. Qin, Y. Xia, and G. Whitesides, "Rapid prototyping of complex structures with feature sizes larger than 20 mu m," *Advanced Materials*, vol. 8, 1996, pp. 917–&.

[133] D. Wu, Y. Luo, X. Zhou, Z. Dai, and B. Lin, "Multilayer poly(vinyl alcohol)-adsorbed coating on poly(dimethylsiloxane) microfluidic chips for biopolymer separation," *Electrophoresis*, vol. 26, 2005, pp. 211–218.

[134] L. Gitlin, P. Schulze, and D. Belder, "Rapid replication of master structures by double casting with PDMS," *Lab on a Chip*, vol. 9, 2009, p. 3000.

[135] Z. Zhang, P. Zhao, G. Xiao, B.R. Watts, and C. Xu, "Sealing SU-8 microfluidic channels using PDMS," *Biomicrofluidics*, vol. 5, 2011, pp. 046503–046503–8.

[136] H.-L. Chang, F. Zhang, J.-L. Ding, F.-L. Chen, S.-J. Hong, M. Kraft, and W.-Z. Yuan, "A highly reliable integrated PDMS interconnector with a long cast flange for microfluidic systems," *Microsystem Technologies*, vol. 18, 2012, pp. 723–730.